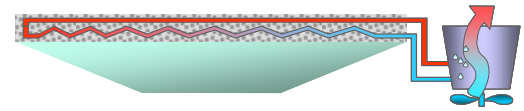

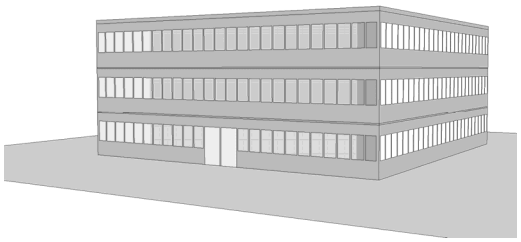

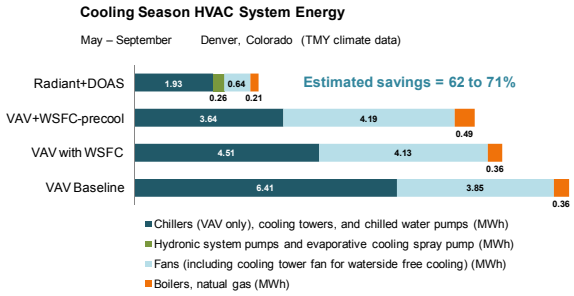

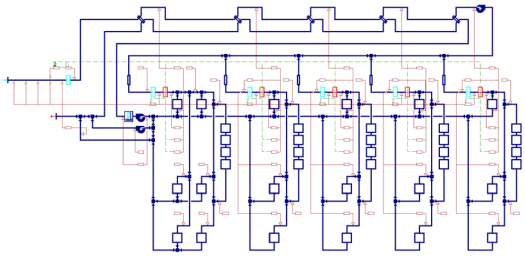

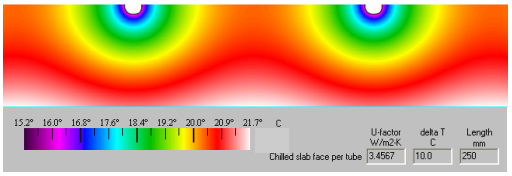

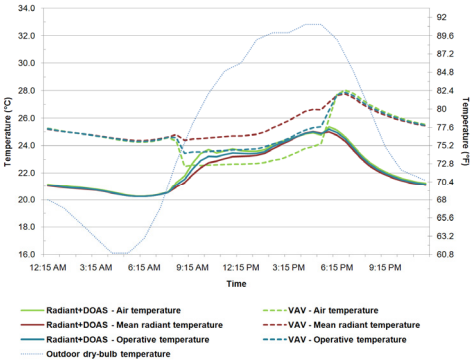

SUMMARY REPORT:

SIMULATION OF RADIANT COOLING PERFORMANCE WITH EVAPORATIVE COOLING SOURCES

TIMOTHY MOORE

CENTER FOR THE BUILT ENVIRONMENT (CBE)

UNIVERSITY OF CALIFORNIA, BERKELEY

MAY 2008

ACKNOWLEDGEMENTS

This work was made possible through the support of the California Energy Commission's Public Interest Energy Research (PIER) Program, funding from industry partners of the University of California at Berkeley Center for the Built Environment (CBE), and the Robert and Patricia Switzer Foundation Environmental Fellowship.

I would like to thank CBE Research Specialists, Fred Bauman and Charlie Huizenga; my advisor, thesis committee chair, and Associate Director of CBE, Professor Gail Brager, and CBE's Director, Ed Arens, for their support, assistance, and encouragement throughout this project. I am also grateful to all of the CBE staff and student researchers for contributing to the valuable work of this organization, which has influenced me in innumerable ways, and for maintaining and growing CBE as one of the finest research centers in the building industry so that students such as me can benefit from participating. Similarly, I would like to thank all of those in the building industry that have generously shared their thoughts, feedback, and time in support of this and related work I have done along the way. Indeed, I have found my interactions with individuals in the field to be among the most valuable elements of my education. The interactive structure and culture of CBE has facilitated these connections with professionals who share the pursuit of better building performance as a means to improving the quality, sustainability, and compatibility of human and natural environments. I wish to thank the USGBC for creating so many new opportunities and my countless building-industry friends and professional colleagues in Colorado that have been so supportive of my efforts in developing a sustainable design consulting practice and the LEED Professional Accreditation Study Guide, both of which have been important sources of financial support. Finally, I would like to thank my family and friends for their encouragement and support when I chose to begin a new career and my dearest Joanna for her patience, love, support, and encouragement in the final months and weeks of this project.

CBE's Industry Partners (as of April 2008):

Armstrong World Industries
Arup*
California Energy Commission
Charles M. Salter Associates
Cohos Evamy
CPP
EHDD Architecture
Engineered Interiors Group
Environmental Systems Design
Flack + Kurtz
Glumac
Haworth
HOK
Johnson Controls*
KlingStubbins
Larson Binkley
Pacific Gas & Electric Company
Price Industries
RTKL Associates
Skidmore, Owings & Merrill
Stantec
Steelcase
Syska Hennessy Group
Tate Access Floors*
Taylor Team: Taylor Engineering
CTG Energetics
Guttmann & Blaevoet
Southland Industries
Swinerton Builders
Trane
Uponor
U.S. Department of Energy*
U.S. General Services Administration*
Webcor Builders*
Zimmer Gunsul Frasca Architects

* *founding partner*

TABLE OF CONTENTS

390 Wurster Hall #1839, Berkeley, CA 94720-1839
tel: 510.642.4950 fax: 510.643.5571
cbe@berkeley.edu | www.cbe.berkeley.edu

ABBREVIATIONS

CHW	Chilled water (*vs*. condenser-water loop)
COP	Coefficient of performance (kW cooling per kW electricity)
CV	Constant volume (*vs*. variable air volume)
DBT	Dry-bulb temperature
DPT	Dew-point temperature
DOAS	Dedicated outside air system (100% outside air; no recirculation)
HVAC	Heating ventilation and air-conditioning
LAT	Leaving air temperature (the temperature immediately downstream of a coil)
MRT	Mean radiant temperature
OA	Outside air (as brought in by the HVAC system fan)
RA	Return air (from conditioned spaces)
RH	Relative humidity (percent of total that would saturate the air at a given temperature)
SAT	Supply air temperature (the as provided to spaces prior to duct gain)
VAV	Variable air volume (*vs*. constant air volume)
VSD	Variable speed drive (via motor electronics)
WBT	Wet-bulb temperature
WSFC	Waterside free cooling (waterside economizer)

EXECUTIVE SUMMARY

This project addresses three closely related and similarly complex questions: First, using currently available simulation software, what methods might be appropriate for comparing slab-integrated radiant cooling to more conventional alternatives, such that the results are sufficiently fair and comprehensive to support system selection and design? Second, what is the relative performance of representative system configurations across a set of climates that test presumed strengths and limitations? Third, what useful conclusions can be drawn from such comparisons to inform the selection, application, design, and control of hydronic radiant cooling?

The particular approach taken to answering these questions is rooted in the contention that useful results must effectively capture five essential aspects of slab-integrated hydronic radiant cooling: a) radiant heat transfer between surfaces; b) the effects of thermal capacity, lag, and decrement in the chilled slab; c) the limitations of evaporative cooling water sources; d) the potential of various control strategies for maintaining thermal comfort while minimizing energy consumption and peak loads; and e) the challenges and benefits of integrating the operation and control of hydronic and airside space conditioning systems.

This report describes whole-building simulations of slab-integrated hydronic radiant cooling with mechanical ventilation, plus a more conventional all-air cooling system as a point of reference. Simulations are performed using Virtual Environment (VE)—an interconnected set of building performance-modeling tools from Integrated Environmental Solutions (IES). Methods are described for the modeling of hydronic radiant cooling slabs. Among these, THERM, a simple two-dimensional finite-element heat transfer tool from Lawrence Berkeley National Laboratory, is used for determining properties of the heat transfer path between the hydronic circuits and cooling surfaces. Attention is also given to modeling limitations of evaporative cooling as a supply water source for the radiant system and waterside economizer for the all-air baseline system. In preparing the models, emphasis was placed on achieving similar degrees of equipment and controls optimization for both systems using methods that could be replicated in the context of practical design processes.

Cooling-season performance is evaluated in terms of system dynamics, thermal comfort, peak loads, and energy consumption for a prototypical office building in Denver, Sacramento, Los Angeles, and San Francisco. The Denver climate was used to optimize system dynamics and performance for minimum energy consumption and peak power. Sacramento—the hottest of the four—was the focus for optimizing and evaluating thermal performance with aggressive hydronic slab nighttime precooling. For the San Francisco climate, added emphasis was placed on optimizing the economizer controls and performance for the all-air baseline system. In all cases, equipment, airflow, and other key parameters were evaluated and re-sized accordingly.

The slab-integrated hydronic radiant cooling is augmented by a dedicated outside air system (DOAS) for conditioning of ventilation air. The hydronic cooling and DOAS utilize only indirect evaporative cooling sources. The supply water source for the hydronic slabs and cooling coils is a closed-circuit cooling tower. The DOAS also incorporates a heat exchanger for sensible energy recovery and indirect-evaporative cooling of ventilation air via a spray chamber in the exhaust air stream. The reference baseline is a modern variable-air-volume system with an efficient water-cooled chiller and fully integrated control resets for supply air temperature and airside economizer operation. A waterside economizer or waterside "free cooling" (WSFC)—essentially the same cooling water source as is used for the hydronic radiant system—and nighttime precooling cycle were modeled as an additional scenario for the baseline system. The DOAS and VAV system use identical high-efficiency fans and motors (differing only in size).

Simulation results (Figures 1–4) suggest strong energy-saving potential for radiant cooling systems in both Colorado and California climates. In Denver (Figure 1), the simulated radiant cooling plus dedicated outside air system (Radiant+DOAS) with precooling uses an estimated 71% less energy than the standard VAV baseline system and 62% less than the same VAV system using waterside free cooling and a nighttime precooling control strategy. This comparison includes heating for cool mornings, which must be coordinated with the nighttime slab precooling strategy. In Sacramento (Figure 2), the Radiant+DOAS uses an estimated 59% less energy relative to the baseline VAV system and 56% less than the VAV with waterside free cooling, regardless of the inclusion of precooling controls. For this hot but relatively dry climate, the added fan energy for precooling with the all-air VAV system, given its capacity for WSFC is sized for chiller heat rejection, offsets the savings from reduced daytime chiller operation. In Los Angeles (Figure 3), where daytime temperature are more moderate and nighttime temperatures tend not to dip quite as low, precooling—in this case used only for the Radiant+DOAS—confers a lesser net benefit. For San Francisco (Figure 4), where cooling loads are reduced and *airside* "free cooling" is readily available through economizer operation (which still requires the use of fans), total energy for both systems is considerably lower. However, the effectiveness of *waterside* free cooling in this climate contributes to even greater reduction of energy consumption for the otherwise already very efficient hydronic radiant system.

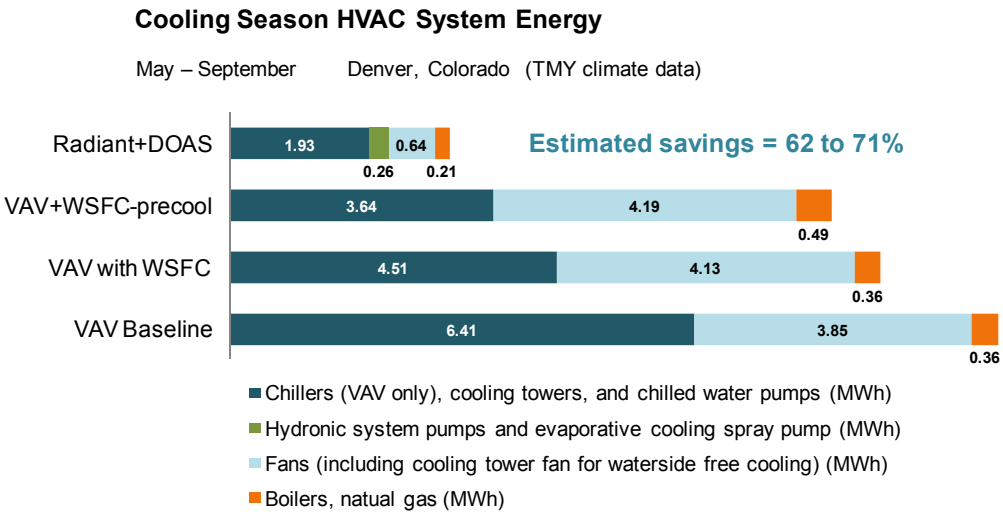

Figure 1: Simulated cooling-season HVAC system energy consumption for Denver, Colorado. The range of estimated saving is relative to the VAV baseline system with and without a waterside economizer.

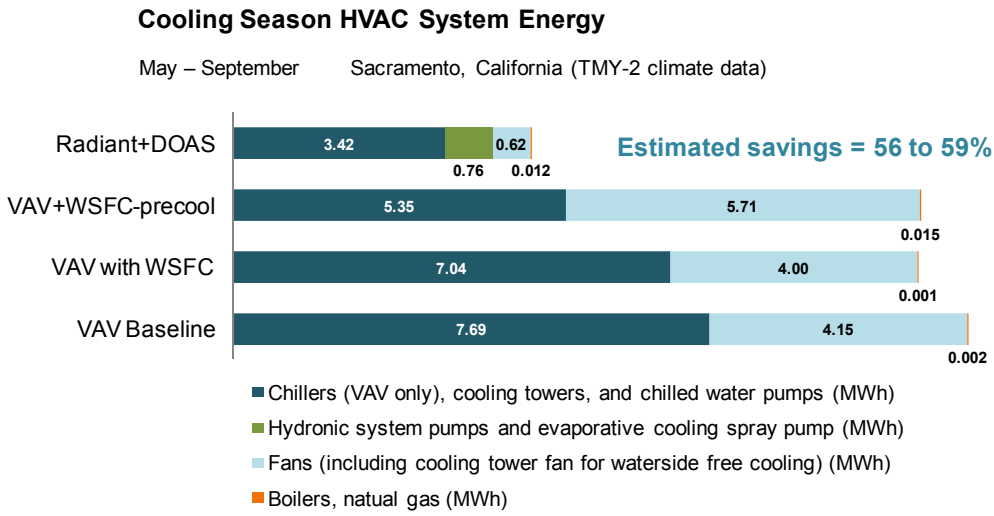

Figure 2: Simulated cooling-season HVAC system energy consumption for Sacramento, CA.

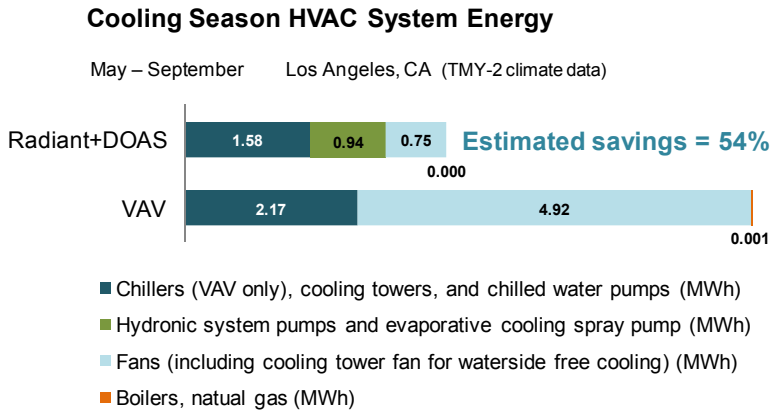

Figure 3: Simulated cooling-season HVAC system energy consumption for Los Angeles, CA.

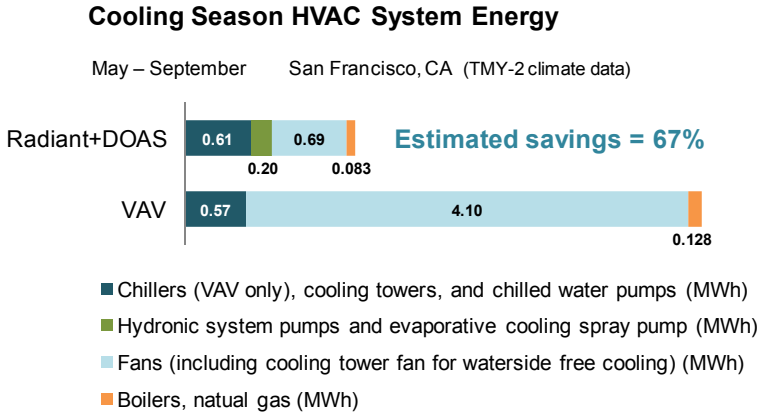

Figure 4: Simulated cooling-season HVAC system energy consumption for San Francisco, CA.

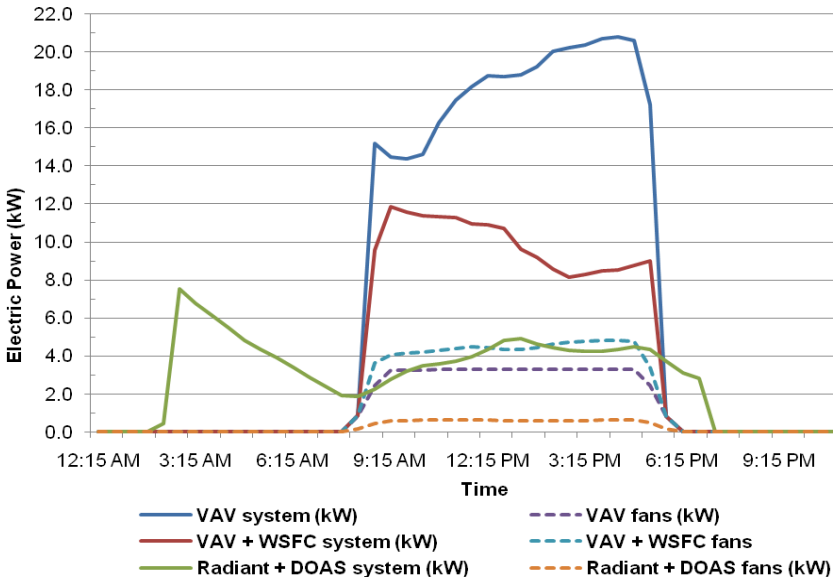

Figure 5: Cooling-system, fan, and nighttime precooling operation in terms of power and energy (the area under the curves) for the Radiant+DOAS, VAV+WSFC, and standard VAV-baseline with water-cooled chiller. The plot is for the day of peak cooling loads in Sacramento, CA (TMY-2 climate data).

Peak power demand for the Radiant+DOAS is both significantly reduced and shifted to off-peak hours (Figure 5): In Sacramento, the VAV baseline system peaks at 20.9 kW on July 19th; on that day, the Radiant+DOAS system peaks at just 9.8 kW—a 50% reduction—and does so at 2:45 AM when utility power demand is very low. During the afternoon hours of July 19th, the radiant-DOAS system peaks at just 2 kW—a 90% reduction. The peak cooling-season demand for the radiant system is 10.4 kW and occurs at 4:15 AM. Evaluating only afternoon hours (noon to 5:00 PM) when electric demands tend to peak, the radiant system has just 34.5 hours of demand over 5 kW, while the VAV system has 504 hours of operation over this same threshold.

Even with aggressive precooling for the hydronic slabs, thermal performance for the two systems in the hot Sacramento climate remains comparable. The greatest difference occurs on the hottest few days in July and August with late-afternoon peak solar gain in the west perimeter zones. At this time, the concrete slabs are relatively warm and the peaking outdoor wet-bulb temperature limits the evaporative cooling of supply water. Under these conditions, operative temperatures for west perimeter zones with Radiant+DOAS cooling exceed 1K (1.8°F) above that of the baseline system only within the very last occupied hour of the day, if at all. For the vast majority of the cooling season, however, the Radiant+DOAS system provides a *lower* operative temperature.

From a gross, whole-building perspective, thermal performance for the low-energy Radiant+ DOAS differs only subtly from that of the baseline VAV system. Even for the afternoon of the *peak* cooling day in Sacramento, with 40°C (104°F) dry-bulb and 23°C (73.4°F) coincident wet-bulb temperatures, the combined average operative temperature for all regularly occupied spaces differs less than 0.5 K (0.9°F) between the radiant-cooling and baseline-VAV cases. This is additionally significant given that the peak cooling provided by the hydronic radiant slabs occurs three hours *after* the hydronic circulation pumps have been shut off to avoid *adding* heat to the slabs. Just 16% of total cooling at that time is provided by the DOAS. However, achieving this with constrained supply water temperatures and at the same time avoiding excessive precooling required careful attention to numerous control parameters. Thus slab precooling with water from

a cooling tower and augmentation by indirect evaporative cooling of ventilation air would appear to be an effective strategy for exceptionally low-energy cooling, even in hot climates such as Sacramento, *if* appropriate attention is paid to the design and control of the system.

There were three essential control strategies employed to utilized the slab thermal mass and the extended nighttime cooling-tower capacity: 1) cut off cooling water to any given slab when the water temperature from the cooling tower exceeds the slab core temperature; 2) avoid cooling the slabs in the late afternoon and evening hours, even when the outdoor WBT is low—*i.e.,* begin the nighttime precooling only after the outdoor WBT has dropped significantly *and* the slab core temperature is approaching equilibrium with the occupied space; 3) constrain precooling to avoid overcooling occupied spaces in early morning hours. Together with the location of hydronic cooling at the core of the massive concrete slabs, these strategies maintained thermal comfort while shifting a large fraction of the cooling load to off-peak hours suited to evaporative cooling.

1. BACKGROUND

To address concerns related to environmental impacts, sustainable resource consumption, and human health and productivity, the building industry is attempting to shift toward both highly efficient or even net-zero energy buildings and improved indoor environmental quality (IEQ). Radiant cooling appears to be among the options with greatest potential for addressing both efficiency and IEQ, particularly in combination with optimized building envelopes, low-energy cooling water sources, and evaporatively conditioned ventilation air and/or natural ventilation. The existence and extent of these various potential benefits are, however, contingent upon one or another degree of design optimization.[1]

Hydronic radiant cooling paired with a dedicated outside air ventilation system (DOAS) appears more energy efficient relative to conventional all-air cooling systems for commercial buildings. In some cases, such as interior spaces in close proximity to glazing heated by solar gains, radiant cooling may offer improved thermal comfort. In climates without large numbers of airside economizer hours, there may also be potential for improved indoor air quality. The first and last of these three potentials stem largely from the extraction of sensible cooling loads via water rather than air, thus leaving the airside system to address mainly ventilation and latent loads.

There are significant additional opportunities that follow from the use of hydronic cooling systems and from the coupling of these systems with massive building components. However, results vary with climate; building design; cooling system components, configuration, and design; controls strategy and sophistication; and integration with ventilation and/or airside cooling. Furthermore, these parameters are all interdependent. As a result, the combination providing the best performance varies with changes in any one of the parameters.

Findings from actual buildings and research suggest energy savings with radiant cooling may be significant (Carpenter and Lay 2003; Roth, et al. 2002; Mumma, 2001a; Stetiu 1999), but it is often unclear to which specific strategies the savings are attributable. In addition to energy efficiency associated with hydronic *vs*. air systems as means of transporting heat (Feustel, H. 1994; FT Energy 2002), some existing designs utilize very low-energy sources of cooling water (McCarry 2003; Moore et al. 2006) and/or have capacity for off-peak operation to reduce peak demand and to improve chiller efficiency via nighttime chiller operation (Olesen 2000; McCarry 2006). Others have investigated the potential for low-energy nighttime precooling of thermal mass with a dry fluid cooler (Meierhans 1996).

Empirical evidence suggests thermal comfort may be improved for human subjects in either asymmetrical environments (Simmonds et al. 2000) or otherwise "neutral" environments (McNall and Biddison 1970; Kulpmann 1993). Potential for improved indoor air quality stems from avoiding recirculation, at least at the building systems level, through synergistic application of radiant cooling with dedicated 100% outside air systems (Mumma 2001; Moore et al. 2006).

With large cooling surfaces and significant thermal mass, hydronic radiant cooling in the form of exposed thermally active concrete slabs offers expanded opportunities for both the use of low-energy sources of cooling supply water and an aggressive nighttime precooling control strategy.

[1] This project and paper build upon the author's earlier work in surveying the existing literature and characterizing the range of available technologies and opportunities for radiant cooling and the potential design challenges that may accompany it (Moore, et al. 2006), as well as the methods for simulation of its performance potential (Moore 2007).

The latter is facilitated in part by the coupling of the cooling source to the *core* of the slab, rather than the room air or surfaces within the conditioned space. This permits more extensive precooling without overcooling in the early morning occupied hours. The extended precooling, in turn, allows for expanded dependence upon evaporative or similar low-energy cooling water sources that may be constrained during midday peak cooling hours but have greater cooling capacity in the context of lower nighttime wet-bulb temperatures.

Thermal mass, constrained cooling capacity, precooling, complex thermodynamics of hydronic radiant slabs, and integration with airside systems each present simulation and control challenges. When combined, and particularly in the context of very hot climates or poorly optimized buildings, the potential for challenges and complexity increases.

Most HVAC designers are unfamiliar with these systems and the challenges present. In addition, while there are several design and simulation tools that appear to readily and appropriately model lightweight metal chilled ceiling panels, this is not the case for thermally activate hydronic cooling slabs, particularly when attempting to evaluate thermal performance with precooling strategies and low-energy sources of cooling water. These obstacles may offer some explanation for the presently very limited use of such systems.

Some real-world examples do not face these challenges, either because the systems are implemented in highly optimized buildings with exceptionally low cooling loads or because they are located in mild climates. Others avoid or alleviate these challenges through greater dependence on parallel airside cooling capacity, use of more conventional cooling water sources that offer greater available capacity throughout the day, or otherwise less aggressive minimization of cooling system energy. Thus these challenges can be addressed in many ways, ideally beginning with a concerted effort to reduce cooling loads. However, if climate change demands the widespread development of net-zero-energy buildings, or something approaching this, and the industry intends to respond accordingly, there will be many buildings and climates for which the challenges described above may need to be addressed. The author has deliberately attempted to target rather than avoid or alleviate these challenges.

The need for effective simulation-based design of radiant cooling systems is being driven by at least three factors: 1) Widespread adoption of radiant systems in North America depends upon understanding the application of these systems in climates and buildings that differ considerably from their European counterparts (where radiant cooling has spread much faster); 2) There is growing interest in capturing and maximizing the benefits of radiant cooling; and 3) While simple in concept, radiant cooling tends to be implemented as part of hybrid mechanical systems requiring sophisticated control, within thermally complex environments, or with thermal coupling to the building fabric in ways that are uncommon for more conventional all-air systems.

While there do appear to be opportunities for simple and yet highly successful applications of radiant cooling in commercial buildings, effectively evaluating the suitability, design options, control strategies and performance potential requires simulation of complex system dynamics.

> *One of the most significant barriers to the specification of radiant systems in buildings is the inability to fairly compare radiant and conventional systems to each other or to combinations of the two. This is really the most pressing need of the radiant community today—to be able to simulate various system types and make energy and/or cost comparisons based on reliable simulation data.* (Strand, 2005)

2. PROBLEM STATEMENT AND INTENT

While many studies have described potential energy savings and comfort characteristics associated with hydronic radiant cooling, and some have compared this type of system with others, there appears to be considerable lack of clarity regarding how slab-integrated hydronic radiant cooling compares to a well-optimized modern all-air system. Furthermore, there appears to be a general lack of information as to how practitioners in the field might best make a fair and appropriately comprehensive comparison between such systems using tools and methods that are well suited to the simulation task and the practical context of a commercial building project. The intention of this report is to address these issues first by describing modeling methods using a simulation tool with a suitably practical interface and appropriately detailed capabilities. The simulation results can then illuminate characteristics of the compared systems and the nature of design parameters that can be with these methods.

3. METHODS AND ASSUMPTIONS

This study investigates performance potential, control strategies, and limitations for slab-integrated radiant cooling using an indirect-evaporative fluid cooler as the primary source of cooling supply water. The analysis focuses on cooling capacity and energy consumption, while maintaining thermal comfort criteria. An appropriately optimized all-air VAV system consistent with the current state of practice for mid-rise commercial buildings is provided as a point of reference for both thermal performance and energy consumption.

Modeling of radiant cooling using Integrated Environmental Solution's Virtual Environment allowed for simulation of radiant exchange between surfaces, direct coupling of thermal mass to the cooling supply water source, nighttime hydronic precooling of the slabs, and detailed integration of controls for hydronic and airside systems. The model also accounts for hydronic tubing size, material, and spacing; density and depth of concrete; convective heat transfer coefficients specific to the chilled surfaces; thermal stratification in the conditioned space; a dedicated outside air system with indirect evaporative cooling; and an evaporative fluid cooler as the primary source of cooling supply water.

This study considers only cooling-season operation (May through September). The four climates selected are Denver, Sacramento, Los Angeles, and San Francisco. These offer cooling-season environmental conditions ranging from hot and dry to cool maritime weather, as well as a variation in the degree of diurnal temperature swing. The selection of the three California climates is in keeping with the California PIER-funded project that supported this study. The Denver climate provides an opportunity to consider greater viability in diurnal and seasonal temperatures. Climate data files for simulation are typical meteorological year (TMY) data as provided by the U.S. Department of Energy. Monthly ground temperatures from the TMY climate statistics file are used to create profiles for the slab-on-grade thermal adjacencies.

While energy performance is reported for San Francisco and Los Angeles, the simulation work and evaluation of thermal performance focused on Denver and Sacramento. With peak dry-bulb temperatures reaching 40°C (104°F) and a coincident web-bulb temperature of 23.4°C (74°F), Sacramento is the hottest and most challenging of the climates with respect to maintaining thermal comfort. Both Sacramento and Denver offer significant seasonal and diurnal variations, which are an opportunity to compare how cooling systems handle transient loads and load diversity with respect to core *vs*. perimeter thermal zones. All of the climates used in the study are suitably dry climate for application of a hydronic cooling system using only an evaporative fluid cooler (closed-circuit cooling tower) as the sole source of cooling water.

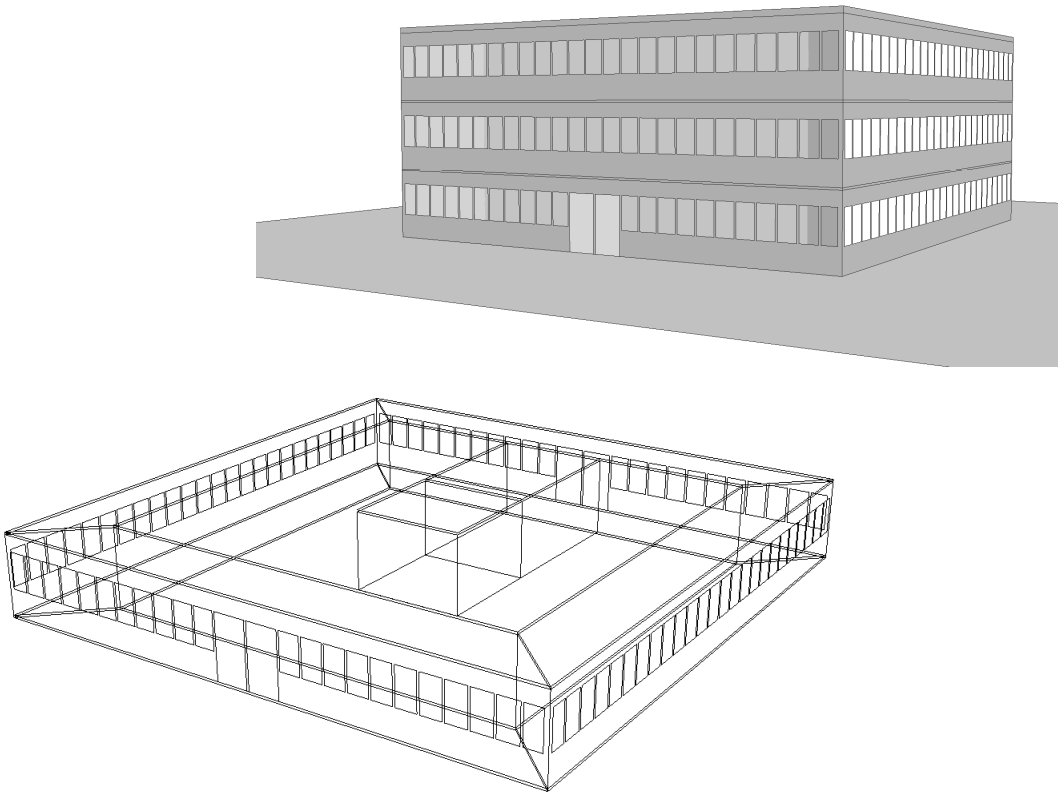

Figure 6: Exterior view (top) and floor layout (bottom) of office building as modeled.

Radiant cooling was modeled, evaluated, and compared to an all-air VAV system in the context of a simple 1,875-m^2 (20,000-sf) three-story office building with typical loads and very modest optimization of the building shell (Figure 6). The simple floor plan and three-story height are intended to represent the essential generic thermal elements for a range of similar buildings. These basic elements include bottom, middle, and top floors with interior plus perimeter zones for each orientation. However, airside configurations (but not sizing) for both the VAV system and DOAS are representative of what might be used in a mid-rise office building potentially several times larger than the three-story building modeled. Thus the simulation results should scale appropriately for consideration with respect to much larger buildings.

The minimal number of stories with identical floor plans kept the model reasonably simple, facilitating exploration of numerous configurations, control strategies, and set points for myriad control parameters. An approximation of overall performance for a taller version of the same building could be readily obtained by multiplying the results for the middle floor by some number of additional floors, at least for cases wherein all systems would scale accordingly.

The fair comparison of very different systems and the development of methods readily applicable to other projects suggested a notably generic with good insulation, tight construction, high-performance glazing, and a high-albedo roof. The building is otherwise relatively sub-optimal in some respects. For example, the square floor plate results in significant solar loads for the east and west facades, its depth does not lend itself to design for daylighting, there are no physical shading devices, and there are no daylighting or occupancy controls for electric lighting.

The total floor area of the building is 1,875 m^2 (20,175 ft^2). The 19 × 19-m (62 × 62-ft) interior zone is open-plan with the exception of a partitioned conference room and 5 × 5-m (16.4 × 16.4-ft) concrete services core with shear walls housing an elevator, stairwell, janitorial closet, and restrooms. As can be seen in Figure 6, the perimeter zones on the first three floors are partitioned off via uninsulated gypsum-board interior walls at a depth of 3 meters (10 ft) from the façade. This provides a means of studying the behavior of the HVAC systems with respect to variation in perimeter loads with orientation— ensuring the systems will have to contend simultaneously with zones that are core-load dominated and those dominated by skin loads that vary throughout the day. While an actual building would almost certainly not have diagonal interior walls at the corners where the perimeter zones meet, these support this analytical endeavor by providing perimeter zones with identical interior volumes, surfaces, and exposure for each façade orientation.

4. COMMON BUILDING ELEMENTS

The building construction, internal loads, schedules, ventilation requirements, and a zone-level exhaust fans common to both simulation runs are as follows:

- Floor decks: All floor decks, including the ground floor and roof deck, are constructed of 200-mm (8-in) cast high-density concrete slabs. While central to the hydronic-cooling scheme, the common application of this construction also affords the all-air system some benefit in terms of the exposed interior thermal mass that buffers midday cooling loads. All floors are covered with a synthetic carpet and pad.
- Foundation: The 200-mm (8-in) concrete slab-on-grade ground floor is insulated to a U-value of 0.44 W/m^2-K (R-13 h-ft^2-°F/Btu) using continuous 50-mm (2-in) polyisocyanurate foam. This provides the baseline with the same thermal mass and insulation benefits as are included for hydronic radiant heating and cooling. This construction then sits on a 50-mm (2-in) layer of gravel and 500-mm (~20-in) of soil, for which thermal properties are included in the model. Adjacent temperatures vary monthly according to TMY-2 ground temperature data.
- Concrete core: A core with shear walls housing stairwells, elevators, etc., is constructed of 150-mm (6-in) cast concrete interior walls, which are directly coupled to all floor slabs.
- Roof: The roof assembly—sitting on top of the reinforced concrete roof deck with embedded hydronic tubing—includes a highly reflective white TPO membrane (initial solar reflectance of 0.85, modeled as 0.30, assuming significant degradation from soiling) and continuous rigid EPS foam insulation. The roofing assembly U-value is 0.19 W/m^2-K (R-30 h-ft^2-°F/Btu).
- Walls: Exterior walls are a lightweight construction of steel-stud framing with gypsum board interior finish, fiberglass batt insulation between the studs, and continuous rigid foam insulating board behind sheet-steel exterior cladding. The U-value for the complete assembly is 0.26 W/m^2-K (R-Value of 22 hr-ft^2-°F/Btu).
- Glazing: The glazed area, including mullions, is 40% of the complete exterior floor-to-floor façade area for all orientations (very slightly more on the north and south ground-floor facades, which included glass doors). The glazing units, using PPG Caribia selective-tint SolarCool-coated semi-reflective exterior glass and SB-60 low-e coated clear interior glass, assembled in Lawrence Berkeley National Lab's Window5, have solar heat-gain coefficient (SHGC) of 0.14, visible transmittance of 21%, and center-of-glass U-value of 1.64 W/m^2-K (0.29 Btu/ hr-ft^2-°F). The window assembly U-factor, including thermally broken aluminum mullions, is 2.1 W/m^2-K (0.37 Btu/hr-ft^2-°F). No exterior shading devices are included and, given their limited benefits and potential for remaining open, no interior blinds are modeled.

- Infiltration and exfiltration: Infiltration is assumed to be 0.1 ACH for all perimeter zones, given relatively tight construction. This equates to 0.067 l/s-m^2 (0.013 cfm/ft^2) of exterior façade area. Exfiltration is driven via building pressurization by the fan-forced supply of outside air to the building, and is thus modeled within the HVAC network as a path from the rooms and return air to the outdoor environment. It is controlled to vary with the outside air volume at the supply fan. In the case of the VAV system, exfiltration varies for the entire building from a minimum of 117 l/s (248 cfm) at the minimum ventilation rate to a maximum of 390 l/s (826 cfm) at maximum fan airflow during 100% outside-air economizer operation. This equates to a range of 0.11 l/s-m^2 (0.02 cfm/ft^2) to 0.37 l/s-m^2 (0.07 cfm/ft^2) of exterior wall area at the minimum and maximum outside air volume, respectively. Maximum exfiltration occurs with maximum supply fan airflow with 100% outside-air economizer operation. For the DOAS, which always uses 100% outside air and has a maximum airflow just 32% of that of the VAV system, the maximum exfiltration is 125 l/s (265 cfm) or 0.35 l/s-m^2 (0.07 cfm/ft^2) of exterior wall area at the maximum supply fan airflow.

  The simulation tool employed has the capability to model infiltration and exfiltration as a function of weather file wind speed and direction and assigned crack areas and exposure factors for all constructions and fenestration. However, this requires somewhat longer simulation run times and was deemed unnecessary for the present study.

- Equipment: The equipment load density is 8 W/m^2 (0.75 W/ft^2). The equipment is assumed to have a radiant heat fraction of 20%, and otherwise contributes to space loads only through convective heat transfer. The schedule for this load is at least 50% 8:00–9:00 AM, ramping to 100% from 9:00 AM until 5:00 PM, then down to 50% again 5:00–6:00 PM. There is a minimum 10% plug load at all times, including nights, weekends, and holidays.

- Lighting: The electric lighting power density is 8 W/m^2 (0.75 W/ft^2), and is 45% radiant and 55% convective. The lighting schedule is identical to the equipment schedule.

- Occupants: Peak occupancy is 135 people (45 per floor). The net regularly occupied space per person is 14 m^2 (150 ft^2). At the gross whole-building level, this is 18.6 m^2 (200 ft^2) per person. The occupancy schedule is 50% minimum for all hours from 8:00 AM to 6:00 PM, ramping to 100% for the hours of 9:00–12:00 and again for hours of 2:00–5:00 PM.

  Occupant heat gains are 90 W (307 Btu/hr) per person sensible and 60 W (205 Btu/hr) per person latent. Sensible gain is split evenly between radiant and convective components; however, in reality, the convective would tend to dominate in an air-cooled environment, where surfaces are warmer, and the radiant component would tend to dominate with cooled surfaces. The specific outcome of this is a function of many parameters, including heat source characteristics, view factors to surrounding surfaces, furniture, clothing, and so forth.

- Cooling control limits for temperature and humidity are set to fall within ASHRAE Std. 55-2004 comfort limits, assuming still air and typical office activity levels and summer clothing as described in the section on HVAC systems below.

- Ventilation: Minimum outside-air ventilation at the zone level is 10.0 l/s (21.2 cfm) per person at peak occupancy and is 0.78 l/s-m^2 (0.15 cfm/ft^2) for the entire building.

- Exhaust fans: Because each is assumed to have similar characteristic efficiency, static pressure, and schedule, exhaust fans for rest rooms, copy rooms, janitor's closets, etc. totaling 250 l/s (530 cfm) are included in the HVAC airside network as a single constant-volume 60% efficient fan and path to the outside with total static pressure of 125 Pa (0.5 i.w.c.).

- Domestic hot water: Because HVAC energy is the focus of this study, and domestic hot water does not make a significant contribution to HVAC loads, domestic hot water is not modeled.

5. HVAC SYSTEMS

The intent of the systems as they have been configured and controlled for this study is to characterize the performance and potential of a low-energy variant of hydronic radiant cooling in the context of a relatively well-understood baseline. The baseline all-air system is therefore intended to represent a widely accepted and applied idea of best practice for mid-rise commercial office buildings—an attempt at fair representation of a common configuration for such buildings. The "plain vanilla" baseline system is thus meant to be both familiar and yet relatively well optimized in terms of equipment, features, and controls.

Room loads as simulated for both systems

Combined total maximum *internal* gains (applies to all occupied zones)	22.4 W/m^2	(2.1 W/ ft^2)
Combined perimeter peak *solar*, *conduction*, plus *infiltration* gains	64.6 W/m^2	(6.0 W/ ft^2)
Maximum perimeter-zone total gains	87.1 W/m^2	(8.1 W/ ft^2)

Comfort criteria

- Maximum of 10% Percent People Dissatisfied (PPD) both for the peak cooling condition during operating hours and for the ASHRAE 0.4% Cooling Design Day conditions
- Clo = 0.6 (Lightweight summer office clothing)
- Met = 1.0 (Standing or sedentary work)
- Air speed = 0.1 m/s (imperceptible)
- Maximum humidity ratio of 12 g/kg or 0.012 kg/kg (0.012 lb/lb).

Climate conditions for meeting design comfort criteria

Peak dry-bulb temperature (DBT) of 40°C (104°F) and a coincident web-bulb temperature of 23.4°C (74°F), which occur both on the hottest July day in the TMY-2 and in ASHRAE 0.4% Cooling Design Day conditions for the month of July (the hottest month), are the environmental conditions under which both systems are required to maintain PPD below 10%. These are also the conditions under which operative temperatures for the radiant + DOAS system is matched to that of the baseline VAV system to ensure adequate sensible cooling capacity.

Interior relative humidity and latent cooling capacity

ASHRAE Std 55-2004 limits the maximum humidity ratio for conditioned spaces to 12 g/kg (0.012 lb/lb). This is equivalent to 64% relative humidity (RH) at 75°F (24°C). Both systems meet this requirement. Suitable interior RH is also reflected in the achievement of PPD below 10% for occupied hours. The baseline system, by virtue of a lower cooling coil temperature, does tend to provide dryer air, resulting in relatively lower PPD values for some peak cooling hours. However, the radiant cooling tends to provide reduced mean radiant temperatures and thus also lower operative (dry resultant) temperatures during all but the most extreme transient cooling loads (for which the systems are closely matched with respect to operative temperature and PPD).

HVAC operating schedules

At minimum, the HVAC systems—fans plus cooling and heating as needed—are set to come on at 8:00 AM as occupants begin to arrive. Available fan airflow *capacity* ramps linearly between 8:00 and 9:00 AM from the minimum ventilation rate to 100% as occupants and equipment ramp up to 100% as well. An inverse ramp-down occurs between 5:00 and 6:00 PM. The actual airflow delivered between 8:00 AM and 6:00 PM is consistently constrained on the low end by the ventilation minimum and on the high end by actual zone demand for each six-minute simulation time step. The radiant slabs also have an additional waterside-only night precooling cycle.

6. VAV RE-HEAT WITH ECONOMIZER AND SUPPLY-AIR TEMPERATURE RESET

The "baseline" system for the comparison is an all-air variable-air-volume (VAV) system with fully integrated outside-air economizer, supply air temperature reset, and terminal re-heat. While the baseline all-air system could have included alternative features, such as indirect and/or direct evaporative cooling, the intent for this study was to provide a well-understood point of reference.

A water-cooled chiller with relatively high performance—approximately 0.6 kW/ton or less from 40 to 80% of maximum cooling load—based on Air-Conditioning and Refrigeration Institute data for chillers with a screw type compressor (ARI 2007) is modeled with load-dependant COPs. The combined COPs for the chiller plus chilled-water pump, condenser-water pump, and cooling tower at 20, 40, 60, 80, and 100% load and ARI standard operating conditions are 3.6, 4.1, 4.5, 4.2, and 3.8 (Table 1). Cooling capacity—at 15% oversize—is 70 kW (20-ton) for Denver.

The Denver climate was used for optimization of

Table 1: Sizing (for Denver climate simulation runs) and coefficient of performance for water-cooled chiller with chilled-water pump, condenser-water pump, and cooling tower.

Coeficient of Performance (COP) for chiller, chilled water pump, condenser pump, and cooling tower							
Required cooling capacity per simulation			Chiller	Pumps	Tower	Combined	Combined
17.3	Load	Load	EER	EER	EER	EER	COP
Oversizing factor	fraction	kW	kW/ton	kW/ton	kW/ton	kW/ton	kW/kW
1.15	1.0	70	0.71	0.10	0.12	0.93	3.8
Maximum cooling capacity	0.8	56	0.63	0.10	0.12	0.85	4.1
20 Tons	0.6	42	0.56	0.10	0.12	0.78	4.5
Maximum cooling capacity	0.4	28	0.61	0.10	0.12	0.83	4.2
70 kW	0.2	14	0.76	0.10	0.12	0.98	3.6

Table 2: Cooling tower design specifications, sizing (for Denver climate simulation runs), and performance for chiller heat rejection plus three operating points during waterside economizer operation.

Cooling tower for chiller condenser-water heat rejection											
Closed-Circuit BAC VF1 Cooling Tower									Waterside eoconomizer operation		
Capacity	Fan	Pump	Flow	Entering	Leaving	Outdoor	EER	COP	Pumps	Combined	
kW	kW	kW	rate l/s	water °C	water °C	WBT °C	kW/ton	kW/kW	EER	EER	COP
75	2.24	0.373	2.0	39	30.0	25	0.12	28.7	kW/ton	kW/ton	kW/kW
53	2.24	0.373	10.0	22	20.7	16	0.17	20.3	0.2	0.3	10.9
42	2.24	0.373	3.0	22	19.1	16	0.22	16.1	0.1	0.3	11.0
33	2.24	0.373	2.0	22	18.0	15	0.28	12.6	0.10	0.38	9.3

The waterside economizer or waterside "free cooling" (WSFC) for the second VAV scenario is based upon an available cooling tower somewhat larger than needed just to reject heat from the fully loaded chiller. Table 2 shows performance at four operating points—one when rejecting heat from the chiller's condenser-water loop, and the other three during WSFC. These values are for an actual available cooling tower selected to meet the heat-rejection needs of the chiller in the Denver climate. Supply water temperature in WSFC mode is constrained by the 3 K (5.4°F) approach. Thus, while the tower has cooling capacity when, for example, outdoor wet-bulb temperatures reach 20°C (68°F) and entering water returning from the cooling coils is just a few degrees warmer, the room cooling supply-air temperature, as reset to meet demand from the warmest zone, may require colder water than the tower can provide. WSFC therefore runs only when it can meet the cooling coil load, and, when it can't, hands off to the water-cooled chiller.

Added WSFC capacity could be obtained using a significantly larger cooling tower. Simulations indicate that additional savings might be obtained by using two cooling towers in an uncommon configuration: one sized for the chiller at average load and the second directly coupled to a precooling coil immediately upstream of the chiller-served coil and capable of switching over to

rejecting added heat from the chiller only when the first tower was inadequate for this purpose. However, for this study, the intent of the VAV scenario with WSFC is to provide an estimate of energy savings related to simply allowing the cooling tower, as sized for rejecting heat from the chiller, to function as the source of cooling water when it can meet the cooling coil load.

The required inputs for the WSFC system are for a single design point, as presented in Table 2 above. The waterside economizer model within the Virtual Environment ApacheHVAC systems simulation module (Figure 7) then determines the cooling tower capacity at any given outdoor wet-bulb temperature and cycles the tower fan between high-speed, low-speed, and off modes as required to meet the cooling coil load with a time-averaged leaving water temperature.

T_1 = cooling tower entering water temperature
T_2 = cooling tower leaving water temperature ($T_2 < T_1$)
L = cooling tower water mass flow rate (assumed constant during tower operation)
G = cooling tower air mass flow rate (varies under fan control)
G_{des} = cooling tower design air mass flow rate
C_{Tdes} = modified cooling tower characteristic at design condition
t_1 = outside air dry bulb temperature
t_{owb} = outside air wet bulb temperature
t_2 = tower exhaust air dry bulb temperature
h_1 = outside air enthalpy
h_2 = tower exhaust air enthalpy (air is assumed saturated)
R = $T_1 - T_2$ = cooling tower range
A = $T_2 - T_{owb}$ = cooling tower approach
ε = heat exchanger effectiveness
T_{1coil} = cooling coil entering water temperature
T_{2coil} = cooling coil leaving water temperature ($T_{2coil} > T_{1coil}$)
T_{coil} = cooling coil metal temperature = $(T_{1coil} + T_{2coil})/2$
m_{coil} = cooling coil water mass flow rate (assumed constant during coil operation)
t_{edb} = cooling coil entering dry bulb temperature
t_{ldb} = cooling coil leaving dry bulb temperature
g_e = cooling coil entering moisture content
g_l = cooling coil leaving moisture content

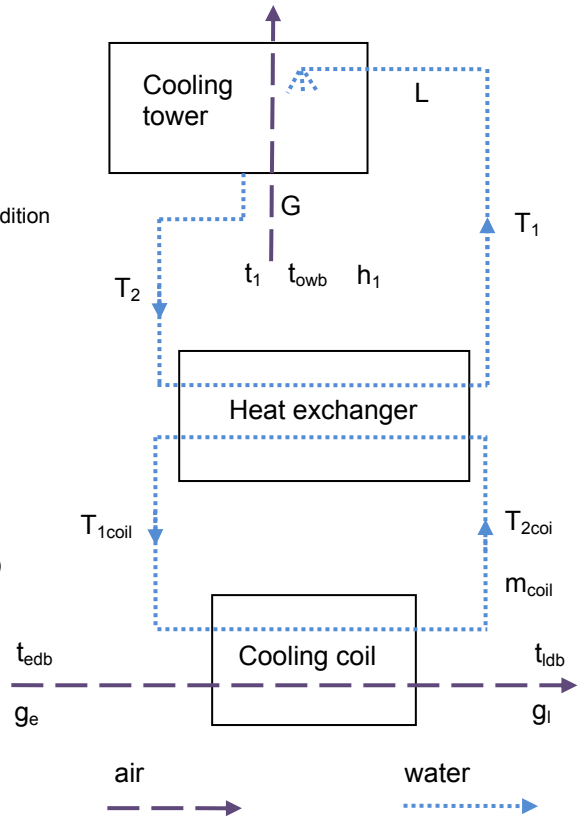

Figure 7: Waterside economizer configuration as implemented in IES Virtual Environment (Gough 2007).

Hot water heating at the air handler and terminal re-heat are provided by a high-efficiency condensing boiler that continuously modulates its output, efficiently meeting the current load by maintaining a set return water temperature. At a return water temperature of 54.5°C (130°F), boiler efficiencies for 25, 45, 65, 80, and 100% load are 93, 92.5, 92, 91.5, and 91%, respectively. The boiler is sized to 25% over maximum simulated heating load. For Denver, boiler capacity is 49 kW (165,000 MBH). The unit is resized accordingly for the other three climates.

Supply airflow is sized 1.15 times that required to maintain 24°C (75°F) in all occupied spaces with 11.11 K (20°F) supply-air delta-T at the 0.4% ASHRAE Cooling Design Day conditions. Maximum supply fan airflows are 4,990 l/s (10,570 cfm); 6,090 l/s (12,900 cfm); 5,680 l/s (12,030 cfm); and 5,510 l/s (11,670 cfm) for the Denver, Sacramento, Los Angeles, and San Francisco climates, respectively. Because the loads differ among spaces based upon interior vs.

perimeter location, façade orientation, and bottom, middle, or top floor, airflows are sized for each zone. Table 3 shows the zone-level airflow sizing for the Sacramento, the climate with the highest solar loads, to illustrate the resulting differences in airflow among zones with various façade orientations and relationships to the ground, adjacent floors, and roof. While these differences are minimized by the reasonably well insulated building shell, high-performance glazing, and reflective roof membrane, they are still sufficient to influence system design. They are most pronounced with respect to transient solar loads for the east and west facades.

The minimum supply airflow, for all VAV cases, independent of the outdoor air ventilation rate (and consistently somewhat larger than this value), is 30% of the maximum for each zone. Total static pressure at the supply fan is 350 Pa (1.4 i.w.c.), assuming ducts, filters, and coils with relatively large cross-sectional area, plus carefully selected and commissioned terminal units, to reduce required velocities and minimize resistance to airflow. Return fan airflow is reduced by exfiltration and by exhaust fan airflow, which must have a separate exhaust air path to avoid being combined with recirculated return air. Return fan airflow is thus equal to the supply fan airflow less the exhaust and exfiltration flows for any given time step. Total static pressure at the return fan is 250 Pa (1.0 i.w.c.). Supply and return fans are modeled with performance curves for high-efficiency backward-curved centrifugal fans (peak fan mechanical efficiency of 80%) with static-pressure reset and premium efficiency motors with variable-speed drives (combined overall fan and motor peak efficiency of 75%).

Table 3: VAV design airflow for Sacramento, CA at 11.11 K (20°F) supply air delta-T.

Design airflow at 11.11 K (20°F) supply-air delta-T			
Conditioned zone	**1st floor**	**2nd floor**	**3rd floor**
N Perim Occ Zn	270	260	270
E Perim Occ Zn	330	320	330
S Perim Occ Zn	380	370	370
W Perim Occ Zn	410	400	410
Interior Occ Zn	580	560	610
Interior Svs Zn	80	60	70
Totals	**2,050**	**1,970**	**2,060**
Total for all three floors			**6,080**

The outside air economizer has a minimum flow equal to the required minimum ventilation, maximum flow equal to the supply fan capacity, and is controlled to deliver a mixed-air temperature that varies inversely in proportion to the return-air temperature. The control uses a sensed-variable midband of 23°C (73.4°F) and 4-K (7.2°F) bandwidth. The target mixed-air temperature at the minimum signal, corresponding to a return-air temperature of 21°C (~70°F), is 24°C (75°F). This is effectively the economizer "high limit." The target mixed-air temperature at the maximum signal, corresponding to a return-air temperature of 25°C (77°F), is 12°C (53.6°F). This control strategy provides mixed-air temperature reset that takes full advantage of airside free cooling, while minimizing mechanical cooling of outside air.

Supply-air temperature reset (*i.e.,* leaving air temperature reset at the cooling coil) with a maximum equal to the room-air cooling midband eliminates unnecessary reheat and permits this system to take full advantage of economizer hours. It also maximizes the chiller part-load COP by reducing the delta between the chilled water loop and outside air temperatures during off-peak cooling hours, which is modeled in this study via improved chiller part-load efficiencies.

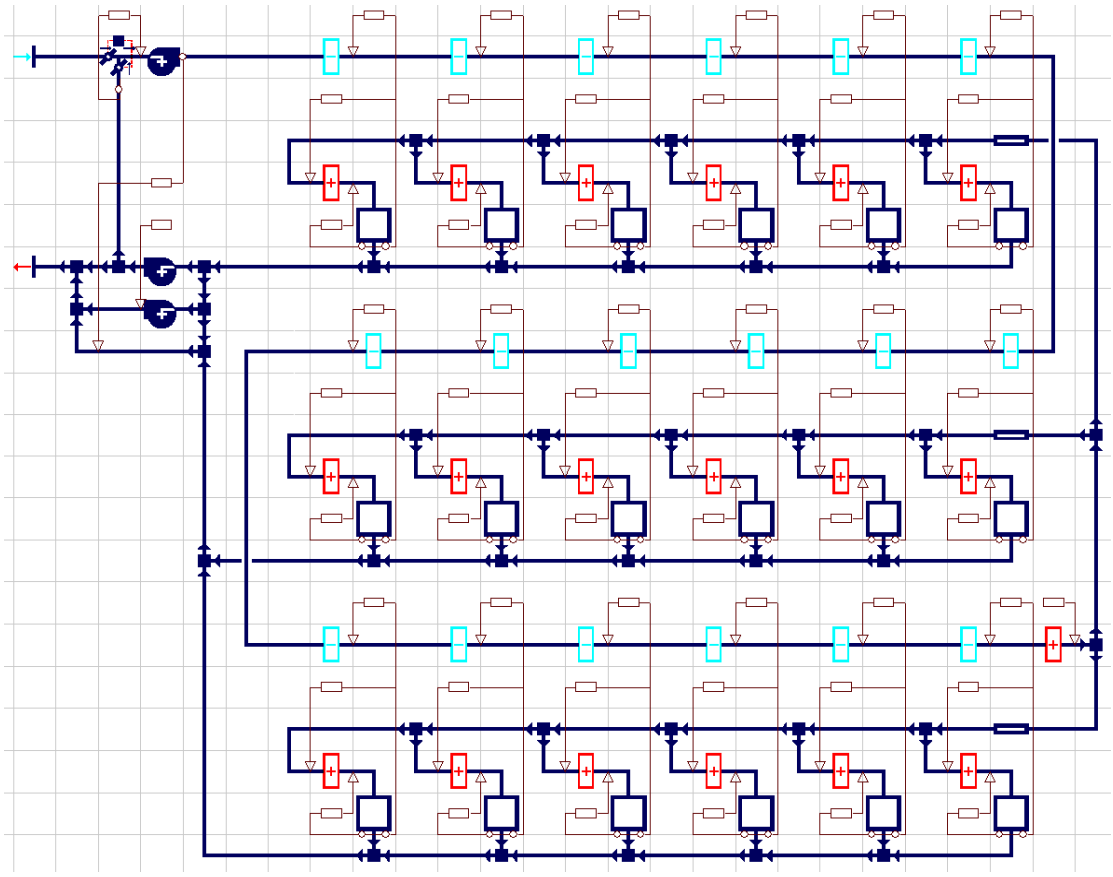

Figure 8: Baseline VAV system airside network in Virtual Environment's Apache HVAC tool.

Cooling supply air temperature reset is modeled and controlled as shown in Figures 8 and 9. A single cooling coil at the air handler is modeled as a contiguous series of coil components on along a common supply air path. Each coil component is associated with a separate zone sensor and controller that can request colder supply air as needed to meet the loads of that zone once airflow has been adjusted up to the maximum permitted by the zone VAV box. Individual zones thus rely first on airflow control and then supply air reset, as is further described below. The composite LAT for the series is thus forced to equal that required by the zone demanding the lowest cooling air temperature at any given time step. Successful supply air temperature reset to maximize economizer hours and operational efficiency of the chiller also requires airflow to interior zones to be sized to permit use of the maximum cooling reset temperature.

Each coil component in this model can be thought of as similar to a row of tubes with fins in a typical multi-row coil. However, this model places all components in parallel with respect to the chilled water loop. Thus it does not capture variations in cooling effect resulting from the degradation of supply water temperature, and thus reduced temperature difference in relation to the air, as would occur for water passing through consecutive rows in an actual cooling coil. In this respect, the model represents a more or less perfect counter-flow coil, whereas real counter-flow coils tend to have a mix of counter-flow and cross-flow characteristics. The result is a small degree of elevation of the coil effectiveness for the ail-air VAV systems in this study. Additionally, while contact factor is modeled for each cooling coil in the network, providing a given amount of cooling via multiple coils in series (each with the same contact factor and the load divided evenly among them) requires approximately 2% less energy than with a single coil.

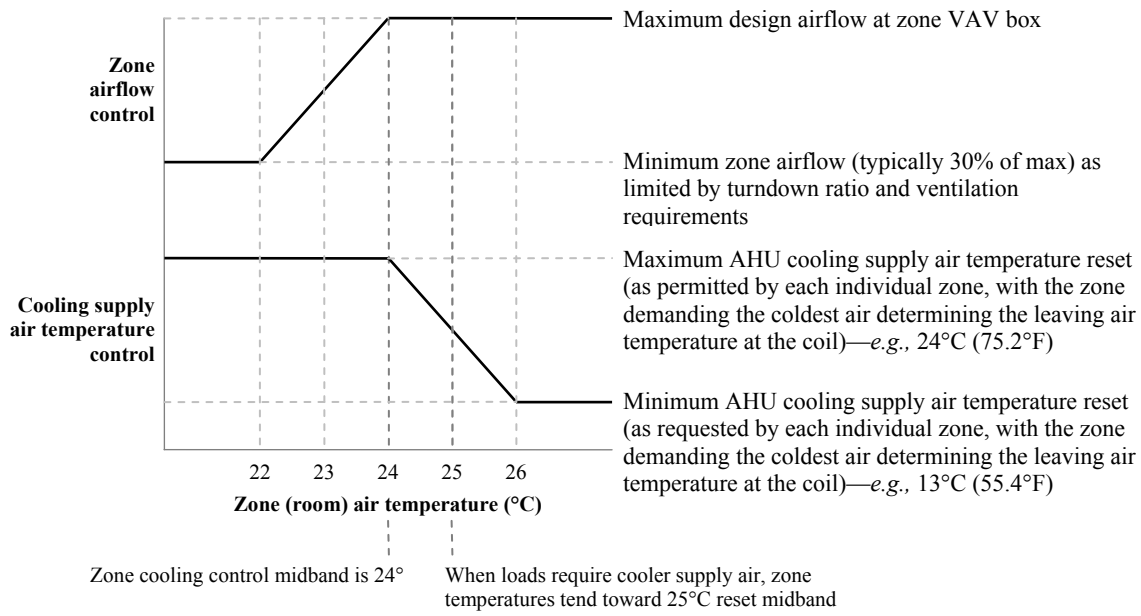

Figure 9: Control sequence for zone airflow and AHU cooling coil supply air temperature reset.

The airflow-first controls sequence used (Figure 9) is a common cooling reset strategy. Swapping the midband temperatures for airflow and cooling controllers—a cooling-reset-first sequence—resulted in 6% higher energy consumption, and thus was not used.

After confirming proper interaction of the zone airflow and cooling coil reset controls, a dehumidification coil with its LAT proportionally controlled to an AHU leaving mid-band DPT of 10°C (50°F) and bandwidth of 5°K was added to the end of the cooling coil reset "string" (just prior to the air-handler heating coil at the far right in Figure 8). Proportional controls were set up such that dehumidification coil operation depressed the zone cooling midband by not more than 1°C (to the airflow control midband). However, having established that this method was sucessful for controlling coil temperature in the VAV system, if indeed dehumidification were deemed necessary, the dehumidication coils and controls were subsequent removed for the resons described below.

Denver and the three California climates modeled are quite dry. Therefore dehumidification does not contribute significantly to determining the cooling coil LAT for the control parameters used. Even with the dehumidification equipment and controls in place, the dry climates permits warmer supply air temperatures based primarily upon sensible cooling loads, extending the number of hours the airside economizer operates. As described in the Results and Discussion section below, the compared systems were able to meet ASHRAE thermal comfort criteria without any dehumidification.

Because the climates in this study are relatively dry, and because dehumidification for the DOAS would involve a desiccant wheel that presently requires an additional workaround for this particular simulation tool, the humidity sensor and its control signal were removed from the supply air temperature reset. The intent of this was to avoid causing the VAV system to control humidity to an extent not yet provided by the DOAS model. For the VAV system, this permits

supply air temperatures based upon sensible cooling demand only, further extending the number of hours the airside economizer operates.

Supply air ductwork passes through the interior zone, as there are no return plenums, and is insulated to a U-value of 1.3 W/m^2-K (R-value of 4.4 h-ft^2-°F/Btu) using continuous 25-mm (1-in) rigid polymer-coated fiberglass duct-liner board. The total surface area of the supply ducts subject to heat gain is 80 m^2 (~861 ft^2) per floor, or 240 m^2 (~2,582 ft^2) for the complete building.

Loops around the return fan and connection to the economizer damper, as shown in Figure 2 are a means of modeling zone-level exhaust fans and exfiltration, appropriately reducing return air and requiring make-up air. Given comparable fan/motor type, performance, and operating schedules, the exhaust fans for restrooms, copy rooms, etc., are lumped together as one fan and airflow. With building pressurization as the primary driver for exfiltration, this path (which has no fan) is proportionally controlled according to the supply fan airflow. Maximum exfiltration is based on the tightness of the construction, number of operable fenestration elements, and design building pressurization.

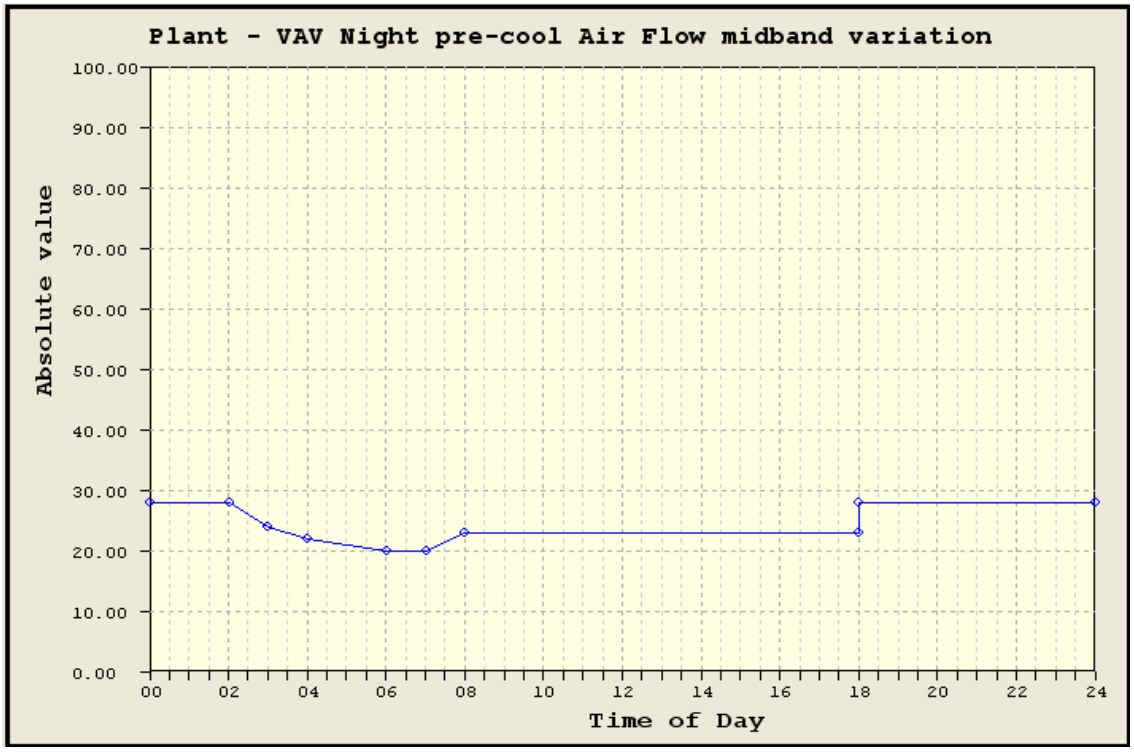

Figure 10: Profile or schedule used to vary the temperature midband in the zone airflow controller.

Figure 10 shows a schedule profile used to alter the room temperature midband setpoint in the VAV box airflow controller during the nighttime precooling cycle. This profile is set up to gradually lower the space temperature during the night in keeping with dropping overnight outdoor air temperatures and without requiring excessive airflow. The room is cooled just to the heating set point and then allowed to float back up slightly just prior to the beginning of occupied hours. This stabilizes the slab temperatures just above the heating setpoint prior to occupancy, maximizing the duration of daytime cooling provided by the thermal mass without triggering counter-productive heating in the morning occupied hours. Profiles are also used to vary the VAV supply-air-temperature reset control mid-bands as well as a range of similar parameters for the Radiant+DOAS alternative.

7. HYDRONIC RADIANT COOLING WITH EVAPORATIVE COOLING WATER SOURCE AND DEDICATED OUTSIDE AIR VENTILATION SYSTEM

The overhead hydronic radiant cooling slab is the primary means by which this system addresses sensible loads in the space. This is augmented by a dedicated outside air system (DOAS) for conditioning of ventilation air. The hydronic cooling and DOAS utilize only indirect evaporative cooling sources—*i.e.*, there is no chiller. The supply water source for the hydronic slabs and DOAS cooling coils is a closed-circuit cooling tower. The DOAS also uses indirect-evaporative cooling of the outside air supply.

A conceptual illustration (top of Figure 11) emphasizes direct coupling of radiant slabs to the closed-circuit cooling tower without the use of a chiller. The Virtual Environment ApacheHVAC airside network in Figure 11 shows the DOAS configuration with indirect evaporative cooling and sensible heat recovery. This network diagram also includes the hydronic slab zones (the five vertical stacks of four room components) on a side loop with zero airflow simply to facilitate faster editing and copying of the hydronic controllers contained within them (these zones would otherwise appear on a list of rooms without air supply).

The hydronic radiant cooling slabs are modeled as fully geometric building components—*i.e.,* with thermal mass, direct absorption of incident solar gain, direct radiant exchange between surfaces, and appropriate convective heat transfer coefficients for the surface-to-air delta-T. Simulated peak radiant slab cooling capacity was 62.5 W/m^2 (5.8 W/ft^2), as augmented by 12.0 W/m^2 (1.1 W/ft^2) coincident cooling from the DOAS, for a total of 74.6 Wm^2 (6.9 W/ft^2).

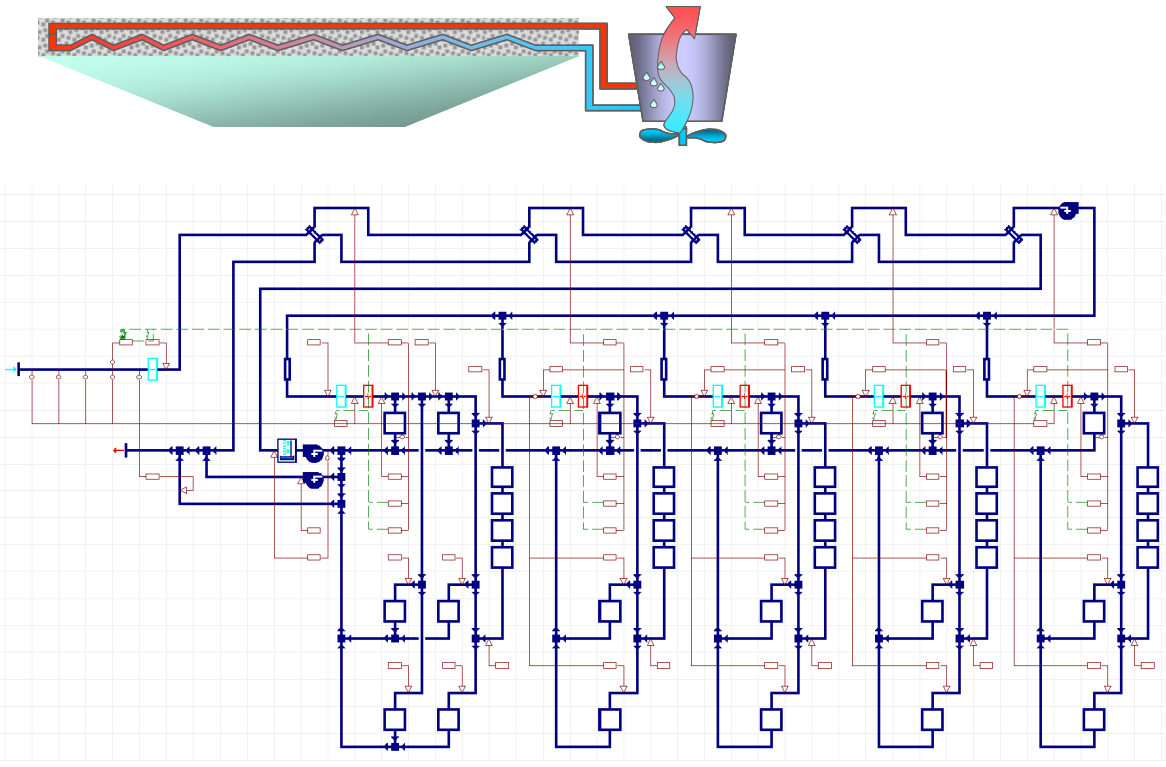

Figure 11: Conceptual illustration of the directly coupled cooling tower and hydronic radiant cooling water loop (top) and schematic airside and controls network (bottom) for the DOAS.

Cooling of ventilation air to augment sensible space conditioning by the hydronic radiant system is provided by indirect evaporative cooling plus a cooling coil using water from the cooling tower. For indirect-evaporative cooling, the exhaust air stream is humidified to near saturation, and thus cooled, prior to passing through a counter-flow heat exchanger. Because 100% of the return air will be exhausted, it is a useful resource as a relatively cool (room temperature) airstream. The ultrasonic humidifier assumed has a saturation effectiveness of 95% and is modeled, given constraints within the simulation tool, with 50 W continuous power consumption as a proxy for the actual consumption of 5 W per kg/h of moisture addition. The counter-flow heat exchanger doubles as an integrated energy recovery device. Based on a face area of 1.5 m^2 (16 ft^2) for an appropriately sized available indirect-evaporative system with counter-flow heat exchanger and mean airflow of 1,650 l/s (3,500 cfm), thus a mean face velocity of 1.1 m/s (217 ft/min), the pressure drop for the heat exchanger is just 50 Pa (0.2 i.w.c.).

Supply airflow with 100% outside air is variable from the design minimum outside-air volume of 1,350 l/s (2,860 cfm) up to 1,950 l/s (4,130 cfm). At the low end, this is 66% of the minimum SA fan airflow for the baseline VAV system and equates to 10 l/s (21.2 cfm) per person and 0.78 l/s-m^2 (0.15 cfm/ft^2). Given the lack of any recirculation, ensuring that all zones will receive at least the design minimum OA is accomplished with minimum supply airflow equal to the sum of zone minimum ventilation requirements. For this configuration, described below, the interior zones are constant-volume at the minimum OA ventilation rate and perimeter zones are variable from the minimum OA ventilation rate to two times that amount. This provides means of "tuning" perimeter space temperatures in response to transient solar loads that may change too quickly for the slow reaction time of the thermally massive chilled slabs. The range of 1.0–2.0 times the minimum ventilation rate was selected based upon six consecutive "trim-and-respond" adjustment runs, beginning with just the minimum ventilation rate, and working upward in 20% increments until the airside system appeared to have just enough capacity, given the evaporative cooling sources, to counter the transient loads not dealt with by the radiant slabs. At the high end, total airflow is 32% of the maximum for the VAV system as sized for Sacramento. This airflow sizing remained constant for all subsequent iterations of the Radiant+DOAS system.

The DOAS configuration is zoned vertically comprising one constant-volume (CV) zone for all interior spaces (on all three floors) and one single VAV zone for the perimeter spaces on each façade orientation. In other words, there are just five airside zones for the entire building. Vertical zoning of the DOAS per space type and façade orientation, including coils, ducts, and controls, is made feasible by the parallel zone-level control, tempering, and buffering of sensible space conditioning by the hydronic radiant slabs. While the airside system is used to adjust space temperatures as solar gain shifts from one façade to the next, the exposed overhead and carpeted floor chilled slabs provide both a buffer to absorb some of the transient solar gain and a means of varying the cooling capacity per floor.

In a real commercial office building with a DOAS such as this, there would almost certainly also be a demand-controlled motorized damper with CO_2 sensor for a conference room sub-zone on each floor. To accommodate this, the supply fan at the AHU would simply modulate to account for the added demand in the sub-zone, while maintaining the CV supply to the remainder of the interior zones. However, since this is a relatively small space and would add the same additional OA requirement to both the baseline and Radiant+DOAS systems, this was not modeled.

More importantly, the approach of grouping zones vertically by façade orientation reduces the number of VAV damper sets to just four and places these at the air handler. Thus there are five supply air ducts, rather than one or two, which does somewhat increase the friction losses for the same cross-sectional area for just the vertical sections from the air handler to each floor.

However, given 65% smaller maximum airflow than the baseline system and leasable floor area within the building as a primary constraint on the number and size of vertical ducts chases, dedicating the same amount of floor area to vertical air distribution would permit a reduction in pressure drop for this portion of the ductwork.

Total static pressure for the DOAS is somewhat lower relative to the baseline VAV system. This is a function of significantly reduced airflow, minimally zoned airside configuration, and relatively lower total duct resistance. The configuration with ducting dedicated to just one interior airside zone and four perimeter zones for all three floors combined eliminates the VAV boxes and permits a reduction in the number of heating coils; where the VAV system has a heating coil at the air handler plus one coil and VAV damper set per zone (19 heating coils and 18 VAV boxes), the DOAS has just five heating coils, four motorized damper sets at the air handler, and no standard VAV boxes. Using the same allotment of space for vertical air distribution in the building, the larger cross-sectional duct area per unit airflow for the main distribution ducts through the core of the building provides lower static pressure for this segment of the distribution system. Similarly, reduced airflow volume over a similar coil area at the air handler reduces the coil face velocity, providing a relatively lower pressure drop across the coils. These measures, along with the absence of VAV boxes and reduction in the number of heating coils, more than offsets the small additional pressure drop associated with the counter-flow indirect-evaporative heat exchanger described above.

The resulting total static pressure is 250 Pa (1.0 i.w.c.) at both the supply fan and the return fan. Both are modeled with performance curves for backward-curved centrifugal fans (peak fan mechanical efficiency of 80%) and NEMA premium efficiency motors with variable-speed drives (combined fan plus motor peak efficiency of 75%).

Supply air ductwork to the perimeter zones passes through the interior zone, as there are no return plenums, and is insulated to a U-value of 1.3 W/m^2-K (R-value of 4.4 h-ft^2-°F/Btu) using continuous 25-mm (1-in) rigid polymer-coated fiberglass duct-liner board. The total surface area of the supply ducts subject to heat gain is 80 m^2 (~861 ft^2) per floor, or 240 m^2 (~2,582 ft^2) for the complete building.

Exfiltration is driven by building pressurization, and varies from 77 l/s (164 cfm) to 125 l/s (265 cfm) with SA fan airflow, since all SA airflow is OA. At its maximum, this is two-fifths of the maximum exfiltration for the baseline all-air system.

Chilled building components and surfaces

Chilled slabs are modeled as separate thermal zones (Figure 12). Hydronic tubing is equidistant—at 100 mm (4 in)—from top and bottom surfaces. With the exception of the slab-on-grade ground floor (insulated as described previously under Common Building Elements), both slab surfaces are thermally active. Ceiling surfaces are exposed and floor surfaces are carpeted.

The internal volume of the slab zone was minimized to 0.1 liter per m^2 floor area (0.57 in^3/ft^2), or an internal height of just 0.1 mm (0.004 in). This essentially elliminates the air volume without having a volume of zero. The Chilled Ceiling component provided within Virtual Environment was then located within the minimized volume of the chilled slab thermal zone. This component amounts to a controllable hydronic loop with thermal capacity, flow, mass, and pump power. The determination of pump power is descibed below. The thermal capacity of this hydronic cooling component was then set to be 100% convective to force its interaction with the slab materials to be similar to that of the water inside of the hydronic cooling loop without the tubing material (which is accounted for in the finite-element modeling of slab conductivity, as described below).

The slabs are cost concrete at 2100 kg/m^3 (131 lb/ft^3) with a specific heat capacity of 840 J/kg-K (0.2 Btu/lb-°F). The conductivity of the concrete was adjusted from 1.40 W/m-K down to 0.55 and 0.84 W/m-K for the interior and perimeter zone slabs, respectively, to account for the size, material, and spacing of the hydronic tubing (Table 4). The difference between the interior and perimeter slabs is a function of the tube diameter. This adjustment was made using THERM—a simple two-dimensional finite element heat transfer model from Lawrence Berkeley National Laboratory (Figures 13a–13d). Air-film resistance and emissivity for the inside surfaces of the slab zones were set to values approaching zero and 1.0, respectively. Because actual zero values are not permitted, a value approaching zero was used to represent these surfaces as if they were in direct contact with the cooling water.

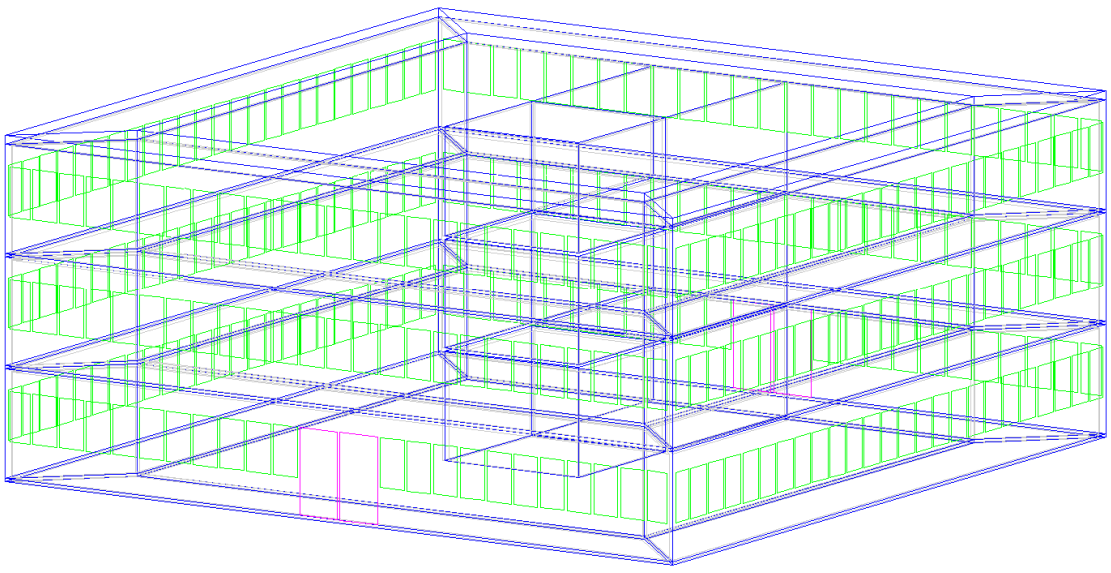

Figure 12: Hydronic radiant slabs (represented as blue lines in the axonometric view above) are modeled as separate thermal zones, with one above and one below each perimeter and interior occupied zone.

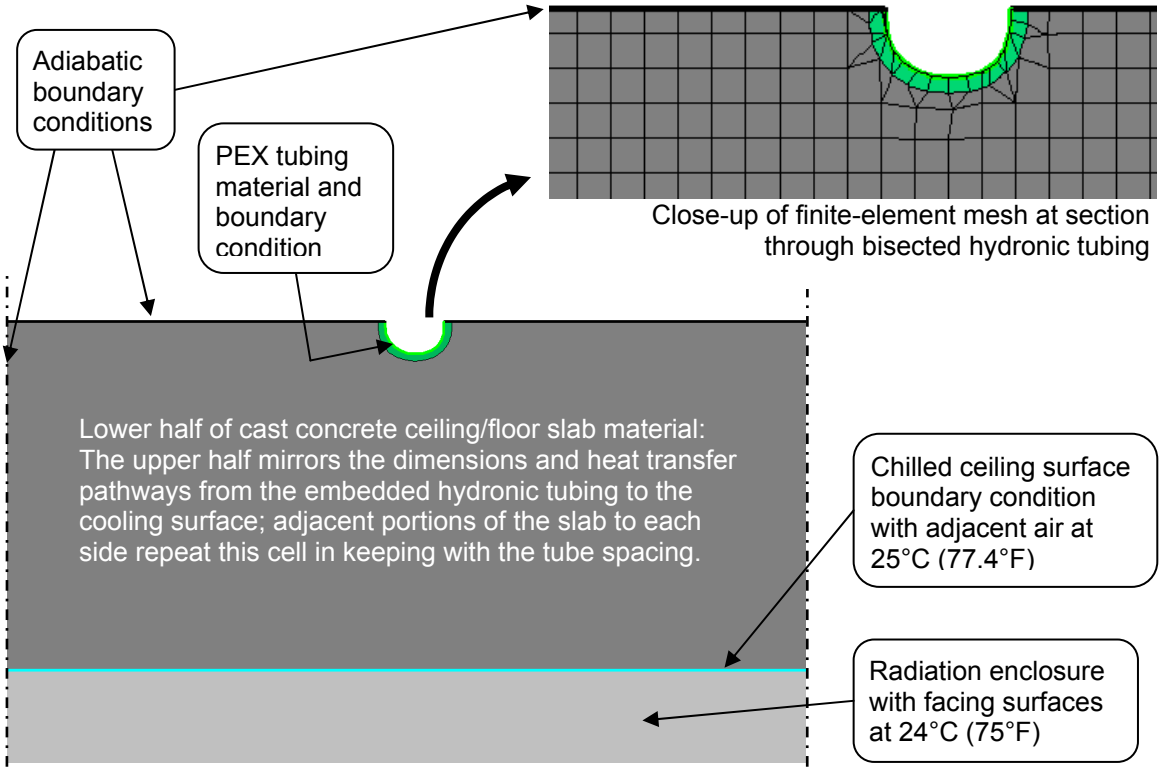

Figure 13a: A cross-section of the concrete slab with embedded hydronic tubing is described in THERM as a repeatable segment bounded by the chilled surface (bottom), center of the tubing (top), and midpoint between tubes (either side). Boundaries other than the tube interior and chilled surface are adiabatic.

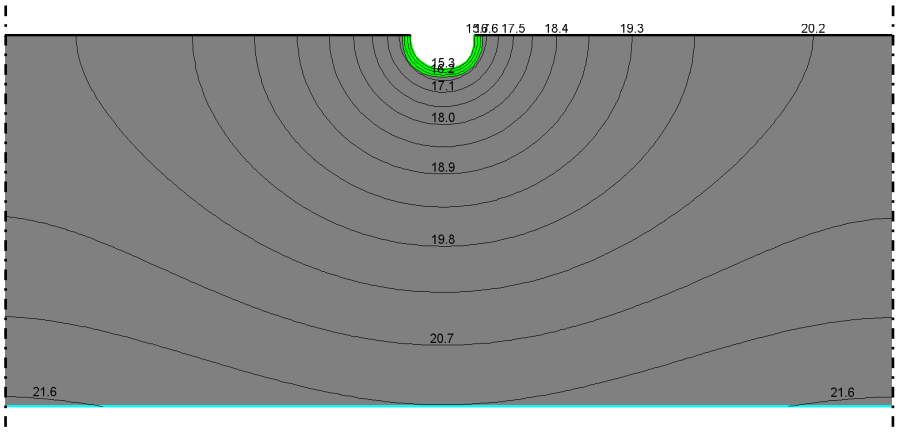

Figure 13b: Isothermal contours indicate the distribution of temperatures resulting from the finite-element model of two-dimensional heat transfer between boundary conditions.

Figure 13c: Isothermal contours as graduated colored/grayscale fills provide a visualization of continuous temperature gradients throughout a cross-section of the chilled slab material.

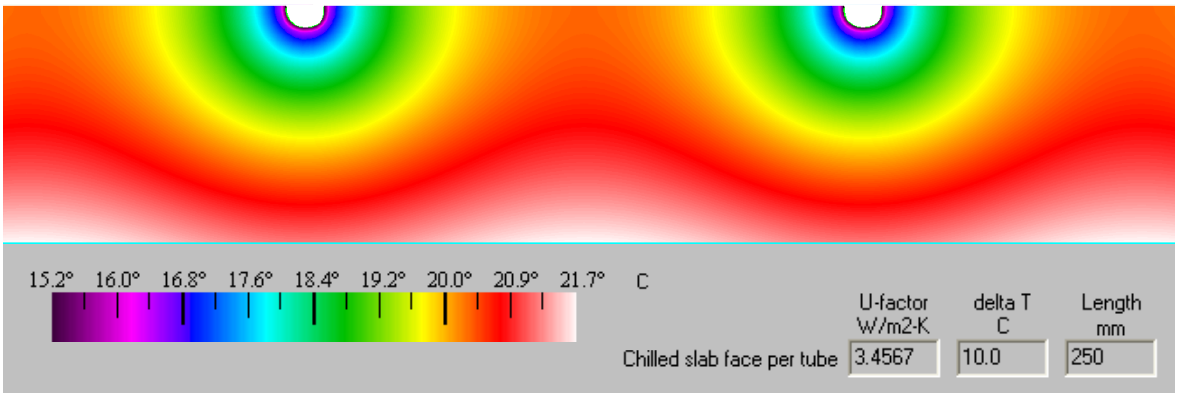

Figure 13d: Colorized/shaded isothermal contours and effective U-values for a chilled slab section bisecting the hydronic tubing at 250-mm spacing in the concrete slab as modeled in THERM.

Table 4: Calculated adjustment of concrete slab material conductivity for 250-mm and 150-mm tube spacing as used in the perimeter chilled slab zones for Denver and Sacramento, respectively.

Adjusted conductivity for 250-mm tube spacing using THERM 2-D heat transfer model

17.3	Hydronic tubing inside diameter, mm
2.5	Hydronic tubing wall thickness, mm
0.25	Hydronic tubing spacing in the slab, m
0.45	Hydronic tubing conductivity (PEX-AL-PEX composite tubing), W/m-k
1.40	Slab conductivity, W/m-K
3.4567	Thermal transmittance or U-value of slab and tubes at 10 K delta-T, W/m^2-K
0.2893	Overall resistance, including water film, tubing, and air film at exposed surface, m^2-K/W
0.1067	Air film resistance on exposed cooling surface, m^2-K/W
0.0007	Water-film resistance at tubing inside surface (forced convection, 0.67 m/s flow), m^2-K/W
0.1818	Resistance for slab plus PEX tubing without air or water films, m^2-K/W
5.499	Conductance for slab plus PEX tubing without air or water films, W/m^2-K
0.100	Slab thickness at perpendicular heat transfer path (center of tubes to cooling surface), m
0.550	Adjusted conductivity for chilled slab material in VE model, W/m-K
60%	Faction of adjusted conductivity value obtained using simple spreadsheet model

Adjusted conductivity for 150-mm tube spacing using THERM 2-D heat transfer model

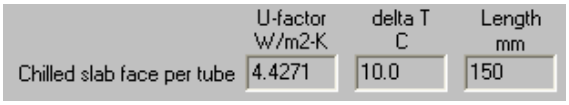

17.3	Hydronic tubing inside diameter, mm
2.5	Hydronic tubing wall thickness, mm
0.15	Hydronic tubing spacing in the slab, m
0.45	Hydronic tubing conductivity (PEX-AL-PEX composite tubing), W/m-k
1.40	Slab conductivity, W/m-K
4.4271	Thermal transmittance or U-value of slab and tubes at 10 K delta-T, W/m^2-K
0.2259	Overall resistance, including water film, tubing, and air film at exposed surface, m^2-K/W
0.1067	Air film resistance on exposed cooling surface, m^2-K/W
0.0007	Water-film resistance at tubing inside surface (forced convection, 0.67 m/s flow), m^2-K/W
0.1184	Resistance for slab plus PEX tubing without air or water films, m^2-K/W
8.444	Conductance for slab plus PEX tubing without air or water films, W/m^2-K
0.100	Slab thickness at perpendicular heat transfer path (center of tubes to cooling surface), m
0.844	Adjusted conductivity for chilled slab material in VE model, W/m-K
72%	Faction of adjusted conductivity value obtained using simple spreadsheet model

An appropriate convective heat transfer coefficient for the cooled slab surfaces is included both in the boundary condition at this surface in the THERM model (Figures 13a–13d) and in the surface properties for the slabs constructions modeled in VE. This determination of this coefficient is discussed in the *Natural convection at actively cooled surfaces* section, below. The PEX tubing boundary condition includes a forced-convection heat transfer coefficient for water flowing in pipes or tubes.

$$h = (1206 - 23.9t)V^{0.8}/(D/1000)^{0.2}$$

Where:

h is the convective heat transfer coefficient in W/(m^2·K)
V is the velocity of water flow in m/s
D is the inside diameter in mm
t is water temperature in °C

Using this simplified equation, which represents a forced convection correlation for water at 3 to 200°C based on Nu = 0.023 $Re^{4/5}Pr^{1/3}$ (ASHRAE 2005), and given 0.67 m/s flow velocity, 15°C water, and a 17.3-mm tube inside diameter, the calculated water-film heat transfer coefficient for the PEX tubing was 1,385 W/m^2·K.

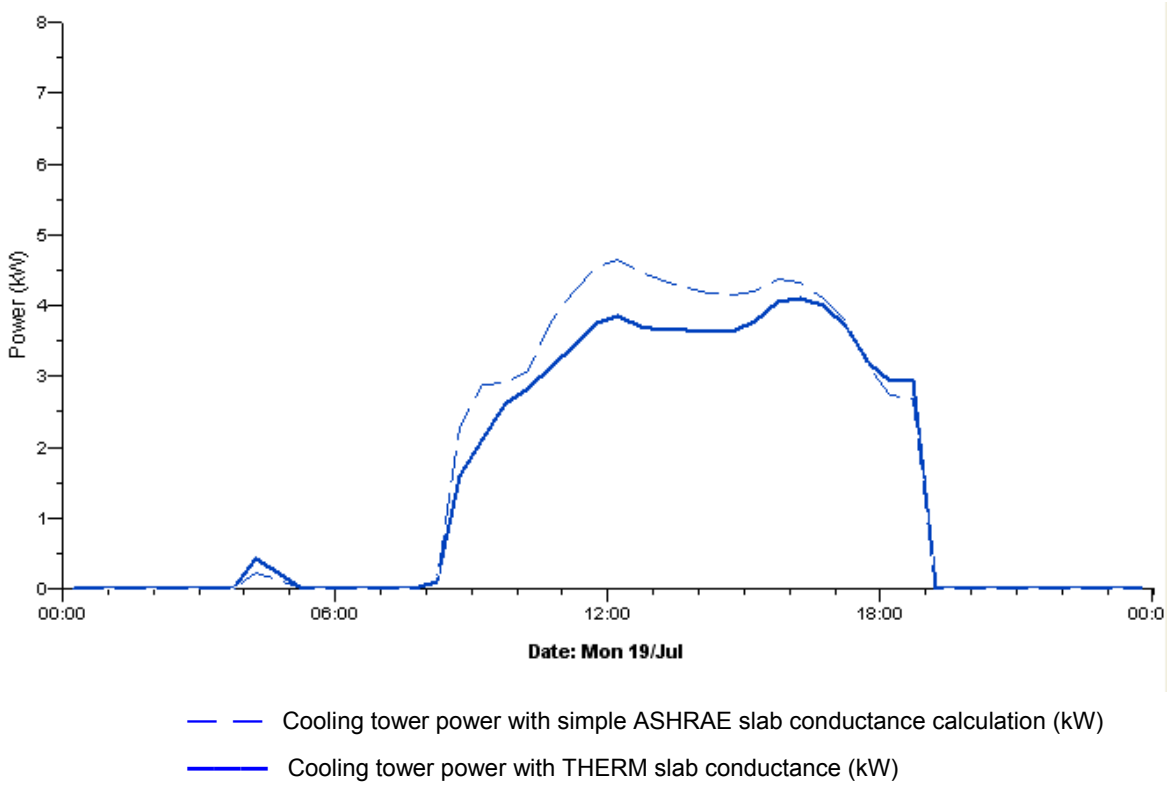

Figure 14: The plot above shows power for the cooling tower (with energy being the area under the curves) for the two different effective slab conductance values on a typical summer day in Denver.

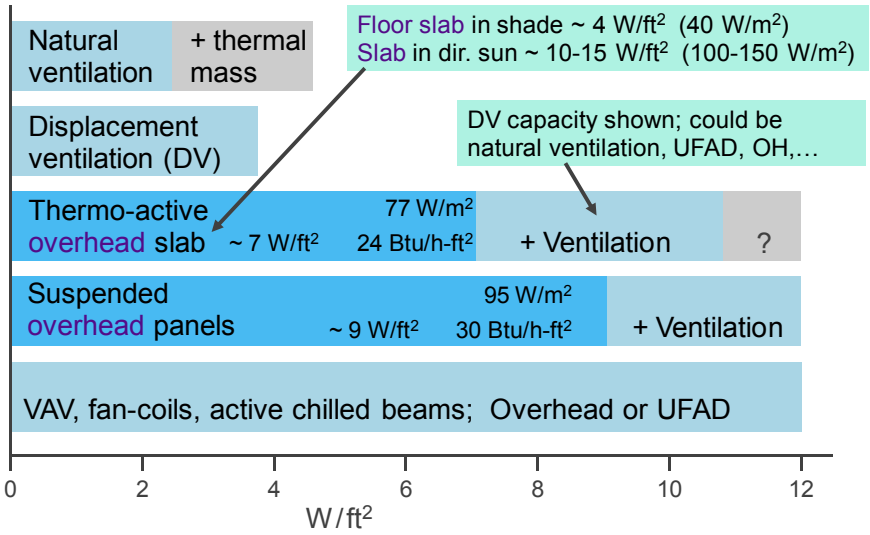

Figure 15: In general, the maximum sensible cooling capacity for overhead hydronic radiant systems falls between the cooling capacity of all-air conventional HVAC and low-energy displacement or natural ventilation strategies (Moore et al. 2006).

While the simpler spreadsheet model (Gough 2007) and hand calculation (ASHRAE 2005) previously used to adjust the slab conductivity for the tube size, depth, and spacing yielded very similar results, both suggested notably higher conductivity than was indicated by THERM. The percentage at the bottom of each section in Table 4 is the fraction of the previous values that is represented by the new values obtained using the THERM model. With the slab conductivity (including PEX tubing material and the forced-convection heat transfer from the water to the tube material) adjusted to a lower value in keeping with the THERM model *vs*. the simplified models, the cooling tower power (Figure 14) for supplying cold water is reduced during periods of transient loads. This is most pronounced early in the day when solar gain is still ramping up and the effect of precooling the slab is spread over a longer period of time.

Simulated peak sensible cooling for the hydronic radiant slab system in a single occupied zone under peak-load conditions was 62.5 W/m^2 (5.8 W/ft^2). This result is 19% below the theoretical and empirically derived potential peak cooling power of 77 W/m^2 (24 Btu/hr-ft^2) for overhead radiant cooling slabs at 18°C (64°F) as described in the literature (Mikler 1999) and shown in Figure 15. This difference can be attributed to four factors: 1) the depth to which the hydronic tubing is embedded in the slab, which is a trade-off between cooling power and faster reaction time, on the one hand, and potential for nighttime precooling, on the other; 2) the tube spacing within the slab; 3) the warmer supply water temperature with just a cooling tower as compared to using a chiller; and 4) the supply water flow rate, which significantly affects circulation pump energy consumption. Furthermore, at the time of this peak hydronic slab cooling power, the DOAS was providing 12.0 W/m^2 (1.1 W/ft^2) cooling to the same occupied zone.

Hydronics

Pump power is minimized through appropriate sizing of the hydronic loops and tubing diameters, as well as the reduced number of elbows afforded by use of flexible PEX tubing for both the zone loops and secondary supply water loop that feeds them. Zone loop flow rates were sized first based upon estimated requirements to meet loads, and then refined over numerous simulation runs to ensure adequate cooling capacity for peak load conditions without significantly oversizing flow rates. Figure 18 provides an excerpt from the spreadsheet set up to calculate pump power for the hydronic cooling circuits as a function of slab area, tubing size, tube spacing, design flow, number of loops, tube material, equivalent pipe lengths, pump efficiency, and pump motor efficiency.

Because they save energy and permit the use of cheaper, simpler 2-way (rather than 3-way) valves for modulating loop flow, the use of variable-speed circulation pumps is growing. However, the most common circulation pumps are still fixed-speed and the simulation tool used for this study is not yet capable of modeling power for pumps with variable speed drives.

For the three-story building, the total pumping electric load for all 20 hydronic slabs (three floor decks plus a roof deck) is just 0.268 kW (0.34 bhp) for Denver and 0.422 kW (0.57 bhp) for Sacramento (Table 5). With a design total flow rate of 5.8 l/s (92.0 gpm) in both cases, these values result in pump power intensity of 46 W/l-s (2.9 W/gpm) and 73 W/l-s (4.6 W/gpm) for Denver and Sacramento, respectively. These power intensities are 15% and 24% of the baseline value of 300 W/l-s (19 W/gpm) given for hot-water circulation systems within the ASHRAE 90.1-2004 Appendix-G Performance Rating Method. As no variable-speed pumps are modeled, these low pump power intensities suggest significant energy savings potential associated with careful design of hydronic circuits to avoid excessive flow rates and minimize friction head loss.

Table 5: Sizing of hydronic circuits and flow rates, associated friction head loss, and resulting pump power for the complete building by zone type for Denver and Sacramento locations.

Hydronic loop sizing and flows - Complete building								
Zone type	**Interior**	**Perim - Den.**	**Perim - Sac.**		**Interior**	**Perim - Den.**	**Perim - Sac.**	
Slab area	1,312	976	976	m^2	14,122	10,506	10,506	ft^2
Slab mass	551,040	409,920	409,920	kg	1,214,492	903,464	903,464	lbs
Tube size	5/8	3/4	3/4	CTS	5/8	3/4	3/4	CTS
Tube ID	14.8	17.3	17.3	mm	0.58	0.68	0.68	in
Spacing	0.25	0.25	0.15	m	9.8	9.8	5.9	in
No. of loops	40	64	64		40	64	64	
Total length	5,248	3,904	6,507	m	17,213	12,805	21,342	ft
Water mass	3,619	3,665	6,108	kg	7,977	8,077	13,462	lbs
Total flow	**0.76**	**5.05**	**5.05**	l/s	**12.0**	**80.0**	**80.0**	gpm
Friction head	7.73	39.264	64.43	m	25.3	128.0	211.3	ft

Complete building	**Denver**	**Sacramento**		**Denver**	**Sacramento**	
Total flow	**5.8**	**5.8**	l/s	**92.0**	**92.0**	gpm
Friction head loss	**47.0**	**72.2**	m	**153**	**237**	ft
Peak pumping power	**0.268**	**0.422**	kW	**0.268**	**0.422**	kW
Pump power per unit flow	**46**	**73**	W/l-s	**2.9**	**4.6**	W/gpm

Each interior zone hydronic slab at 328 m^2 (3,530 ft^2) as ten parallel 131-m (430-ft) loops of 5/8" SRD-9 CTS[2] cross-linked polyethylene (PEX) tubing with a 14.8 mm (0.58-inch) inside diameter spaced 0.25 m (9.8 in) apart and just 0.019 l/s (0.3 gpm) flow per loop, or 0.19 l/s (3.0 gpm) for one complete interior zone slab.

Piping friction head loss for one interior zone hydronic at the design flow velocity of 0.11 m/s (0.36 ft/s) is 0.0015 m-H_20/m-pipe (0.15 ft-H_20/100-ft-pipe), as calculated using the Hazen-Williams equation for pressure loss in piping with a roughness constant of 150 for thermoplastic tubing. Accounting for equivalent total tubing and pipe length of 1,327 m (4,362 ft), including risers, valves, and headers, pump efficiency of 65%, and pump motor electric efficiency of 78%, total friction results in electric pump power per interior zone slab of just 0.007 kW.

The 905 liters (239 gal) of water in the tubing in one interior zone slab has a mass of 905 kg (1,994 lbs). This is embedded in the center of a 0.2-m (~8 in) thick high-density cast concrete slab with mass of 137,760 kg (303,620 lbs. or ~152 tons).

Perimeter zone hydronic slabs, including four zones per floor or one per façade orientation at 61.4 m^2 (657 ft^2) each use four parallel 61-m (200-ft) loops of 3/4" SRD-9 CTS[3] cross-linked polyethylene (PEX) tubing with a 17.3 mm (0.68 inch) inside diameter. For Denver, perimeter-zone tubes are spaced 0.25 m (9.8 in) apart. For Sacramento, perimeter-zone tubes are spaced 0.15 m (~6 in) apart. In both cases, maximum flow per loop is 0.079 l/s (1.25 gpm), or 0.32 l/s (5.0 gpm) for each complete perimeter zone slab.

Piping friction head loss for each perimeter zone at the design flow velocity of 0.34 m/s (1.1 ft/s) is 0.0097 m-H_20/m-pipe (4.9 ft-H_20/100-ft-pipe), as calculated using the Hazen-Williams roughness constant of 150 for thermoplastic tubing.

In the Denver case, total hydronic loop friction results in electric pump power per perimeter zone slab of just 0.015 kW. This accounts for equivalent total tubing and pipe length of 254 m (832 ft), including risers, valves, and header pipes, pump efficiency of 65%, and pump motor electric efficiency of 78%. For Sacramento, total hydronic loop friction results in electric pump power per perimeter zone slab of 0.025 kW. This accounts for equivalent total tubing and pipe length of 416 m (1,366 ft), including risers, valves, and header pipes, pump efficiency of 65%, and pump motor electric efficiency of 78%.

For both Denver and Sacramento, the 229 liters (60.5 gal) and 382 liters (101 gal) of water in the tubing in the interior zone slabs have a mass of 229 kg (505 lbs) and 382 kg (841 lbs), respectively. This is embedded in the center of a 0.2-m (~8") thick high-density concrete slab with mass of 25,800 kg (56,870 lbs. or ~ 28.4 tons) for each perimeter zone.

---

[2] SRD is an abbreviation for standard dimension ratio and CTS is an abbreviation for standard copper tube size for which outside diameter is CTS plus 1/8 inch and SRD is equal to outside diameter divided by wall thickness. PEX tubing for hydronic systems typically has an SRD of 9.

[3] SRD is an abbreviation for standard dimension ratio and CTS is an abbreviation for standard copper tube size for which outside diameter is CTS plus 1/8 inch and SRD is equal to outside diameter divided by wall thickness. PEX tubing for hydronic systems typically has an SRD of 9.

Hydronic loop sizing and flows per zone - Perimeter				
Slab area	61	m^2	657	ft^2
Slab mass	25,620	kg	56,466	lbs
Tube size	3/4	Specify in CTS (nominal IP-unit fraction)		
Tube ID	17.3	mm	0.68	in
Spacing	0.15	m	5.9	in
Total length	407	m	1334	ft
Water mass	382		841	lbs
Spec'd flow	0.32	l/s	5.00	gpm
# of loops	4		4	
Loop length	101.7	m	333	ft
flow / loop	0.079	l/s	1.25	gpm
Flow velocity (*v*) in each individual loop				
	0.34	(m/s)	1.10	(ft/s)
Friction head loss (*f*) per linear unit of tubing at flow velocity				
c =	150	Hazen-Williams roughness constant		
q =	0.079	l/s	1.25	gpm
d_h =	17.3	mm	0.68	in
f =	0.0097	m-H_20/m	0.97	ft-H_20/100-ft
Pump Power - Perimeter zone (per zone and per unit flow)				
See ASHRAE table of Equivalent Length for elbows at flow velocity				
0.32	*q - flow capacity (l/s)*		1.14	*(m^3/h)*
407	*tube length (m) without fittings, elbows, etc.*			
5	*riser length (m) without fittings, elbows, etc.*			
4.8	*EPL - equivalent pipe length (m) for elbows, etc.*			
416	*EPL total (m), including elbows, fittings, valves, etc.*			
0.0097	*pipe head loss (m) per 1-m length at design flow*			
4.0268	*design system head loss (m) - resulting from friction*			
0	*static head (m) - height of open system components*			
4.0268	*h - Total differential head (m)*			
1000	*ρ - density of fluid (kg/m^3) initial value assumes water*			
9.81	*g - gravity (m/s^2)*	*standard terrestrial value*		
0.012	*Hydraulic power (kW)*			
0.017	*Hydraulic power (bhp)*			
0.65	*η - pump efficiency*			
0.019	*Shaft power (kW)*			
0.026	*Shaft power (bhp)*			
0.78	*η_e - pump motor efficiency (incl. power electronics)*			
0.025	*Electrical power per zone (kW)*			
78	*Electrical power per unit flow (W/l-s)*			
4.9	*Electrical power per unit flow (W/gpm)*			

Figure 16: A spreadsheet set up to calculate pump power for the hydronic cooling circuits as a function of slab area, tubing size, tube spacing, design flow, number of loops, tube material, equivalent pipe lengths, pump efficiency, and pump motor efficiency.

Natural convection at actively cooled surfaces

Previously established variable heat transfer coefficients for natural convection, including those from Alamdari & Hammond (1983), Awbi & Hatton (2000), and CIBSE appear poorly suited to modeling chilled ceiling surfaces. Correlations—"Equation (8)" in Figure 17, below—developed in laboratory experiments by Novoselac et al. (2006) at Pennsylvania State University indicate higher rates of convective heat transfer for chilled surfaces, and thus greater cooling capacity than would be predicted using each of the other coefficients noted.

Correlations developed by Novoselac et al. are for a flat horizontal overhead cooling surface with hydraulic diameter ≥ 1 m (3.3 ft) and surface-to-air temperature difference (delta-T) greater than 2 K (3.6°F). With a corresponding Rayleigh number greater than 2×10^8, these properties indicate turbulent natural convective flow for horizontal surfaces (Kakac 1987). Experiments were conducted with mixed radiative and convective heat sources representative of an office environment having both internal and solar loads. Experimental radiant panel systems extracted 60% and 40% of the space-cooling load by radiative and convective heat transfer, respectively.

The convective heat transfer coefficient from Novoselac et al., for which correlations are presented in Figure 19, below, was used for the downward facing surfaces of the chilled slabs as modeled for this study.

$h_c = 2.12 \times \Delta T^{0.33}$ W/m^2-K ($h_c = 0.308 \times \Delta T^{0.33}$ Btu/h × ft^2 × °F)

Where: h_c = convective heat transfer coefficient

ΔT = surface-to-air temperature difference in K (°F)

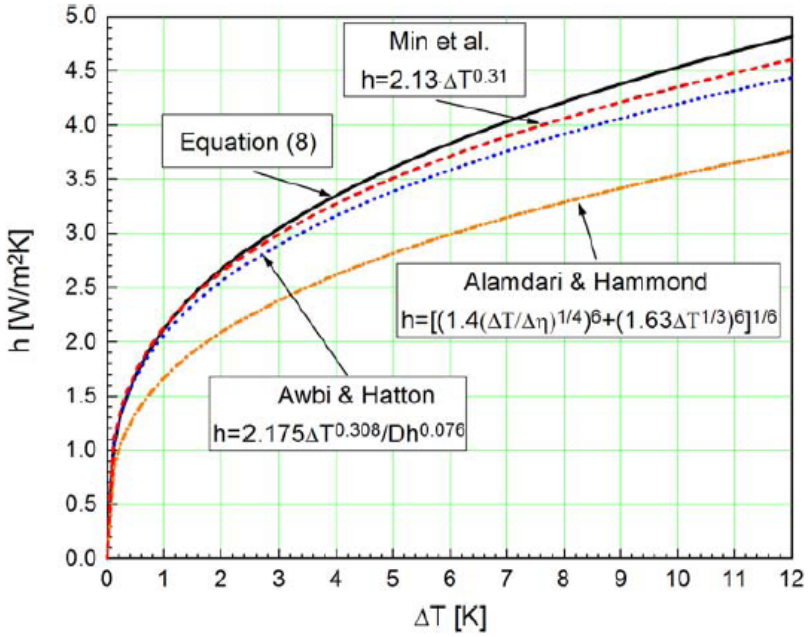

Figure 17: Novoselac et al. (2006) plot of convective heat transfer correlations for chilled overhead surfaces (Equation 8) as developed in controlled laboratory tests.

$h_c = b(DT)^{0.33}$ is the simplified form for natural convection correlations with buoyancy-driven turbulence, where DT is the surface-to-air temperature difference and b is the constant for turbulent natural convection. This form results from substitution of appropriate Prandtl, Nusselt, and Grashof numbers in the expression relating them: Nu = C_T(Gr*Pr)$^{0.33}$ (ASHRAE 2005).

In simulation runs performed using the dynamic thermal model presented in this study, the newly developed convective heat transfer coefficient from Novoselac et al. increased chilled slab cooling capacity by 5–6% as compared to using the Alamdari & Hammond variable coefficient. Relative to that modeled with the CIBSE variable coefficient, cooling capacity was increased 3–4%. Although it was not possible to introduce a variable coefficient within the simulation tool used for this study, the difference with the Awbi & Hatton coefficient is consistently, over a range of surface-to-air temperature differences, approximately one-third of the difference indicated for the CIBSE coefficients. In all cases, differences in predicted capacity depend upon the surface-to-air delta-T and the relative mix of convective and radiant heat sources in the space. In the case of the CIBSE variable coefficient, the predicted result also depends upon mean air velocity in the space and how this is reflected in the model.

The convective heat transfer coefficient and resulting air-film resistance used for chilled ceiling surfaces in the dynamic thermal model, as well as the calculated intermediate values, are as follows:

6.00	Input design surface-to-air delta-T (degrees C or K), minimum valid entry is 2K
3.83	Heat transfer coefficient for turbulent natural convention at chilled surface (W/m^2-K)
0.90	Surface Emissivity on cooling surface (bottom) facing room
6.156	Constant relating radiative heat transfer rate and emissivity
5.540	Derived radiative heat transfer coefficient (W/m^2-K)
9.360	Surface air-film conductance (W/m^2-K)
0.107	Surface air-film resistance used for chilled ceilings in VE model (m^2-K/W)

Cooling Tower

The supply water source for the hydronic slabs and DOAS cooling coils is a closed-circuit cooling tower. Because there is no chiller, and thus generally a lower water temperature entering the tower at *all* times—*i.e.,* not only when in a waterside-economizer mode—a slightly larger closed circuit cooling tower is required for the Radiant+DOAS system modeled for this study. However, there are three reasons that the cooling tower does not have to be as large for the hydronic cooling system as it would have to be if it were the sole source of supply water for the VAV system: 1) because the radiant system uses the large surface area of the chilled slabs, in this case both above and below the occupants, it can provide effective cooling with much warmer water; 2) the large cooling surface also permits use of supply water at temperatures closer to the return water temperature (a smaller delta-T for the water loop), which, for a given approach, extends the useful range of tower operation with respect to outdoor WBT; 3) because it cools the core of the slab, and not the air in the room or surfaces closest to the occupants, the radiant system can rely more heavily upon a nighttime precooling cycle when the outdoor wet-bulb temperatures tend to be much lower.

For Los Angeles, and San Francisco climates, a relatively typical tower with 2.2 K (4°F) approach is used. For Denver, two smaller cooling towers—each 75% of the fan and pump power of the tower for Denver—are configured in series on the water loop. This simple and relatively

common series configuration provides an approach that is half that of a single tower or parallel configuration. For Sacramento, the tower approach to outdoor WBT is thus 1.1 K (2°F). This approach and the performance values for a range of operating points calculated for these cooling towers using a selection and sizing tool from Baltimore Air Coil (BAC 2008) are presented in Table 6, below. These and additional operating points were used to populate a matrix of load and temperature-dependent COPs for the source of cooling water in the ApacheHVAC module of Virtual Environment. While somewhat oversized for the application, the tower sized for the Denver climate was used in the Los Angeles and San Francisco climates as well. In each case, however, the towers and associated fan and pump power are still relatively small within the range of available cooling towers for commercial buildings.

In contrast to the cooling tower provided to reject heat from a chiller in the baseline VAV system and its WSFC variant, the cooling tower for the hydronic radiant cooling system without a chiller needs to be and can be somewhat larger, since there is no chiller to purchase. Thus, for a given set of operating conditions, it can have a somewhat smaller approach to the outdoor WBT and/or provide greater cooling capacity. This selection needs to balance a range of parameters: there may be added energy consumption associated with a large, low-cost unit operating much of the time at part load if it does not include variable-speed fans and pumps. The relatively common practice of staged operation of multiple smaller units might overcome this limitation to some extent. However, it may also come with lower peak efficiency for the smaller fans and will very likely add to the system cost.

A simplified model of cooling tower operation maintains supply water temperature for the hydronic radiant slab and DOAS cooling coil in keeping with the cooling tower approach and hourly outdoor wet-bulb temperatures in the TMY weather file. Based upon performance for an actual available cooling tower (Table 6), this simplified model provides 10 to 19 kW of cooling per kW electric input (*i.e.,* 0.36–0.19 kW/ton cooling), including tower fan, tower spray water pump, and primary chilled-water (CHW) loop pump. In other words, the combined performance for these components in the simplified cooling tower model excludes only the zone circulation pumps, for which pump power is separately assigned to each chilled slab zone.

Table 6: Cooling tower performance for a range of operating points as sized and configured for the Denver and Sacramento climates.

Cooling Tower for direct coupling to hydronic system - Denver											
Single Closed-Circuit BAC FXV-L423 Cooling Tower							Tower	Tower	CHW Pump		Combined
Cooling	Fan	Pump	Flow	Entering	Leaving	Outdoor	EER	COP	EER	EER	COP
kW	kW	kW	rate l/s	water °C	water °C	WBT °C	kW/ton	kW/kW	kW/ton	kW/ton	kW/kW
45	3.73	0.187	6.0	24	22.2	20	0.31	11	0.05	0.36	10
73	3.73	0.187	6.0	21	18.2	16	0.19	19	0.05	0.24	15
100	3.73	0.187	6.0	18	14.0	10	0.14	26	0.05	0.19	19

Cooling Tower for direct coupling to hydronic system - Sacramento											
Two 25% smaller Closed-Circuit Cooling Towers in series on loop							Tower	Tower	CHW Pump		Combined
Cooling	Fan	Pump	Flow	Entering	Leaving	Outdoor	EER	COP	EER	EER	COP
kW	kW	kW	rate l/s	water °C	water °C	WBT °C	kW/ton	kW/kW	kW/ton	kW/ton	kW/kW
71	5.6	0.373	9.0	23	21.1	20	0.30	11.9	0.05	0.35	10
90	5.6	0.373	9.0	19.5	17.1	16	0.23	15.1	0.05	0.28	12
109	5.6	0.373	9.0	24	21.1	20	0.19	18	0.05	0.24	14
109	5.6	0.373	9.0	23	20.1	18	0.19	18.2	0.05	0.24	14
109	5.6	0.373	9.0	21	18.1	16	0.19	18.2	0.05	0.24	14
141	5.6	0.373	9.0	19.5	15.8	14	0.15	23.6	0.05	0.20	18
150	5.6	0.373	9.0	18	14.0	10	0.14	25	0.05	0.19	19

Within Virtual Environment's Apache HVAC systems simulation module, the cooling tower for the Radiant+DOAS is modeled as a chilled water source with supply water temperature limited to be no cooler than permitted by the tower approach to the hourly outdoor wet-bulb temperature. This was modeled by a proportional control in each chilled ceiling slab zone. Within the "chiller" component type used to model the energy performance of the cooling tower, the model uses a matrix of coefficient of performance (COP) values varying from 10 to 19 for sixteen different operating points. Each operating point in the matrix represents a unique combination of cooling load and outdoor wet-bulb temperature, with the latter ranging from 10 to 20°C (50 to 68°F). This "chiller" module then interpolates between points on the matrix as a map of performance.

While this matrix of operating points provides a reasonable approximation of cooling tower performance, actual COP and approach vary with both the outdoor WBT and the entering water temperature as a function of part-load conditions. Furthermore, given limited resources for determining relationships between cooling tower capacity and fan power with a variable-speed drive, fan and pump power are fixed in the calculation of operating points. For this reason, low part-load fractions (below ~50%) were omitted from the matrix. Thus simulated operation below ~50% load uses the COP of the lowest load fraction in the matrix column for the outdoor WBT most closely corresponding to that of the current simulation time step. In the interest of energy efficiency, one might want to specify a cooling tower with variable-speed fan and pump. Thus the assumption of fixed fan and pump power leaves some room for improvement.

To lower the CHW loop temperature further with respect to outdoor WBT (potentially below the WBT), as might be desirable for either higher cooling loads or more humid environments, a precooling coil can be included on the tower air inlet. While limited in its capability to produce water much below the WBT, the most energy-efficient and cost effective option among multi-stage evaporative cooling configurations appears to be a single-stage, direct-coupled configuration, wherein the precooling coil gets its water from the sump of the same tower (Seidl 2005). This precooling coil circulates water from the cooling tower sump through a coil to lower the entering air temperature. For example, directly coupled single-stage precooling could lower the entering air temperature for Sacramento at the ASHRAE 0.4% Cooling Design Day DBT of 36.4°C (97.5°F) of by 9K (16°F), thus reducing the WBT of the entering air by 3K (5.4°F). The temperature of the water leaving the tower is thus also reduced by 3K (5.4°F). Given an approach of 2.2K (4°F), and a precooling reduction of 3K (5.4°F), the leaving water temperature would be 0.8K (1.4°F) below the outdoor wet-bulb temperature.

The psychrometrics of precooling the cooling-tower entering air and the effect of this upon supply water temperature for the cooling design day example above are illustrated in Figure 18. The upper and lower enthalpy differences (Δh_1 and Δh_2) indicated are for the same tower first without and then with precooling. If the precooling energy were rejected elsewhere—*i.e.,* other than in the same tower—the total Δh between entering air and leaving air would remain the same. If precooling energy is rejected in the same tower, however, this energy would be added, resulting in Δh_3. The saturated leaving air state would once again be that of the upper one of the two points on the saturation line.

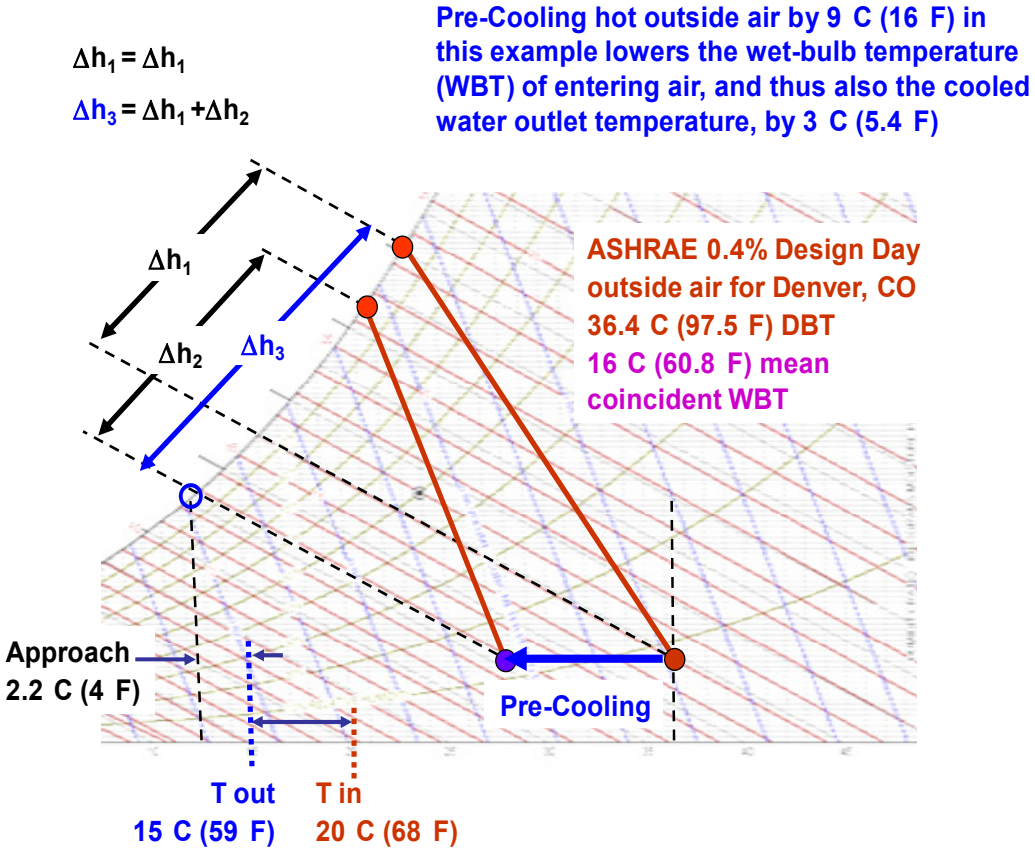

Figure 18: The psychrometrics of precooling the cooling-tower entering air via a directly coupled pre-coiling coil (i.e., a coil using the water from the same tower) and its potential effect on supply water temperature.

Rejecting the additional precooling energy in the same tower—*i.e.,* in the case of a single-stage, directly coupled precooling coil—requires that the size of the tower be increased to provide the added heat-rejection capacity. While the theoretical limit of this precooling approach is the outdoor dew-point temperature (DPT), fan-energy trade-offs and practical considerations of tower size and cost will tend to come into play prior to reaching that limit.

Cooling system controls

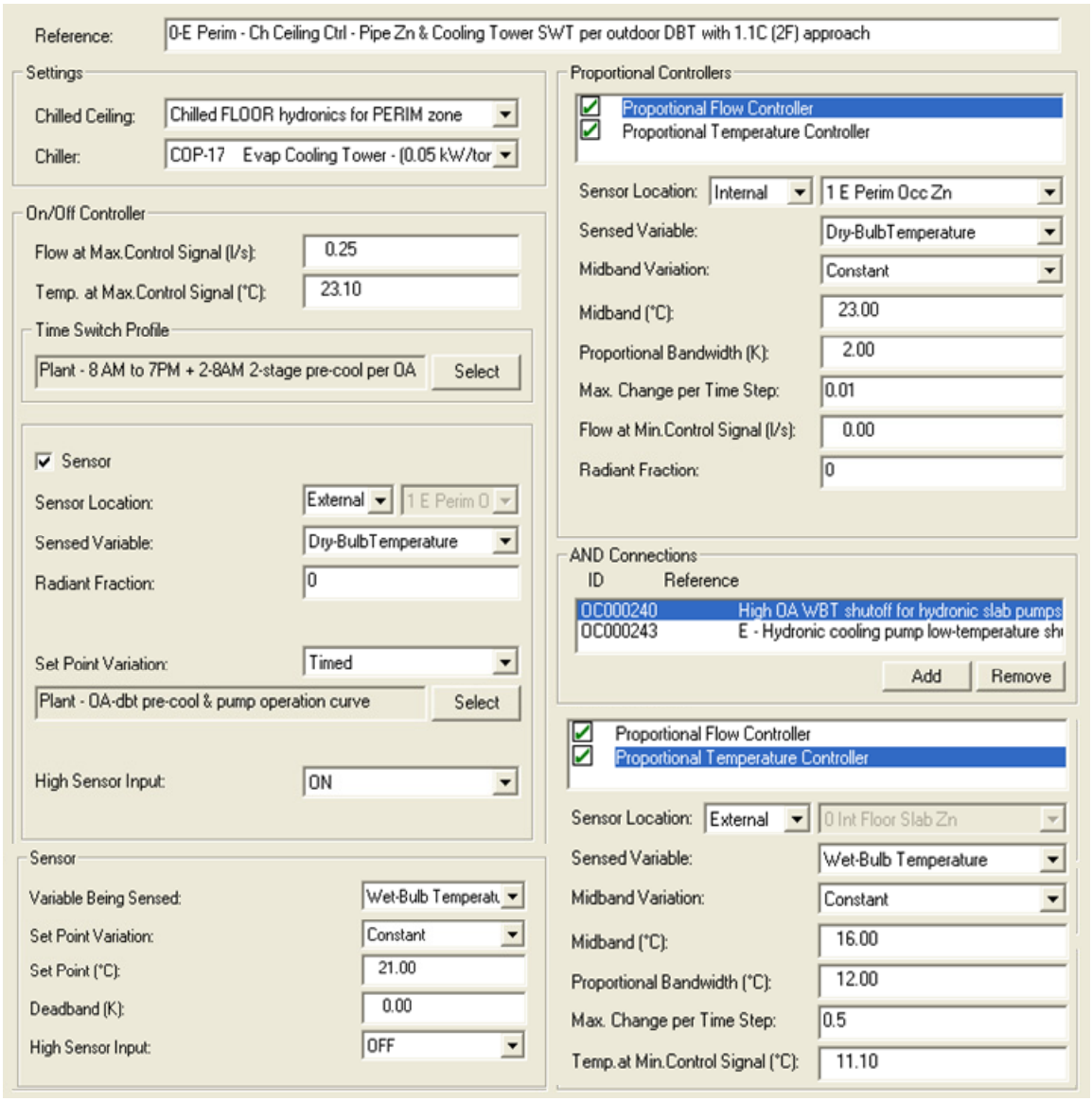

Figure 19: A composite view of the zone-level controller, including nested or associated dialog boxes for specific parameters, linked logical (AND/OR) controllers, and references to formula control profiles.

Each hydronic slab zone has a separate "room unit" controller (Figure 19) capable of controlling the circulation pump on/off status, water flow, and water temperature. The temperature control is proportional to the outdoor WBT to maintain supply water in keeping with the cooling tower approach—*i.e.,* the supply water can be no colder at any given time step than would be possible with the specified cooling tower. The flow control is proportional in relation to the temperature within the adjacent occupied zone and has its maximum volume set to meet the zone cooling load in combination with the DOAS. The on/off control is used, as further described below, to determine night precooling, to prevent overcooling in the early morning hours, and to prevent introducing warm water from the cooling tower in the hottest part of the day when the slab has already been cooled down. Figure 19 also includes nested or associated dialog boxes for specific parameters, linked logical (AND/OR) controllers, and references to formula control profiles.

These various control parameters and linked controllers or formulae can reference a broad array of interior space conditions, exterior climate conditions, conditions anywhere on the airside HVAC network, as well as the on-off signal from any other controller (the latter is presently limited to referencing controllers that can be placed on the airside network). Profiles can be prepared to vary control parameters and operating states according to date, day, and time; absolute values, or a user-defined formula. The formula profile may include the full range of indoor and outdoor climate conditions, room references, controller references, and additional sensors, such as daylight levels recorded in daylighting simulation runs. These formula profiles can then be use to vary time schedules, set points, or the midband for a proportional controller.

While the pump power is fixed within each chilled ceiling module (each of which represents a set of hydronic loops in a single interior or perimeter zone), pump power can be switched on and off independently for each zone, thus providing some approximation of a variable-speed pumping on the whole-building level with respect to the number of zones operating at any given time. However, the modulation of flow at the zone level affects only the cooling performance, and not the energy consumption.

Nighttime hydronic precooling runs first from 2:00 AM to 6:00 AM (when the lowest outdoor WBT of the typical diurnal cycle provides the best cooling tower performance) if the outdoor DBT is at least 15°C (59°F), and then from 6:00 AM to 8:00 AM if the outdoor DBT is at least 18°C (64.4°F). Daytime hydronic cooling from 8:00 AM to 7:00 PM runs if the outdoor DBT is at least 21°C (69.8°F).

Between 7:00 PM and the 2:00 AM start of the precooling cycle, operation of the hydronic cooling in the slabs is prevented by a simple time-based on/off control. During this off period, the slabs act as passive sinks, soaking up heat that will be rejected during the precooling cycle.

Flow to each slab is modulated between zero and the maximum design flow during precooling according to a temperature sensor in the adjacent occupied space, as needed to prevent the occupied space from being significantly overcooled. This involves two linked controllers to facilitate temperature control and appropriate accounting of pump energy,: the first is the proportional flow controller with occupied-zone cooling temperature target, which is already included in the "chilled ceiling" controller for the slab zone; the second is a low-temperature shutoff control placed in the conditioned zone on the airside network and linked to the chilled ceiling controller via an "AND" connection. The reason for this arrangement is that the software currently forces the user to place the on/off time-switch control for the chilled ceiling unit (the hydronic loop in this case) within the same zone (the chilled slab). Thus, placing the on/off sensor in the adjacent occupied zone via the logical AND connection permits the cooling effect to remove heat from the full thickness of the slab prior to triggering the shutoff limit control. While some overcooling could occur as a result of thermal inertia, the massive slabs change temperature gradually enough during precooling so that the overshoot in terms of slab temperature tends to stay within the comfort range. Resulting space temperatures are discussed in Section 7, below.

Even with this control strategy, there is, however, still a very minor tradeoff in the form a very slightly greater required heating energy under certain circumstances for the hydronic radiant system. This stems from the lower temperature of the floor and ceiling slabs during cooling season, even when the nighttime precooling cycle has not run the night before, which tends to slightly overcool the conditioned space on the mornings of uncommonly cool days. Refinement of cooling and precooling controls in keeping with multi-day trends might alleviate this.

There is an additional sensor and formula profile to turn off the pump whenever outdoor WBT plus the 1.1 K (2.2°F) tower approach (the temperature of the coldest water the tower can deliver at any given time) exceeds the temperature at the core of the hydronic cooling slab. The logic for doing so is that this occurs only during periods of high midday outdoor temperatures when the pre-cooled mass of the hydronic slabs remains useful as a passive heat sink. However, because ventilation air must still be brought into the building, the cooling tower, airside coils, and airside indirect evaporative cooling spray chamber remain on for OA conditioning. Indeed, ~23–25°C (73–77°F) ventilation air is more desirable than the 35–40°C (95–104°F) outdoor air that is coincident with Sacramento peak outdoor wet-bulb temperatures in excess of 21°C (70°F). Although not as critical for addressing peak cooling loads, the same control logic is used in Denver, Los Angeles, and San Francisco to avoid throwing away invested cooling system energy.

Figure 20, below, illustrates the controls and system behavior of the Radiant+DOAS on a hot and sunny Denver Monday in August following an equally hot weekend with HVAC systems off and lighting and equipment remaining at their 10% minimum unoccupied loads.

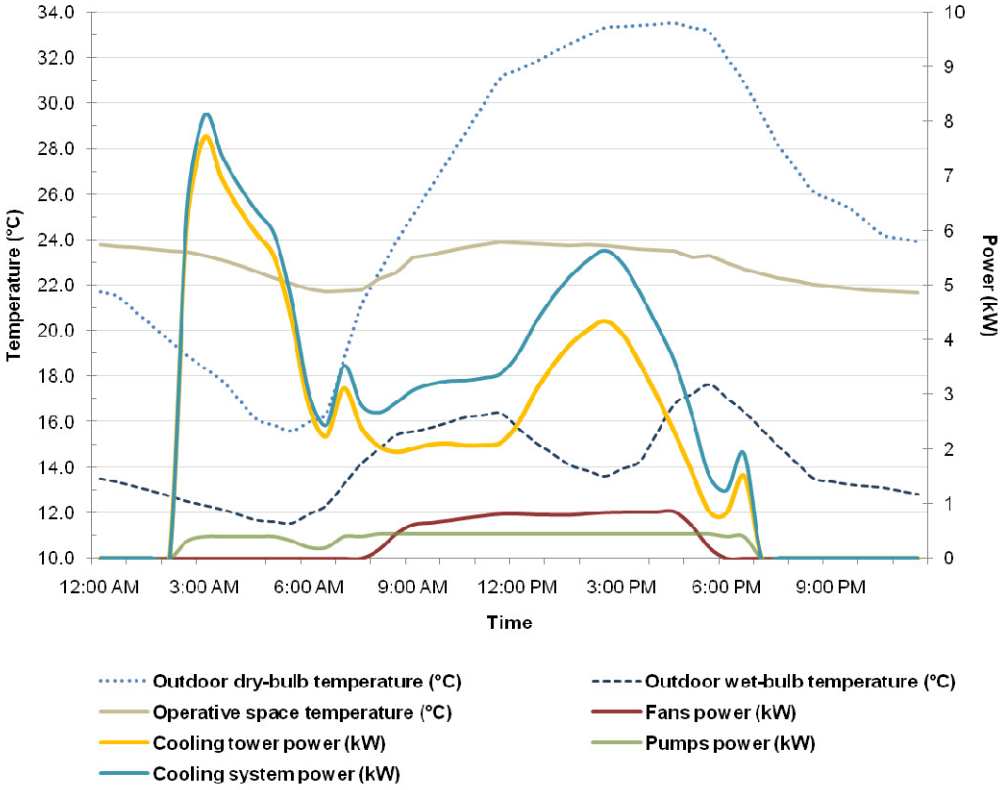

Figure 20: A plot of cooling system component and total electric power in the context of indoor operative temperature and outdoor DBT and WBT on a typically hot and sunny Denver Monday in August.

Energy consumption

Simulated cooling system energy consumption for May through September (Tables 7, 8, 9, and 10; Figures 21, 22, 23, and 24, below) suggests considerable energy savings potential with radiant cooling in climates suited to evaporative cooling of supply water via a cooling tower. An alternate VAV system scenario with waterside economizer or waterside "free cooling" (WSFC) demonstrates the extent to which the baseline VAV system could capture a portion of the same benefit from the use of its cooling tower as cooling supply water source when conditions permit. In all cases, WSFC still uses cooling tower fan and pump energy, plus distribution pumps in the case of the hydronic systems and supply and return fans in the case of the all-air system.

Across all four climates, cooling system energy saving during the May–September cooling season for the Radiant+DOAS relative to the baseline VAV system ranged from 54% to 71%. For the Denver and Sacramento climates, a detailed cooling tower model for waterside economizer operation or waterside "free cooling" (WSFC) was added to the baseline VAV system (see Figure 7) to investigate the extent to which this would affect relative differences in energy performance. In these cases, the WSFC was modeled to operate in place of the water-cooled chiller otherwise modeled for the baseline VAV system whenever the WSFC was capable of meeting the entire

Table 7: Radiant+DOAS May–September HVAC system energy in the Denver climate relative to the baseline VAV system and variants of the baseline system with WSFC and precooling.

Cooling Season HVAC System Energy May–September Denver, CO	VAV Baseline (MWh)	VAV with WSFC (MWh)	VAV with WSFC Savings *vs.* VAV	VAV+WSFC-precool (MWh)	VAV+WSFC-precool Savings *vs.* VAV	Radiant+DOAS (MWh)	Radiant+DOAS Savings *vs.* VAV	Savings vs.VAV+ WSFC-pc
Chillers (VAV only), cooling towers, and chilled water pumps	6.41	4.51	30%	3.64	43%	1.93	70%	57%
Hydronic system pumps and evaporative cooling spray pump	n/a	n/a	n/a	n/a	n/a	0.26	n/a	n/a
Fans (including cooling tower fan for waterside free cooling)	3.85	4.13	-7%	4.19	-9%	0.64	83%	84%
Boilers, natual gas	0.36	0.36	0%	0.49	-36%	0.21	41%	41%
HVAC system electricity	10.26	8.33	19%	8.33	19%	2.82	72%	66%
Total HVAC system energy, including natural gas	**10.62**	**8.67**	**18%**	**8.06**	**24%**	**3.03**	**71%**	**62%**

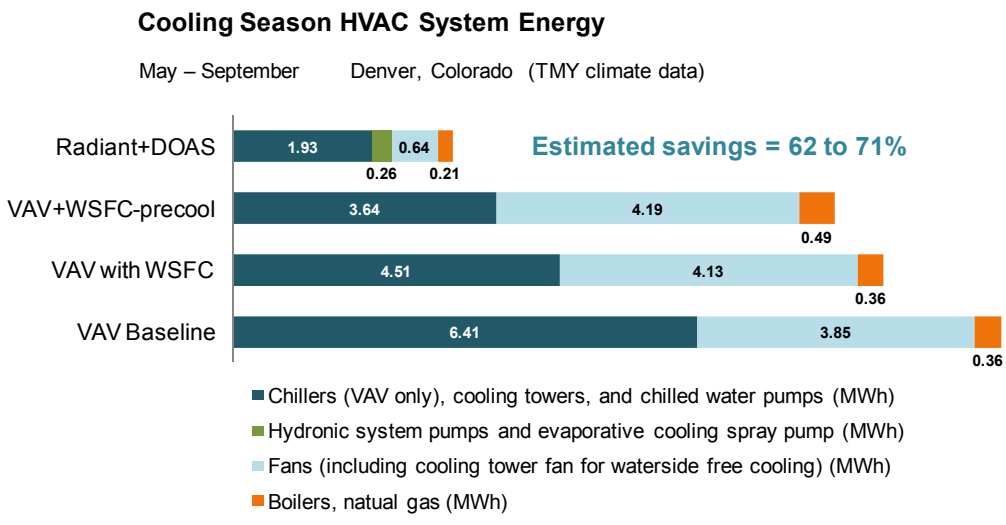

Figure 21: Estimated May–September HVAC system energy for VAV and Radiant Cooling alternatives in the Denver climate. The range of potential savings given for the Radiant+DOAS is relative to the VAV system with and without waterside free cooling (waterside economizer operation) and a precooling cycle.

Table 8: Radiant+DOAS May–September HVAC system energy in the Sacramento climate relative to the baseline VAV system and variants of the baseline system with WSFC and WSFC plus precooling.

Cooling Season HVAC System Energy May–September Sacrameto, CA	VAV Baseline (MWh)	VAV with WSFC (MWh)	VAV with WSFC Savings *vs.* VAV	VAV+WSFC-precool (MWh)	VAV+WSFC-precool Savings *vs.* VAV	Radiant+DOAS (MWh)	Radiant+DOAS Savings *vs.* VAV	Savings vs.VAV+ WSFC-pc
Chillers (VAV only), cooling towers, and chilled water pumps	7.69	7.04	8%	5.35	30%	3.42	56%	51%
Hydronic system pumps and evaporative cooling spray pump	n/a	n/a	n/a	n/a	n/a	0.76	n/a	n/a
Fans (including cooling tower fan for waterside free cooling)	4.15	4.00	4%	5.71	-38%	0.62	85%	85%
Boilers, natual gas	0.002	0.001	58%	0.015	-705%	0.012	-531%	-1398%
HVAC system electricity	11.84	11.04	7%	11.04	7%	4.79	60%	57%
Total HVAC system energy, including natural gas	**11.84**	**11.04**	**7%**	**11.08**	**6%**	**4.87**	**59%**	**56%**

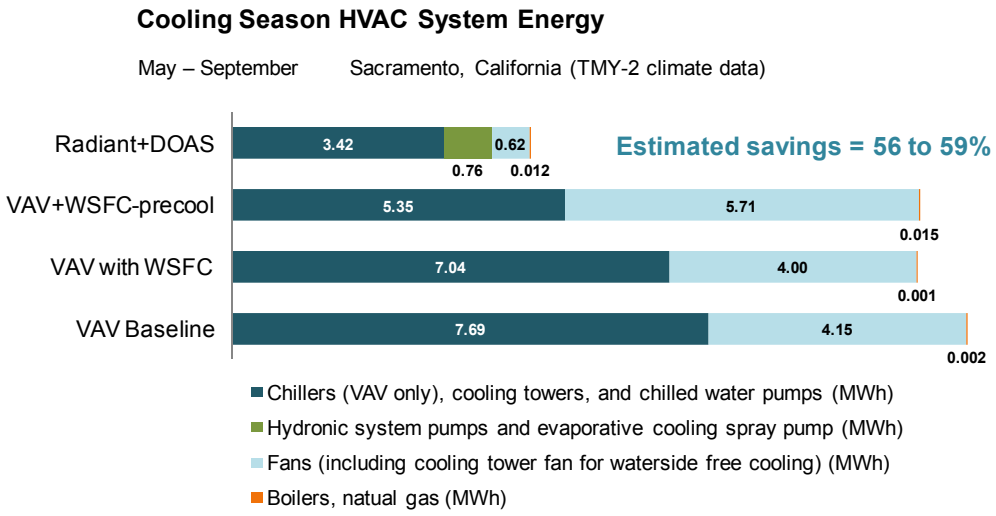

Figure 22: Estimated May–September HVAC system energy for VAV and Radiant Cooling alternatives in the Sacramento climate. The range of potential savings given for the Radiant+DOAS is relative to the VAV system with and without waterside free cooling (waterside economizer operation) and precooling.

cooling load. Results for this additional investigation indicate reduced relative energy savings for the Radiant+DOAS of 62% and 56%, respectively, for the Denver and Sacramento climates.

There is a design trade-off between chiller energy and fan energy plus free cooling via airside economizer operation that occurs in mild climates such as San Francisco, when airside systems are downsized in light of the parallel sensible cooling capacity of a radiant system. In such cases, the airside capacity is typically made subordinate to the hydronic radiant cooling. In other words, for hybrid systems that include radiant cooling and mechanical ventilation (as opposed to natural ventilation), the trade-off between maximized airside economizer operation and elimination of redundant airside capacity appears to be a key design consideration in mild cooling-dominated climates. Inclusion of appropriately integrated and controlled cooling tower and waterside economizer or other low-energy cooling supply water source therefore may be important considerations. The system characteristics that support this conclusion also point to the value of harnessing natural ventilation as a source of cooling in any climate where a more typical all-air mechanical HVAC system would be afforded a large number of economizer hours.

Table 9: Radiant+DOAS May–September HVAC system energy in the Los Angeles climate relative to the baseline VAV system.

HVAC System Energy, May - September	VAV	Radiant	Estimated Savings
Chillers (VAV only), cooling towers, and chilled water pumps (MWh)	2.17	1.58	**27%**
Hydronic system pumps and evaporative cooling spray pump (MWh)	n/a	0.94	
Fans (including cooling tower fan for waterside free cooling) (MWh)	4.92	0.75	**85%**
Boilers, natual gas (MWh)	0.001	0.000	**100%**
HVAC system electricity (MWh)	7.09	3.28	**54%**
Total HVAC system energy, including natural gas (MWh)	7.09	3.28	**54%**

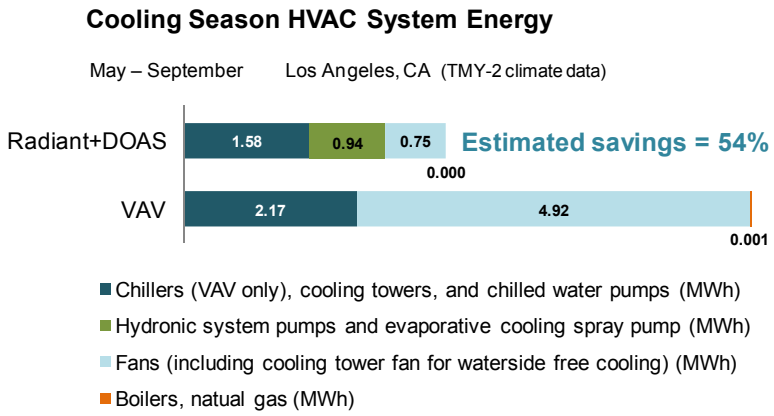

Figure 23: Estimated May–September HVAC system energy for Radiant Cooling (Radiant+DOAS) relative to the baseline VAV system in Los Angeles.

Table 10: Radiant+DOAS May–September HVAC system energy in the San Francisco climate relative to the baseline VAV system.

HVAC System Energy, May - September	VAV	Radiant	Estimated Savings
Chillers (VAV only), cooling towers, and chilled water pumps (MWh)	0.57	0.61	**-7%**
Hydronic system pumps and evaporative cooling spray pump (MWh)	n/a	0.20	
Fans (including cooling tower fan for waterside free cooling) (MWh)	4.10	0.69	**83%**
Boilers, natual gas (MWh)	0.128	0.083	**35%**
HVAC system electricity (MWh)	4.68	1.50	**68%**
Total HVAC system energy, including natural gas (MWh)	4.81	1.58	**67%**

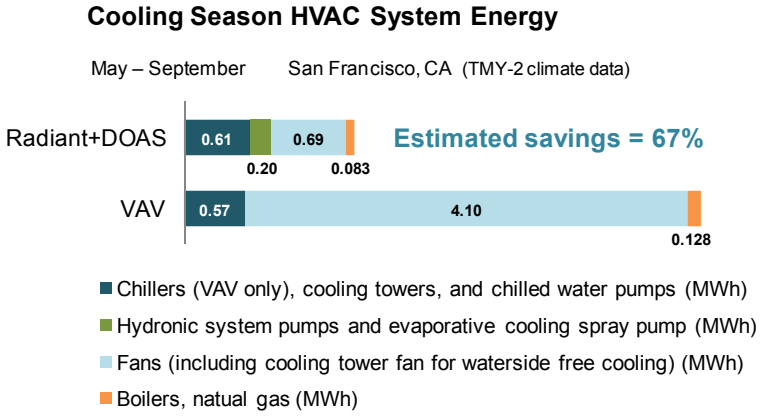

Figure 24: Estimated May–September HVAC system energy for Radiant Cooling (Radiant+DOAS) relative to the baseline VAV system in San Francisco.

Circulation pump power is a potentially significant contributor to hydronic radiant cooling system energy consumption. Because pump power is sensitive to the combination of water flow rate, tube sizing, and loop length, the degree to which these are optimized can significantly affect system energy consumption and the achievement of predicted savings. This stems from two basic pump laws: 1) pump head varies directly with the square of water flow velocity, and 2) pump power varies directly with the cube of flow velocity and volume. Thus, for example, if flow rate remains constant and tubing diameter is reduced by just one step in standard copper tube size—*e.g.,* from 3/4" to 5/8"—pump power for a representative set of system design parameters will more than double. If flow volume (and thus also flow velocity) is doubled for a given diameter and length of tubing, this will result in roughly 3.6 times the friction head loss per unit length of tubing and, for a representative set of pump and system parameters, on the order of 7.2 times the pump power. Apparently small changes in the design of individual hydronic loops can add up to significant differences in building energy consumption.

For *both* the Radiant+DOAS and VAV baseline systems, the combination of solar-control glazing and sufficiently optimized HVAC controls fully eliminates *simultaneous* heating and cooling for the months of May through September (this can otherwise be a significant source of energy consumption for VAV and similar system configurations using terminal re-heat as means of addressing the differing demands of perimeter zones with disparate solar loads). There is, for both systems, however, a small amount of non-coincident heating for the coolest mornings simulated.

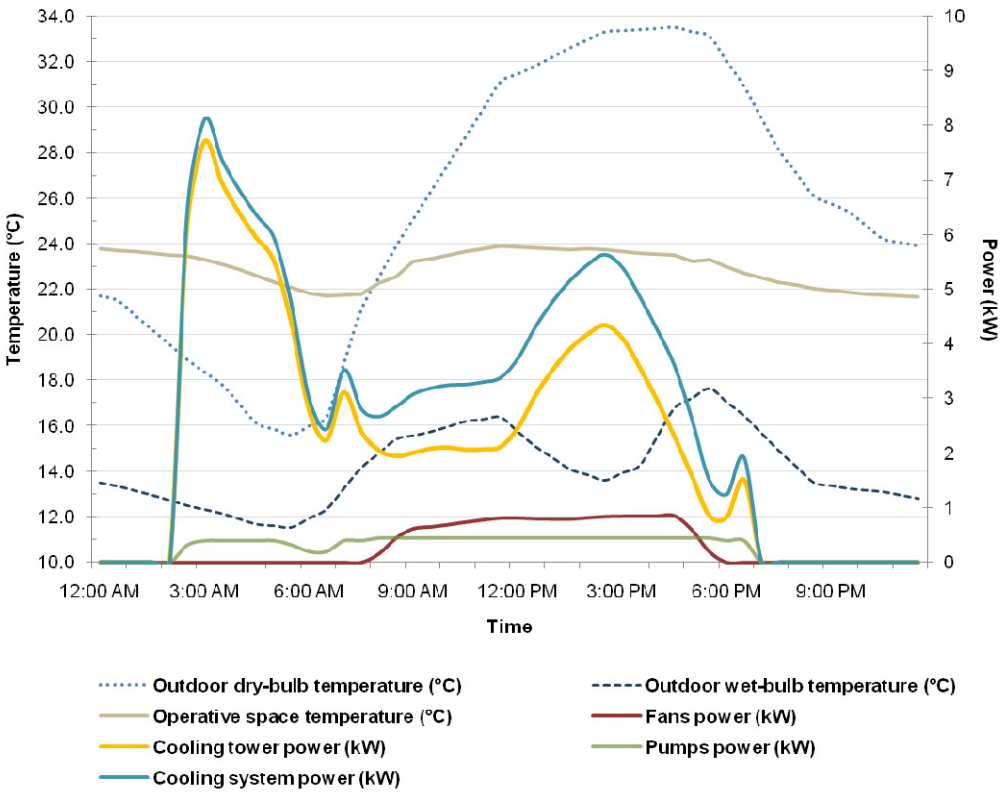

Figure 25: The same plot presented earlier in Figure 20 to illustrate the system operation and controls on a typically hot, sunny Denver Monday in August also illustrates the relative distribution of energy consumption (the area under each of the power curves) for the components of the Radiant+DOAS for the nighttime precooling cycle followed by normal daytime operation.

Peak power demand and precooling potential

Table 11: Cooling system peak power demand for the day and time of peak zone-level cooling, day of peak building-level cooling, all hours for the entire cooling season, and just the high-demand afternoon hours for the cooling season.

Building-level cooling system electrical power demand			Reduction from	
Day of peak *zone*-level sensible cooling (per top-floor west perime			VAV baseline	VAV+WSFC
VAV	22.6 kW	4:15 PM on 26 July	0%	
VAV+WSFC	11.83 kW	9:15 AM on 26 July	48%	
Radiant+DOAS	6.06 kW	12:45 PM on 26 July	73%	49%
Day of peak *bulding*-level sensible cooling (per combined demand for all zones)				
VAV	21.02 kW	12:45 PM on 16 August	0%	
VAV+WSFC	12.16 kW	9:15 PM on 16 August	42%	
Radiant+DOAS	6.56 kW	1:45 PM on 16 August	69%	46%
Cooling-*season* peak system-level electric demand (encompassing all hours)				
VAV	21.02 kW	12:45 PM on 16 August	0%	
VAV+WSFC	12.60 kW	10:45 AM on 2 August	40%	
Radiant+DOAS	8.32 kW	10:45 AM on 6 September	60%	34%
Cooling-season peak demand *during high-demand hours* (Noon to 6:00 PM)				
VAV	21.02 kW	12:45 PM on 16 August	0%	
VAV+WSFC	10.91 kW	12:15 PM on 3 August	48%	
Radiant+DOAS	6.56 kW	1:45 PM on 16 August	69%	40%

Cooling-season hours of high system-level electric demand during high-demand hours	
Number of hours of system electric power exceeding 6 kW between 12:00 noon and 6:00 PM	
VAV	408 hours
VAV + WSFC	402 hours
Radiant Cooling + DOAS	35 hours

The baseline VAV system electric demand tends to peak in the mid to late afternoon when loads are greatest. The VAV with WSFC system electric demand tends to peak in the mid to late morning when evaporative cooling opportunities overlap most with the typical midday rise in loads—*i.e.,* when significant loads coincide with relatively low outdoor wet-bulb temperatures. The system electric demand for the hydronic radiant cooling tends to peak in the very early morning hours when the precooling cycle begins, the slabs are still warm from the previous day, and evaporative cooling potential is greatest This is because the hydronic radiant cooling can take greater advantage of nighttime precooling to cool the core of the building fabric.

For the Denver climate, the combination of evaporative cooling and nighttime precooling opportunities, system efficacies, and thermal inertia of the slab-integrated hydronic cooling system reduced the seasonal peak cooling system power by 69% relative to the baseline all-air VAV system and 40% relative to the all-air VAV system with WSFC (Table 11, above).

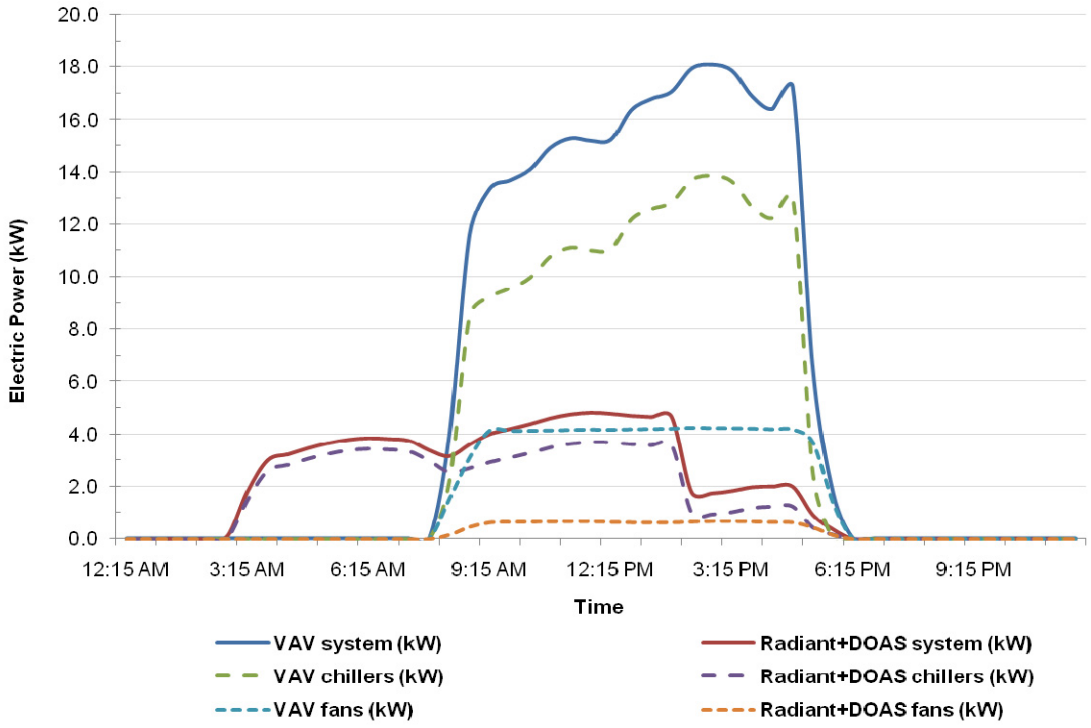

Figure 26: Cooling system, chiller/cooling tower, and fan power and energy (the area under the curves) for the radiant-plus-DOAS and VAV-baseline systems on a typical warm summer day in Denver, CO.

Figures 26 plots VAV baseline and Radiant+DOAS chillers, fans, and total HVAC system power over the hours of the day of peak cooling loads for the Denver climate. Chiller and fan operation are included in the cooling system total and plotted separately to show their contribution and operating profile for each of the two systems.

Figure 27 shows the chiller, fans, and cooling tower pump power for the VAV+WSFC system with and without precooling on a typical Sacramento, CA day in July with late-afternoon 35°C (95°F) DBT high, 21°C (70°F) coincident WBT, and preceding overnight low DBT of 12°C (54.6°F) at 5:00 AM. For this particular day, precooling permits the WSFC to operate for approximately three hours longer than in the VAV+WSFC system without precooling. For the control sequence and parameters modeled, this comparison shows how the increased fan energy approximately offsets the reduction in chiller operation associated with nighttime precooling.

Note that cooling tower pump power in Figure 27 is represented separately only when the system is in WSFC mode, and thus is an indicator of this mode. Pump power is combined with the chiller power whenever the chiller runs. Fan power for the cooling tower is added to the airside supply and return fan power. For the non-precooling case, fans run only from 8:00 AM to 6:00 PM (*i.e.*, there is no nighttime cycling). The afternoon fan-power plateau for both systems indicates maximum supply fan airflow, which is always the condition at which the system switches from WSFC mode to chiller operation for lack of sufficient WSFC capacity. Together, the cooling tower pump power and fan power plots indicate the operation of the WSFC mode, which tends to follow a drop-off in useful airside economizer operation and thus, outside of the precooling mode, occurs when supply airflow is at its maximum and OA is just slightly too warm to meet cooling loads. The systems then shift to chiller operation when the rising outdoor WBT and/or building loads result in cooling demand greater than the available WSFC capacity at that time step.

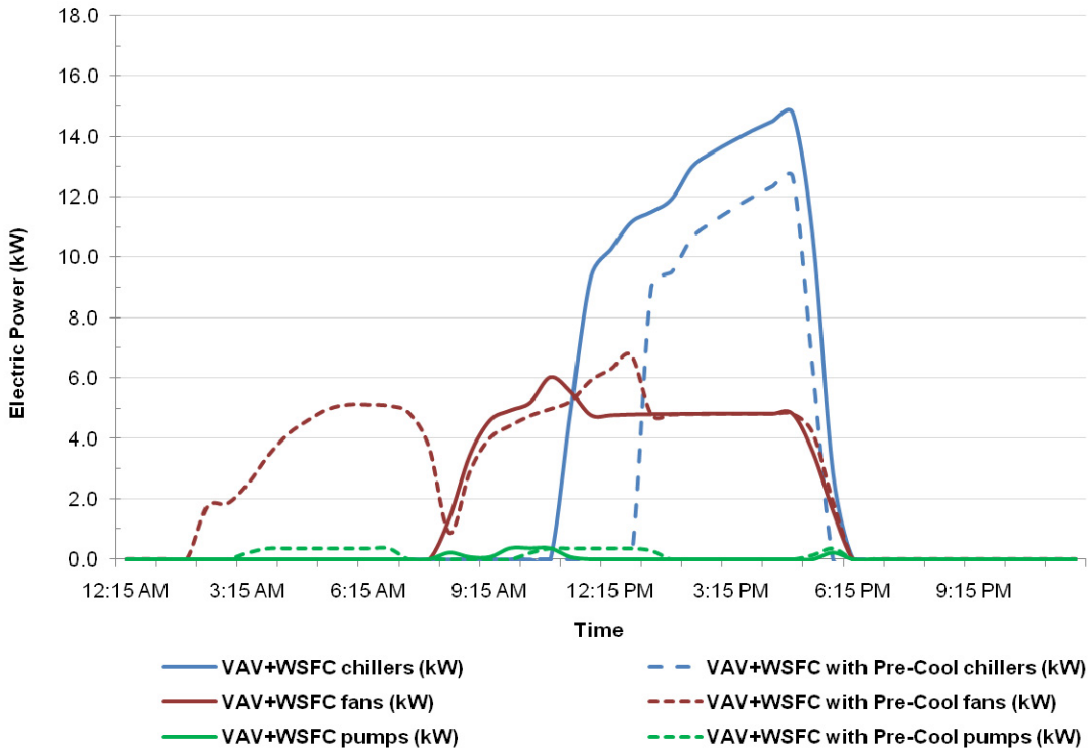

Figure 27: Chiller, fans, and cooling tower pump power for the VAV+WSFC system with and without precooling during a typical hot mid-July day in Sacramento, CA (TMY-2 climate data).

The baseline VAV system control strategy does not use night precooling. However, for the Denver and Sacramento climates, a VAV system with WSFC and a pre-cooling control strategy was modeled to determine the extent of saving associated with this approach.

The Denver VAV case showed energy savings for nighttime precooling with WSFC (Figure 21), but the Sacramento VAV case did not (Figure 22). The lack of energy savings with precooling in the Sacramento climate results from increased fan energy relative to the VAV baseline, which offsets the reduction in daytime chiller operation. This appears to stem from both the lesser WSFC capacity in that climate and limitations of the precooling strategy with the all-air system, as described below, in the context of warmer overnight temperatures. Relative to the Denver climate's cooler overnight temperatures, those of the Sacramento climate increase the amount of air needed to precool the space to the same temperature and/or the need for conditioning the air as a precooling medium. This increases the dependence upon WSFC as means of utilizing the wet-bulb depression in this relatively dry climate. Thus it appears that climates with warm overnight dry-bulb temperatures are less well suited to precooling with all-air systems with WSFC wherein the cooling tower is sized for chiller heat rejection (*i.e.,* the tower is not sized for meeting peak loads with just WSFC).

Where cooling energy was reduced for the Denver case (Figure 21), this was limited by two characteristics of the all-air system: 1) the tendency for overcooling the space at the start of the day; and 2) the limited capacity for WSFC when the cooling tower is sized to meet just the heat-rejection requirements of the chiller. The reason for the former is that the all-air system cools the surfaces in the occupied space, which then cool the occupants by radiant exchange when they arrive early in the morning, rather than the core of the building fabric. In Figures 28 and 29,

precooling with the VAV system brings the operative space temperature down to that of the precooling of the hydronic slabs. However, given the relatively superficial character of cooling the slabs via convective heat transfer at their surfaces, there is somewhat limited benefit from precooling with the all-air system once morning solar loads and internal gains begin to ramp up. In contrast to this, the hydronic radiant system cools the concrete slabs from the inside, and the delay of that cooling effect reaching the surface extends the potential for precooling the building without overcooling the occupants in the early part of the day.

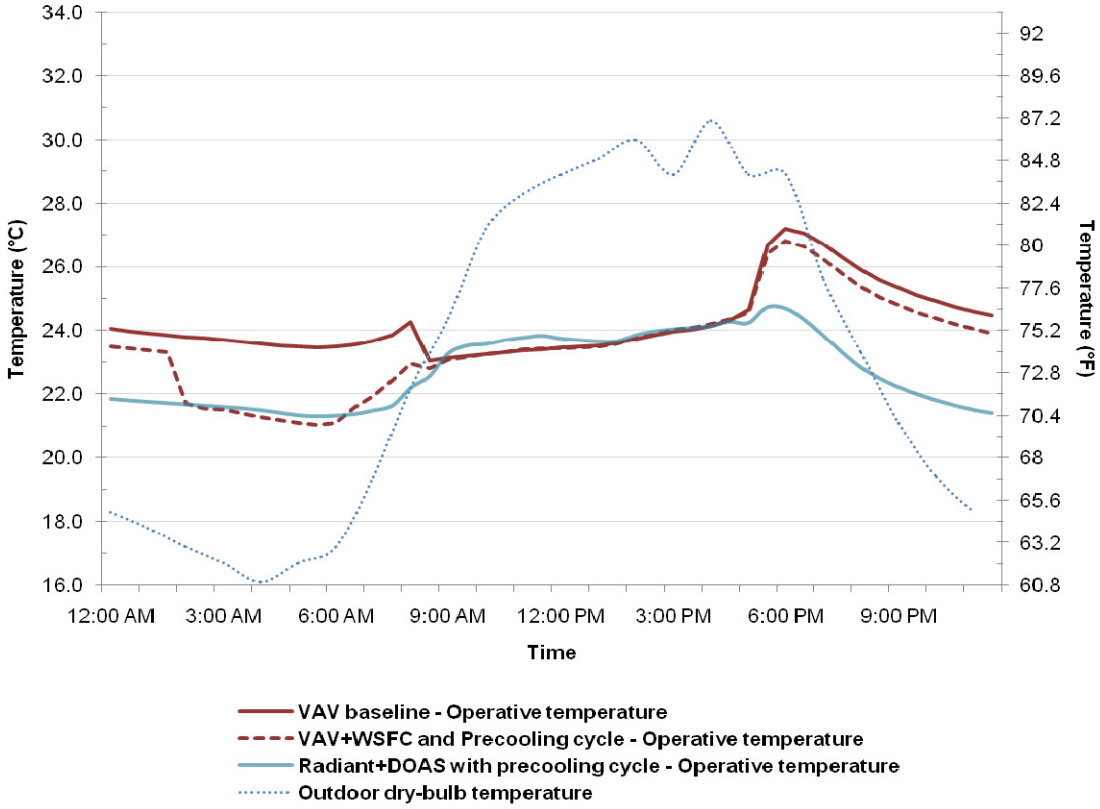

Figure 28: Outdoor dry-bulb and representative operative temperatures for a top-floor south perimeter zone for three alternative systems on the day of peak cooling loads in Denver CO (TMY-2 climate data), including the radiant-plus-DOAS, VAV-baseline, and VAV with WSFC and precooling cycle.

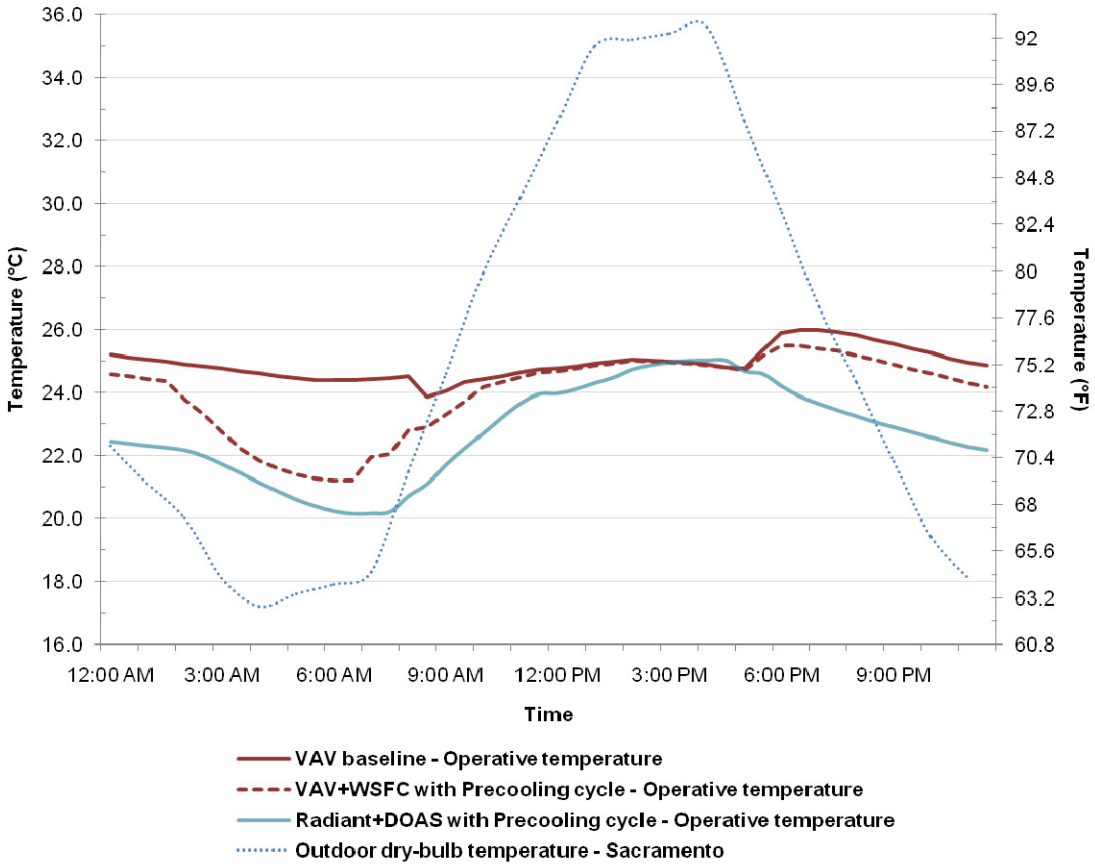

Figure 29: Outdoor dry-bulb and representative operative temperatures for a top-floor south perimeter zone for three alternative systems on the day of peak cooling loads in Sacramento CA (TMY-2 climate data), including the radiant-plus-DOAS, VAV-baseline, and VAV with WSFC and precooling cycle.

The reason for the sizing of the cooling tower in the all-air system just for chiller heat rejection is twofold: the use of air and cooling coils requires colder water, and thus a larger cooling tower as WSFC resource than is the case for the radiant-DOAS system and the all-air system still includes the cost of the chiller, since it cannot effectively make use of the relatively warm daytime supply water from WSFC. However, it is possible that some projects would opt for redundant chiller and WSFC capacity with large cooling towers, in which case the potential for precooling with WSFC would be that much greater. Indeed, there may be an optimal tower size that maximizes WSFC for some large fraction of typical cooling loads thus justifying a degree of redundant upfront investment in cooling capacity; however, determining this was not within the scope of this study.

Because the building fabric is consistent for both cases, and given climates with typical diurnal temperature swings above and then below the building balance-point temperature, the VAV system does benefit to some degree from the interior exposed mass of the concrete core, floor decks, and roof deck as thermal buffers (ceilings and core walls are exposed; floors are covered only by carpeting).

Cooling capacity

Peak radiant slab cooling capacity, as simulated within the top-floor west perimeter zone was 62.5 W/m^2 (5.8 W/ft^2). This was augmented by 12.0 W/m^2 (1.1 W/ft^2) coincident cooling from the DOAS, for a total of 74.6 Wm^2 (6.9 W/ft^2) peak sensible cooling. As discussed previously under *Chilled building components and surfaces*, this peak simulated cooling capacity is ~19% less than the theoretical maximum of 77 W/m^2 (7.2 W/ft^2 or 24 Btu/h-ft^2) for overhead chilled slabs that is described in the literature, even without counting the contribution from the carpeted floor slab surface. Simulations performed for this study indicate that this difference can be attributed to four factors: 1) the depth to which the hydronic tubing is embedded in the slab, which is a trade-off between cooling power and faster reaction time, on the one hand, and potential for nighttime precooling, on the other; 2) the tube spacing within the slab; 3) the warmer supply water temperature with just a cooling tower as compared to using a chiller; and 4) the supply water flow rate, which significantly affects circulation pump energy consumption. Furthermore, at the time of this peak hydronic slab cooling power, the DOAS was providing 12.0 W/m^2 (1.1 W/ft^2) cooling to the same occupied zone.

Modification of the chilled surface convective heat transfer coefficient according to correlations established by Novoselac et al. (2006) appear to provide a better representation of cooling capacity, even as a fixed coefficient based on design delta-T. In addition, given the effect is small when delta-T is small, replacing the variable coefficient that uses equations from Alamdari & Hammond (1983) with a fixed coefficient for just the chilled surface should not lead to significant errors either with a variable delta-T or when the chilled surface is inactive and allowed to drift toward equilibrium with the conditioned space. Using widely accepted variable coefficients for natural convection (Alamdari & Hammond 1983; CIBSE 2005), on the other hand, tends to underestimate radiant cooling capacity for overhead chilled surfaces by 3–9%, depending on the surface-to-air temperature difference and the mix of radiant vs. convective loads in the space. The less well-established—thus less likely to appear in any simulation tool—Awbi & Hatton (2000) equations, however, appear to predict cooling capacity within 1–3% of the experimental correlations developed by Novoselac et al. While the differences in convective heat transfer coefficients are closer to 20% in the case of the Alamdari & Hammond, the mix of radiant *vs*. convective loads and the predominantly radiant cooling effect of flat overhead chilled surfaces dilute the difference with respect to overall cooling capacity of the chilled surface.

As described in the previous section on cooling system controls, flow to each hydronic cooling slab is modulated between zero and maximum design flow during precooling according to a temperature sensor in the adjacent occupied space, as needed to prevent the occupied space from being overcooled. There is potential for some overcooling to occur as a result of thermal inertia. However, the massive slabs change temperature gradually enough during precooling that the slab surface temperature overshoot tends to stay within the comfort range. For example, even on a relatively cool morning following a full precooling cycle—*i.e.,* a nighttime precooling cycle that includes peak cooling tower heat rejection as well as operation for the maximum duration of the cycle—operative temperatures for all spaces are tightly grouped within the target space-conditioning temperature range (Figure 31), in the Thermal comfort section below).

Simulation results indicated an unanticipated synergy between pre-cooled exposed ceilings in the interior zones and the conditioned ventilation air ducts passing through those zones: For the baseline VAV system, wherein the room surfaces tend to be much warmer, the ductwork near the ceiling picks up heat from both warm air and warm surfaces; the ducts adjacent to chilled slabs, however, were able to transfer some of the relative excess cooling capacity from the interior to perimeter zones, where peak loads per unit area are on the order of four times as high.

Thermal performance and thermal comfort

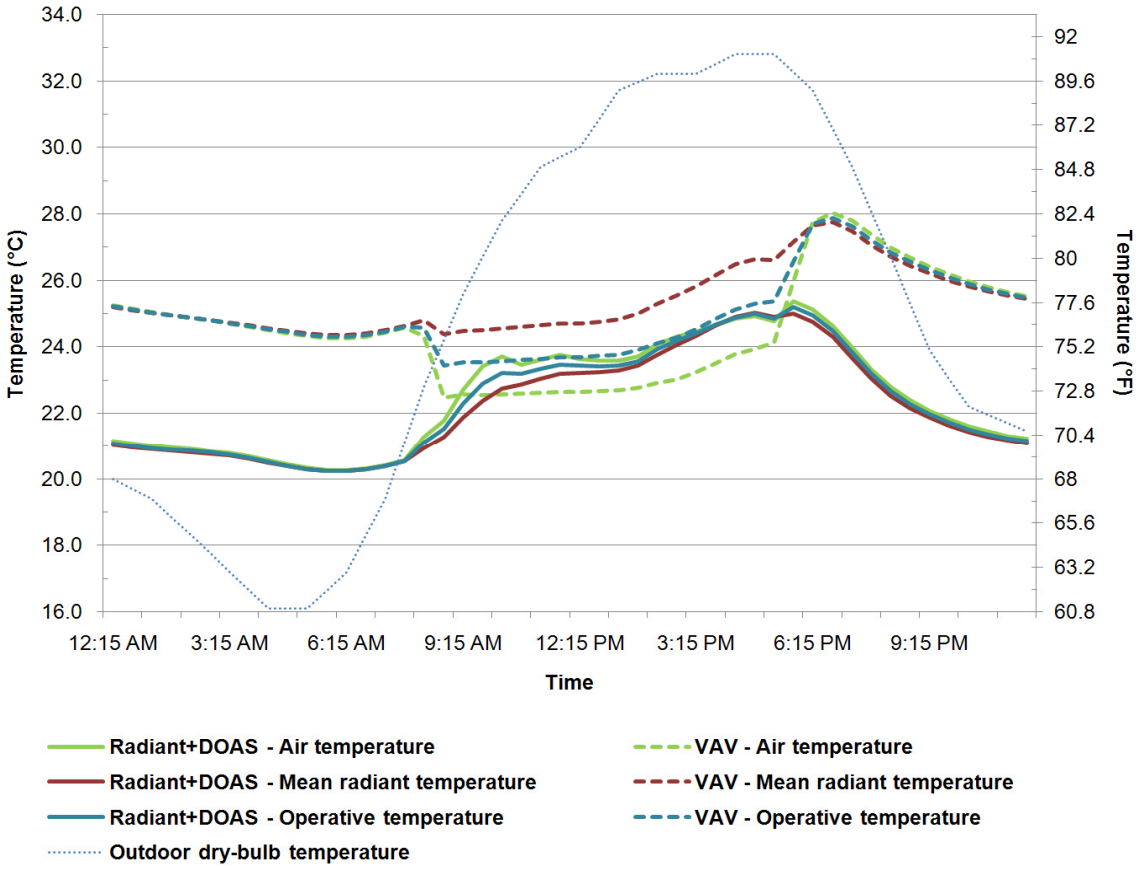

Figure 30: Air, mean-radiant, and operative temperatures for Radiant+DOAS vs. baseline VAV systems for the top-floor west perimeter zone on a typical warm, clear day in Denver.

Both systems were capable of controlling the interior *air* temperature consistently below 25°C (77°F) for *all* hours of the May through September cooling season. However, because the all-air system must cool surfaces via convective heat transfer; all interior surfaces tend to be warmer than the air during cooling operation. When there is significant incident solar radiation striking the window glazing, the mean radiant temperature (MRT) in the spaces conditioned by the all-air system tends therefore to be considerably more elevated than for the same set of surfaces in the spaces conditioned by the radiant cooling system. Figure 30 provides a clear illustration of how the all-air VAV system maintains the desired air temperature while allowing the surface temperatures to run considerably higher. This spread between air temperature and MRT results in an elevated operative or dry resultant temperature.[4] In contrast to this, the radiant cooling system maintains the MRT just *below* or equal to the air temperature, with the most pronounced difference occurring at the beginning of the day, when both internal and solar gains are ramping up and the chilled slab is at its coolest temperature for the day.

[4] Dry resultant temperature is the combined effect of the dry-bulb air temperature and the mean radiant temperature at a given location in a space. Operative temperature is similar to dry resultant temperature, but also includes the effects of air movement. However, in cases where air movement is assumed to be 0.1 m/s or less—essentially still air—operative and dry resultant temperature are effectively the same.

Figure 31 shows the number of May through September hours for which the operative or dry resultant temperature is elevated above 25°C (77°F). This is accounting for both air and mean radiant temperatures. These results suggest that the simulated radiant cooling capacity and control strategy exceed the goal of ensuring comparable performance. Furthermore, they suggest that radiant cooling may provide improved comfort in certain perimeter-zone environments.

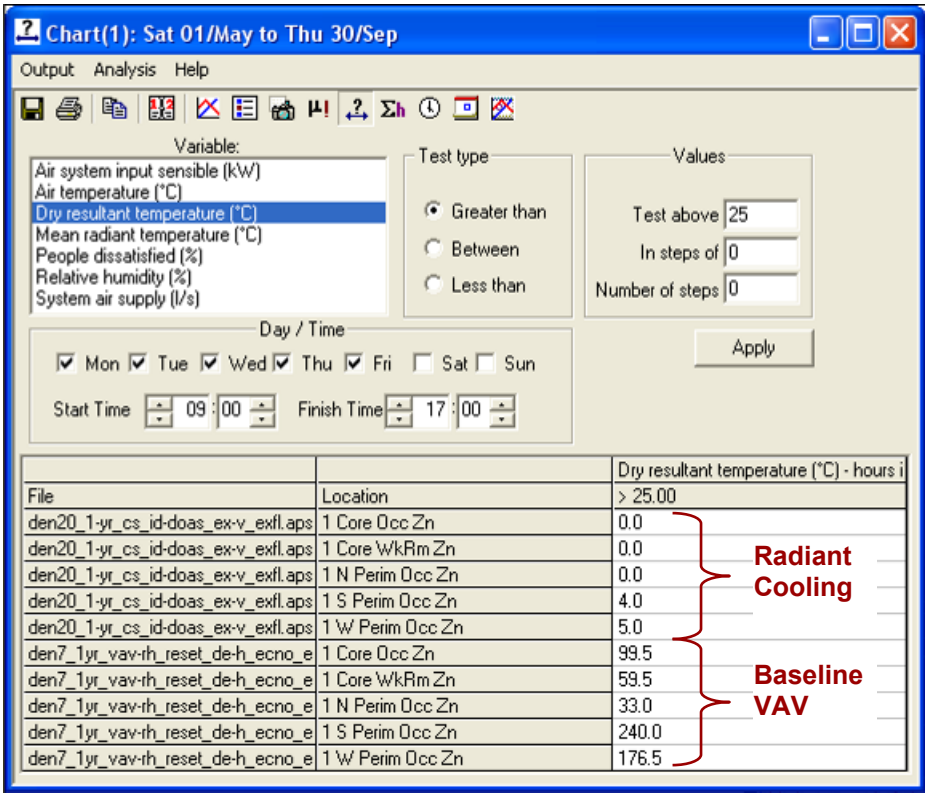

Figure 31: Comparison of May through September hours within the conditioned spaces that exceeded 25°C dry resultant (operative) temperature.

Thermal comfort results for the radiant cooling were in compliance with ASHRAE Standard 55-2004 for all regularly occupied hours in May through September. The standard requires that percent people dissatisfied (PPD) be maintained below 10%. This was determined with a 75 W occupant activity level (equivalent to a 70-kg person performing sedentary office work at a metabolic rate of 1.0 Met) and minimal monthly adjustment of clothing, with the lightest clo value equal to 0.5 for the hottest month.

Even with aggressive nighttime precooling of radiant slabs, as evidenced by peak cooling tower operation between 2:00 and 8:00 AM following a hot weekend, the conditioned spaces are not overcooled (Figure 32): operative temperatures in three representative spaces are maintained well within the desired range for thermal comfort. In addition, the mass and thermal decrement of the concrete chilled slabs evens out the fluctuating cooling capacity of the cooling tower over the course of the day such that interior operative temperatures remain relatively constant.

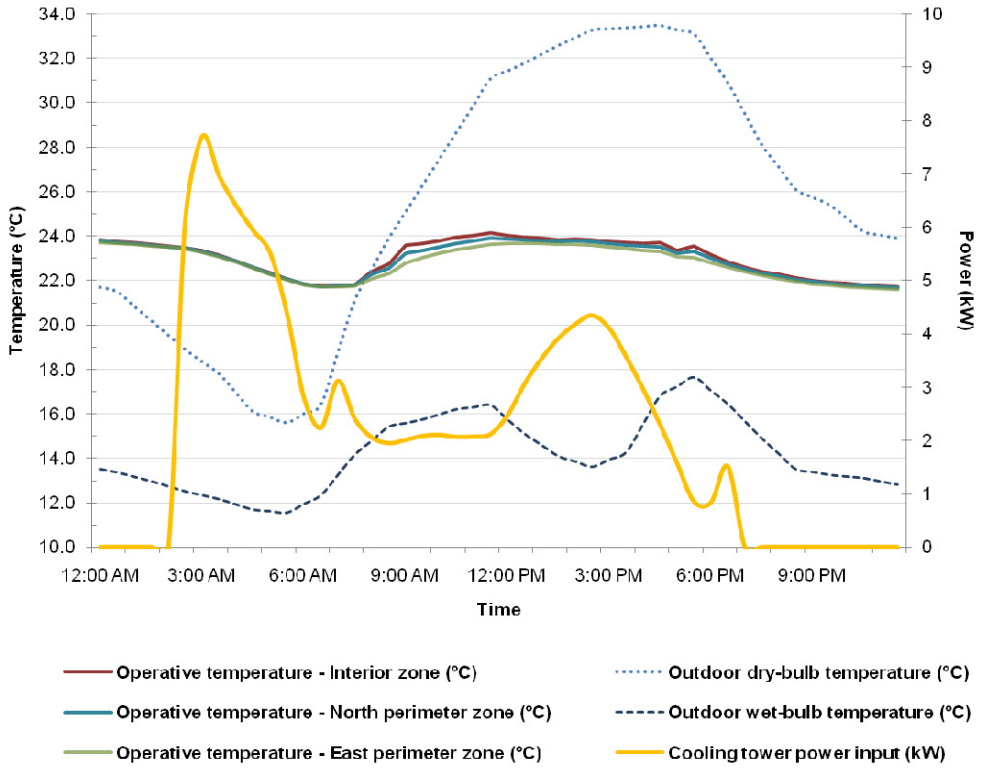

Figure 32: Nighttime precooling of radiant slabs and maintenance of thermal comfort within conditioned spaces are illustrated by cooling tower operation between 2:00 and 8:00 AM at the start of a cool Monday morning proceeded by a hot weekend and followed by similarly hot midday temperatures.

In the case of Sacramento, outdoor WBT tends to be higher than for the other three climates investigated. On many typical summer days it is high enough that the cooling tower can provide very little useful cooling capacity above and beyond what is already stored in the mass of the concrete slabs. The effectiveness of the precooling scheme is therefore much more critical to maintaining thermal comfort in the conditioned spaces. This is particularly the case for the west perimeter zones where the peak solar loads are greatest at the very end of the day. At this time, the slab thermal mass has been soaking up heat throughout the day and there has been insufficient early-afternoon evaporative cooling capacity to re-charge the depleted slabs. Thus, while the outdoor WBT may have dropped somewhat by this time of day, the cooling effect reaching the surface of the slab will need to have been introduced hours earlier. Even under such conditions, however, precooling of the slab core resulting in early morning space temperatures of 21°C (~70°F) led to a peak operative temperature of 26.5°C (79.7°F) at 5:00 PM. As shown in Figure 34, this is consistent with the operative temperature for the baseline VAV system at the end of the day under the same conditions. And, even without a change in activity or clothing level throughout the day, the pre-cooled slabs in the Radiant+DOAS system maintained the ASHRAE Standard 55 thermal comfort criteria of 10% maximum PPD during the occupied hours of that day (Figure 33).

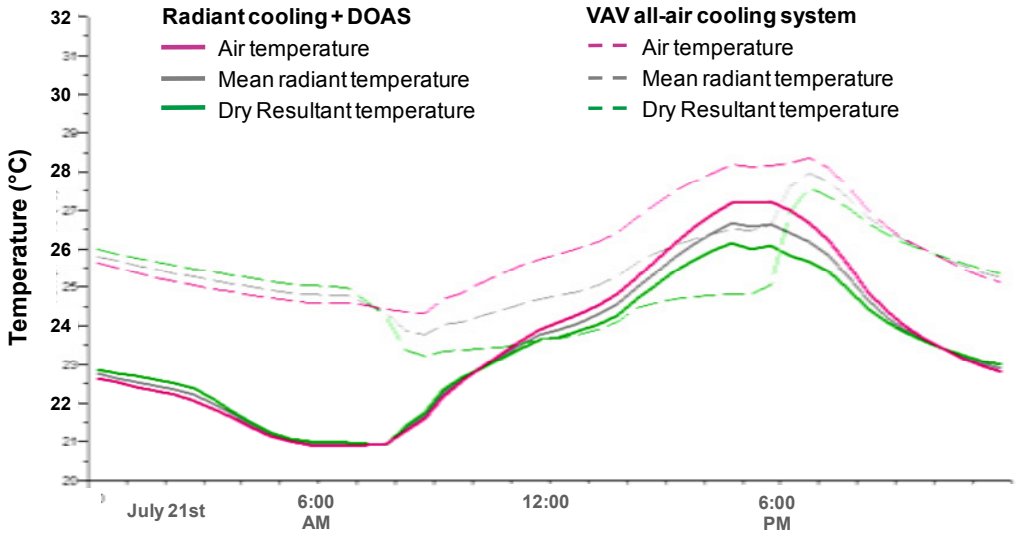

Figure 33: Air, mean-radiant, and dry-resultant temperatures for the Radiant+DOAS vs. baseline VAV systems for the top-floor west perimeter zone on a very typically hot, clear summer day in Sacramento with peak outdoor DBT of 33°C (91.4°F) and WBT in excess of 20°C (68°F).

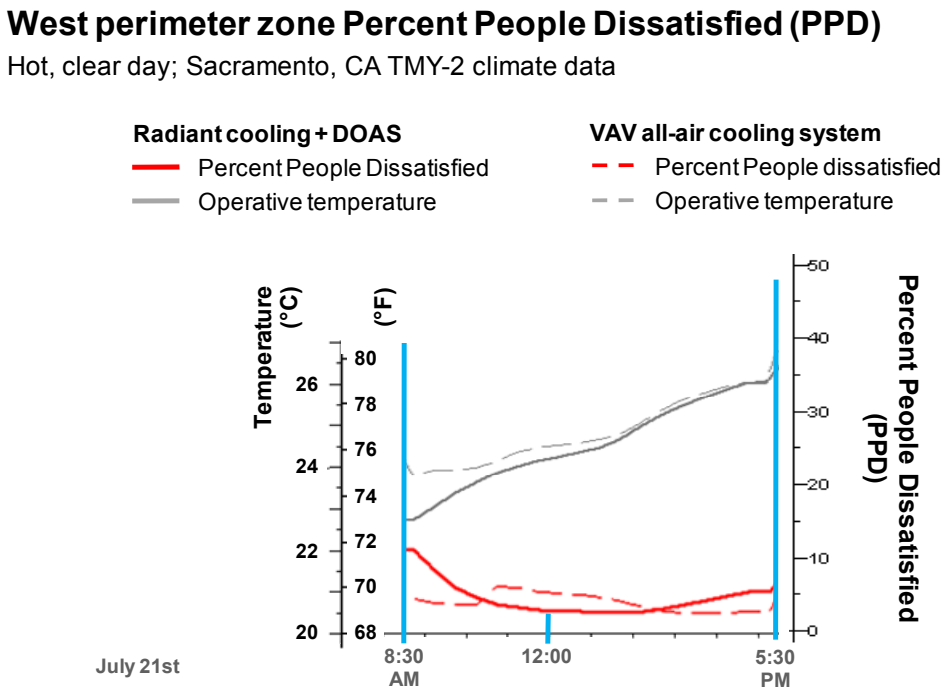

Figure 34: Operative temperature and percent people dissatisfied thermal comfort rating in a critical space—the top-floor west perimeter zone—on a hot, clear day in Sacramento.

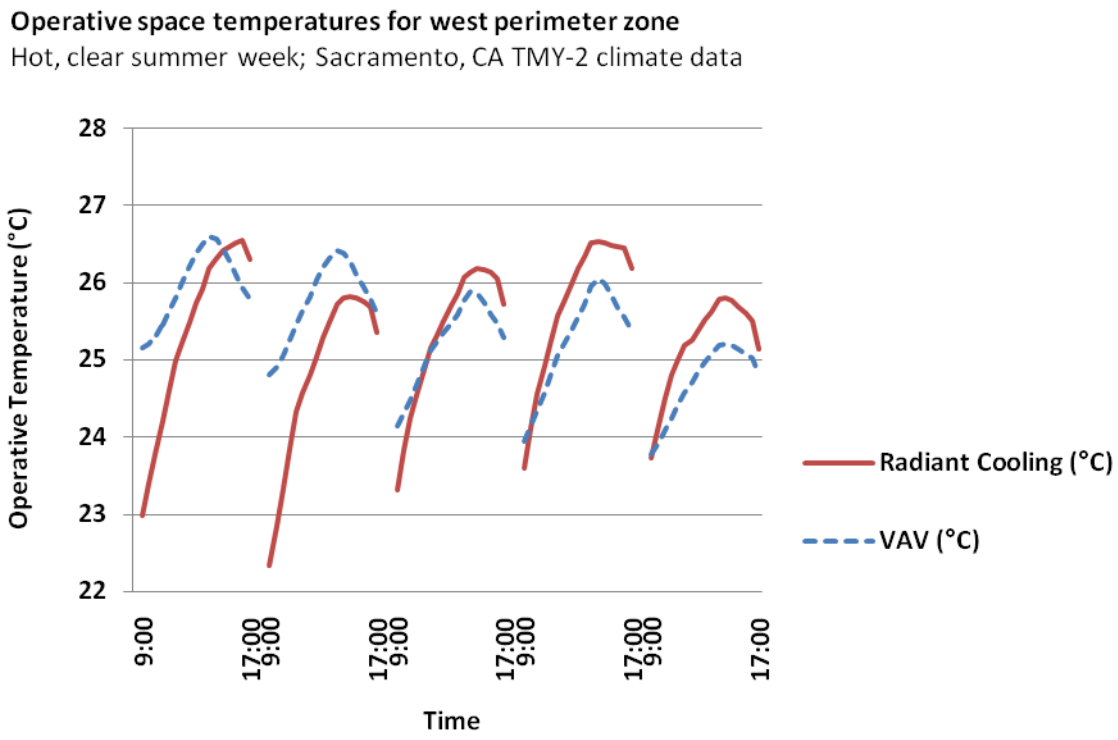

Figure 35: Operative space temperatures during occupied hours for the VAV and radiant cooling in the top-floor west perimeter zone during a hot summer week in Sacramento, CA.

Figure 35 shows a pattern that was relatively common during extended periods of consecutive hot days with wet-bulb temperatures high enough to significantly constrain both the midday and nighttime indirect-evaporative cooling capacity of the radiant system. In this extreme case, including the two hottest days in the Sacramento climate data operative space temperatures gradually rise during the three days in the middle of the week. This five-day period immediately follows an equally hot weekend during which all mechanical systems were off and the building was soaking up heat. While the VAV system gradually recovers from the preceding weekend "hot soak," the peak operative temperature for the Radiant+DOAS at the end of Thursday is similar to that of the preceding Monday.

Even without humidity control (see system descriptions in previous sections), and given the dry Denver climate, both systems provided interior conditions reasonably consistent with ASHRAE Standard 55: Both had fewer than 10 operational hours within the cooling season for which the humidity ratio exceeded 0.012 kg/kg (0.012 lb/lb). This limit is equivalent to 64% relative humidity (RH) at 75°F (24°C). Both had fewer than 5 hours with RH greater than 64%, and in no instance was this coincident with peak cooling loads or space temperatures. For more humid climates, however, these systems would be set up and operated to control humidity using an appropriate cooling coil temperature reset for in the all-air VAV system and desiccant-wheel dehumidification in the case of the DOAS.

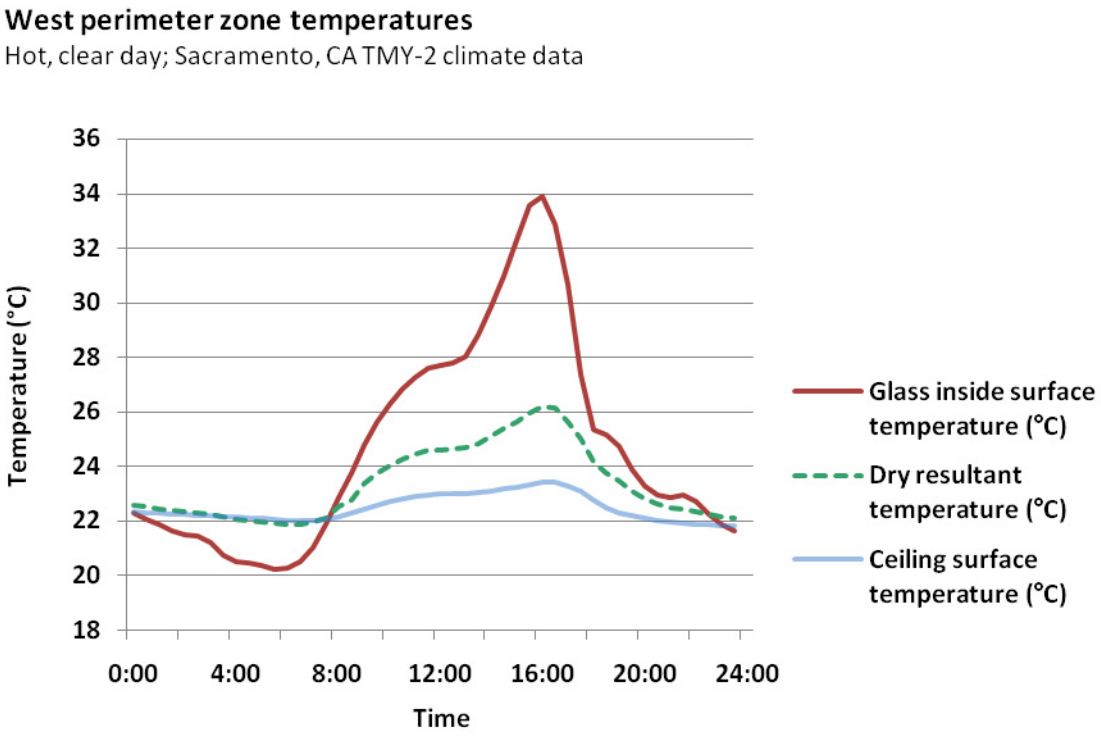

Figure 36: Elevated window glass inside surface temperatures are offset by much lower ceiling surface temperatures associated with a chilled overhead hydronic radiant cooling slab in a west-facing perimeter zone on a hot, clear day in Sacramento.

While radiant asymmetry is increased with radiant cooling when inside glass surface temperatures are significantly elevated, as is the case for in the west perimeter zones of the modeled prototype building on this hot day in Sacramento (Figures 36), CBE research completed for the National Fenestration Rating Council (Huizenga et al. 2006) suggests that this degree of asymmetry is not problematic and that the balancing effect of the chilled ceiling results in occupant comfort in keeping with the resulting operative space temperature.

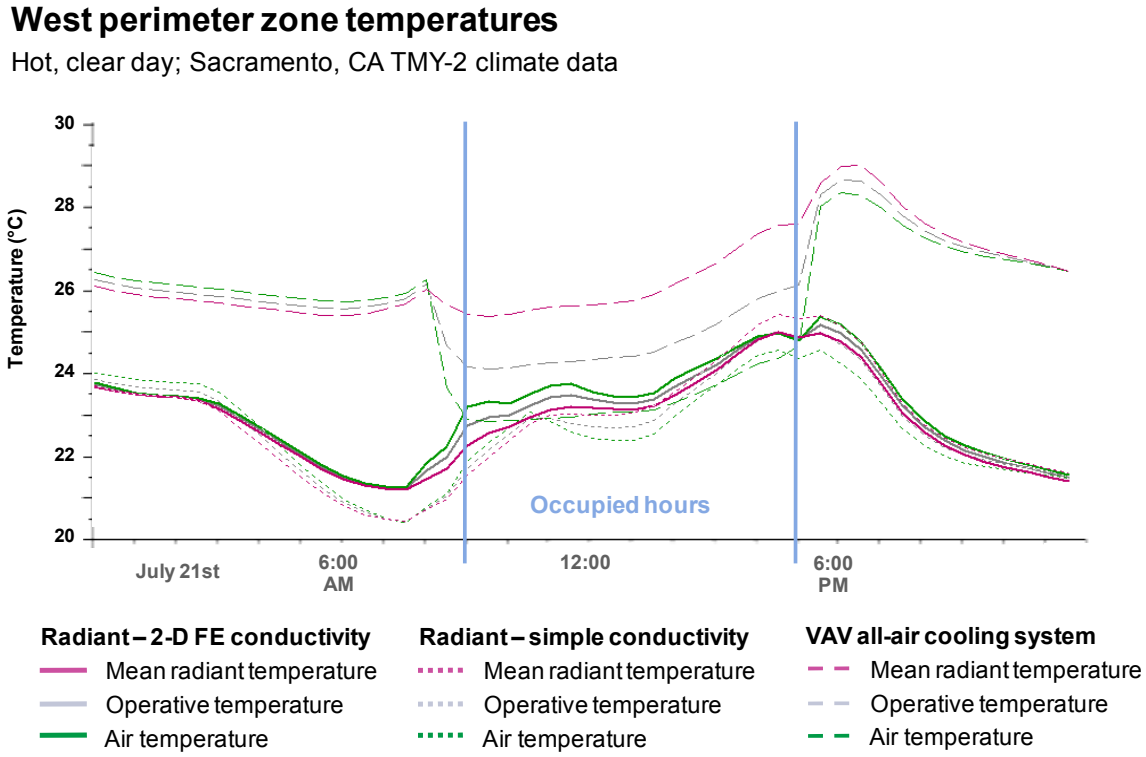

Figure 37: Operative space temperatures during occupied hours for the VAV and radiant cooling in the top-floor west perimeter zone during a hot summer week in Sacramento, CA.

Two-dimensional finite-element modeling of heat transfer paths between the hydronic tubing and cooling surface of the chilled concrete slab yielded 20–40% lower effective conductivity for a given tube size, spacing, and depth than was calculated via alternate methods (ASHRAE 2005; Gough 2007). This difference is most pronounced for larger hydronic tube-spacing values. The principal implications of the reduced conductivity are reduced peak cooling power of the chilled surface for a given supply water temperature and flow rate, a longer slab temperature time constant resulting in slower reaction to changes in load or supply water parameters, and added capacity for precooling in advance of midday and afternoon peak cooling loads for a given slab mass and hydronic tubing depth.

The reduced conductivity of the slab material shifted and slightly reduced the temperatures fluctuations during occupied hours as shown in Figure 37. The pattern of operative space temperatures with the Radiant+DOAS with the reduced slab conductivity more closely follows the pattern of the air temperatures for baseline VAV system over the same occupied hours. In this instance, the operative temperatures for the VAV baseline are consistently higher as a result of solar heating of the building envelope.

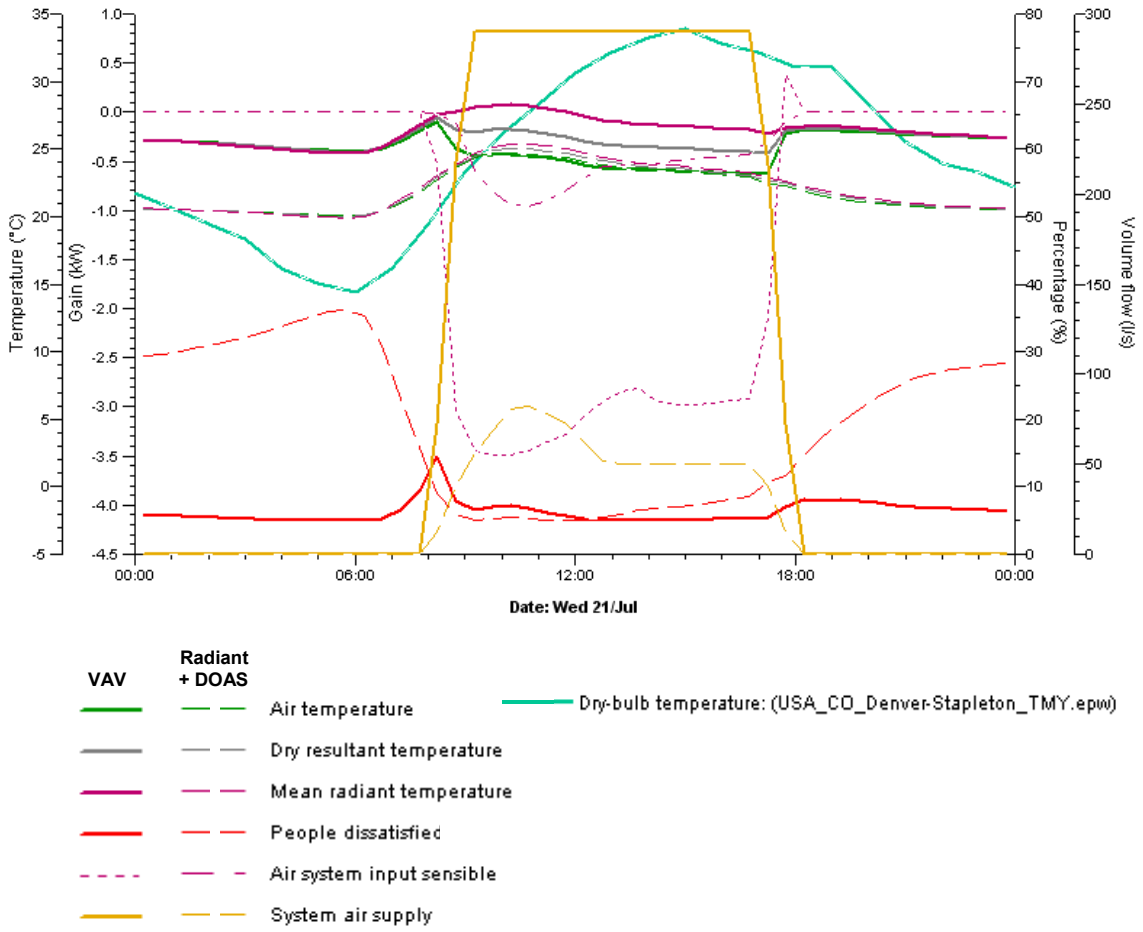

Figure 38: Simulation results show the relative behavior of the two systems in terms of sensible space conditions, airflow volume, airside sensible heat extraction, and PPD for an east perimeter zone on a typical hot day.

Figure 38 illustrates typical behavior of the radiant cooling system as compared to the VAV system for an east perimeter zone: The radiant cooling system begins the day with stored cooling capacity and a low space temperature and then, relative to that of the VAV system, maintains similar air temperatures, a lower MRT (more consistent with the air temperature), and thus lower operative temperature. Whereas the VAV system has a peak airside extraction rate from the zone of approximately 3.5 kW (shown in Figure 39as air system sensible input in the form of negative gain), the airside extraction rate for the DOAS that is paired with the radiant cooling system is less than 1.0 kW. In parallel with sensible cooling from the slower-responding chilled thermal mass and its buffering potential, this roughly 70% smaller peak airside cooling effect is sufficient to manage the transient solar gain peak just as well as the VAV system.

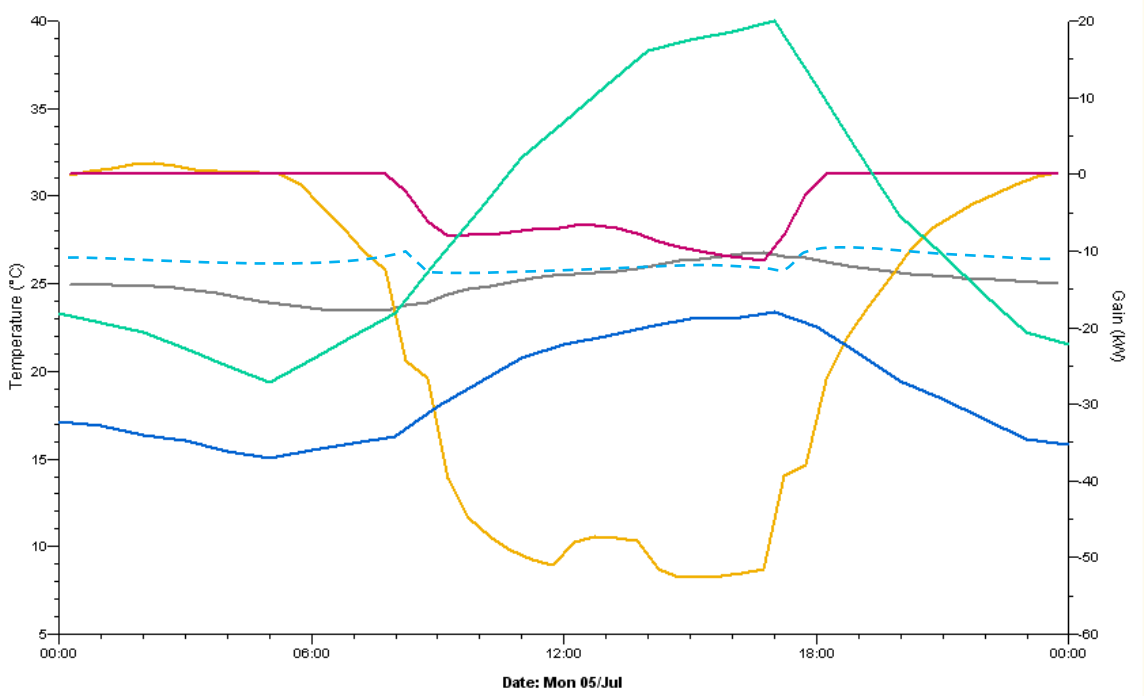

Operative space temperature using radiant cooling plus DOAS (°C)
Operative space temperature using VAV system as point of reference (°C)
Sensible cooling provided by hydronic radiant slabs – negative heat gain (kW)
Sensible cooling provided by DOAS ventilation – negative heat gain (kW)
Outdoor dry-bulb temperature (°C)
Outdoor wet-bulb temperature (°C)

Figure 39: Space temperatures, cooling heat transfer, and coincident outdoor environmental conditions for the day of peak cooling loads in Sacramento CA (TMY-2 climate data).

From a gross, building-wide perspective, the thermal performance of the modeled low-energy radiant cooling plus DOAS differs only subtly from that of the baseline VAV system. Figure 39, illustrates this: even on the hottest day in the TMY-2 climate data file for Sacramento, which is the most challenging of the four climates with respect to capacity and control of the precooling strategy, the combined average operative space temperature for all regularly occupied zones (solid gray line) closely follows that of the same parameter for the VAV system (dashed light-blue line). The peak sensible cooling provided by the hydronic radiant slabs in Sacramento occurs at 3:15 in the afternoon that day when the outdoor wet-bulb temperature is 23°C (73.4°F) and the hydronic pumps have been shut off for over three hours to avoid adding heat to the slabs. At that time, just 16% of the total cooling is provided by parallel sensible cooling via the DOAS. Thus precooling of the slab with water from a cooling tower and augmentation by indirect evaporative cooling of ventilation air would appear to be an effective strategy for low-energy cooling in climates such as Sacramento.

Continued development of the model and methods

While the model and methods presented here begin to get at some of the nuances associated with hydronic radiant cooling with a cooling tower as chilled water source and indirect-evaporative-cooled ventilation air, there is still plenty of room for improvement in terms of accurate representation of system dynamics and practical application in the design context.

Targeted future developments include refinement of four essential components of the radiant cooling and DOAS models: 1) The cooling tower model should be further developed to reflect variations in the supply water temperature range and approach to the outdoor wet-bulb temperature with changes in both the entering water temperature and outdoor wet-bulb temperatures; 2) There should be means of coupling this more complete cooling tower model directly to the hydronic cooling loop; 3) The waterside hydronic cooling model should permit supply water temperature and/or flow control to a slab *surface* temperature, rather than slab core or room temperature; 4) The dedicated outside air system would benefit from an appropriate desiccant wheel component in the airside HVAC network. The latter would permit modeling heat-driven regeneration of a desiccant wheel for dehumidification of supply air, thus extending the range of climates in which the radiant cooling plus DOAS could be effectively simulated and thus more effectively explored as a design option.

9. CONCLUSIONS

The simulations demonstrate that hydronic radiant cooling using an evaporative supply water source in conjunction with a dedicated outside air system has significant potential for energy savings. As compared to a well-optimized conventional VAV system in the Denver, Sacramento, Los Angeles, and San Francisco climates, with and without a waterside economizer or "free cooling" and a nighttime precooling cycle, estimated energy savings ranged from 54% to 71%. Peak cooling-system electric power demand on hot summer afternoons was similarly reduced. Furthermore, the Radiant+DOAS was capable of providing comparable and sometimes improved thermal comfort. However, the extent of energy savings achieved while meeting high standards for thermal comfort, particularly under extreme conditions in the hottest two of these climates, appears significantly dependent upon design and control strategies that take advantage of the large cooling surface and thermal mass associated with the radiant chilled slabs.

Dynamic thermal simulation tools with practical capability for modeling and examining building physics, systems, and controls are valuable not only for evaluating potential energy savings, but also for informing design and control strategies. Furthermore, fair comparison of alternatives, including combinations of air and water systems and varying degrees of mixed-mode operation, requires the simulation tool to be equally capable of modeling a range of airside options and configurations, including natural ventilation. For this project, the ability to model sophisticated controls for the VAV system on the one hand and integrated operation of the hydronic-radiant and airside systems on the other was essential to the determination of their relative merits.

Energy use for the Radiant+DOAS was minimized by careful design of the system and controls. Component sizing and configuration contributed significantly to reducing energy consumption for the pumps, cooling tower, fans, and indirect-evaporative spray pump. Controls were designed to maximize nighttime precooling and passive operation of the slab as a heat sink. Three control strategies were essential: 1) turn off cooling water to any given slab when the water temperature from the cooling tower exceeds the slab core temperature; 2) avoid cooling the slabs in the late afternoon and evening hours, even when the outdoor WBT is low—*i.e.,* begin the nighttime precooling only after the outdoor WBT has dropped significantly *and* the slab core temperature is approaching equilibrium with the occupied space; 3) constrain precooling to avoid overcooling occupied spaces in early morning hours. Together, these control strategies fully utilize the slab thermal mass and the extended nighttime cooling-tower capacity.

While it reduced the peak cooling power of the radiant slabs with respect to transient loads, embedding the hydronic tubing in the center of 200-mm (8-in) thick concrete floor/ceiling slabs facilitated the indirect-evaporative precooling strategy. Had the slab mass been less or the tubes closer to the surface, the useful precooling capacity would have been reduced. In hot climates, successful reliance upon an evaporative source of supply water for this system may depend on such a strategy to maximize both the capacity of the slab as a heat sink and the usefulness of cooling hours when the outdoor WBT is low. Clearly, such a system would also benefit from minimization of transient loads. A simple two-dimensional finite-element model proved valuable in determining the effective conductivity of the heat transfer paths from the hydronic tubing to the slab surface, and thus the thermal behavior of the system design and controls.

A similar precooling control strategy was applied to the VAV system with WSFC—emphasizing nighttime availability of cool outside air and efficient WSFC operation as needed during those hours to arrive at a comparable operative temperature prior to daily building occupancy. This yielded energy savings up to 24% relative to the baseline VAV (without WSFC). In contrast, the Radiant+DOAS achieved energy savings as high as 71% relative to the baseline VAV system. The difference can be explained by the reduced energy intensity of moving heat via water rather than air and by the capability of the hydronic radiant system to much more effectively take advantage of the thermal mass in the concrete slabs.

APPENDIX A:

VISUALIZATION OF CLIMATE-RELATED OPPORTUNITIES FOR LOW ENERGY SUPPLY-WATER, LOAD-SHIFTING, AND DEHUMIDIFICATION STRATEGIES FOR RADIANT COOLING SYSTEMS

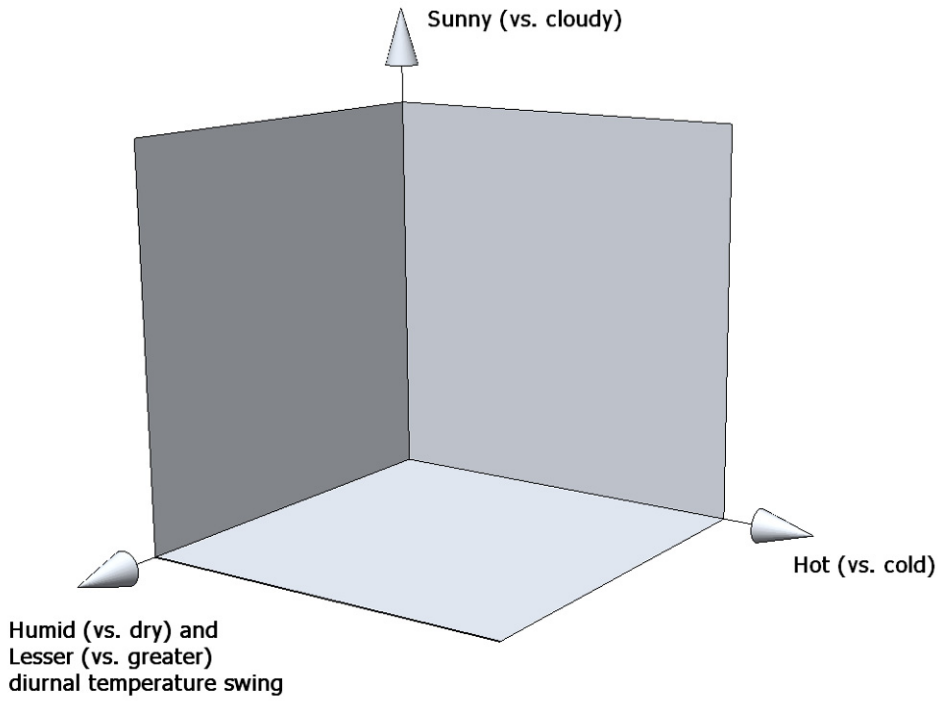

Figure A1: A three-dimensional chart affords visualization of relevant climate parameters for climate-based selection and design of low energy supply-water, load-shifting, and dehumidification strategies for radiant cooling systems. These climate parameters include cooling-season temperatures, humidity, and solar resources. This might be thought of as similar to a psychrometric chart with the added dimension of clear vs. cloudy skies. While there may be exceptions, the extent of diurnal temperature swing tends to increase with dryness of climate, and thus this parameter has been paired with humidity. It's important to keep in mind that for core-load dominated buildings the cooling season may encompass the entire year.

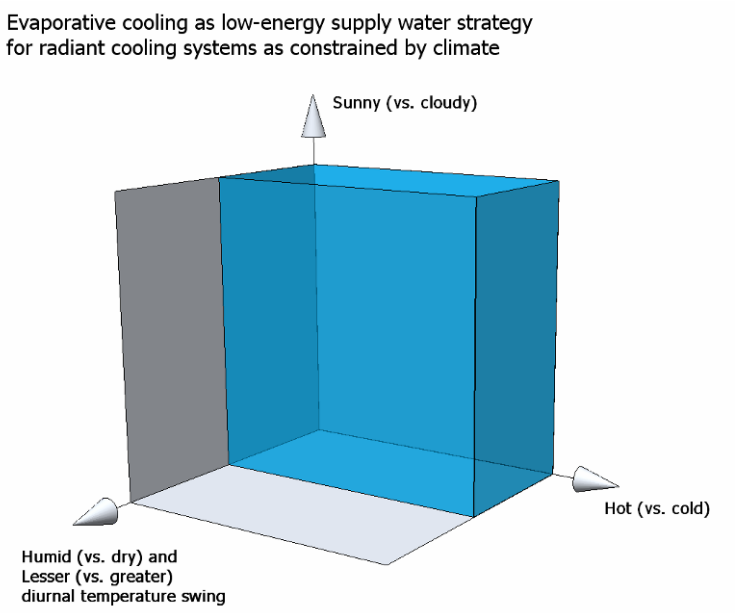

Figure A2: Evaporative cooling as a low-energy source of supply water (e.g., cooling tower only) for radiant cooling systems is most effective in dry climates. If humidity varies significantly, this can constrain the supply water temperature and thus cooling capacity. Indirect evaporative cooling of supply water may be extended to more humid climates with desiccant pre-treatment systems. Just as for evaporative cooling of ventilation intake air without increasing its moisture content, drying by desiccants can increase the evaporative cooling potential in an evaporative water cooler. However, the desiccant requires a regeneration heat source (Figure A5).

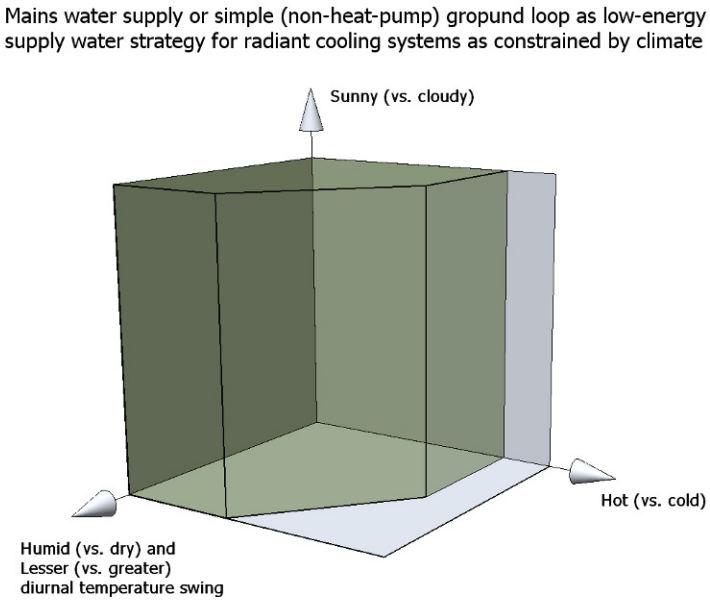

Figure A3: Use of cold water from municipal mains or a simple ground loop (i.e., without heat pump) is limited by two climate parameters: Depending on the building, the cooling capacity provided by ground-temperature water may limit applicability in very hot climates; Hot, humid climates will tend to have less diurnal and seasonal temperature swing, and thus ground temperatures closer to summer ambient air temperatures.

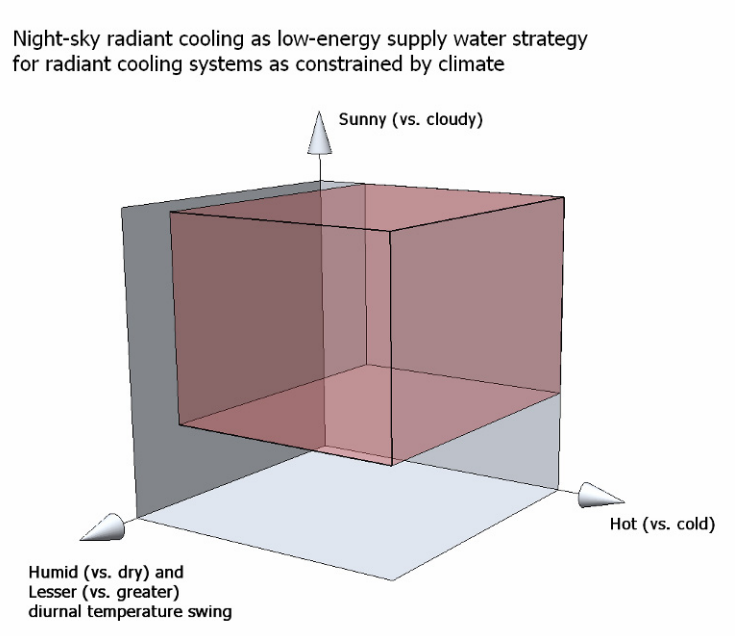

Figure A4: Night-sky radiant cooling requires access to the clear sky and is thus limited mainly by cloud cover. Some daytime radiant cooling of supply water may even be feasible with appropriate roof-top emitter design and clear-sky conditions—especially for core-load-dominated buildings in cooler climates. However, to the extent that cooling is required in winter conditions, night-sky radiant cooling will be constrained by need for freeze protection.

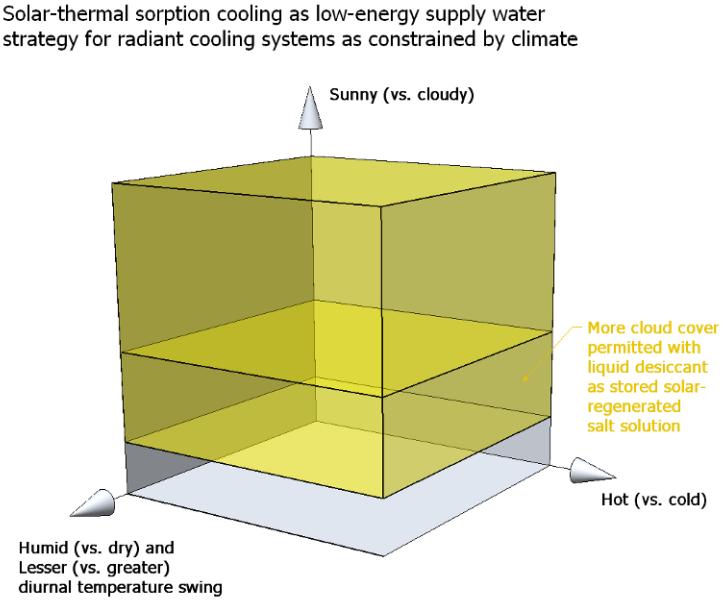

Figure A5: Solar-thermal sorption cooling depends mainly upon sufficient solar input. The relatively low COP of most sorption chillers makes the heat source, whether solar, waste heat, or a combined heat and power system, essential to achieving low-energy operation. Solid desiccant systems using an adsorption cycle can be used in combination with evaporative cooling of supply water to extend the capacity or climate range of that strategy (Figure A2). Liquid Such systems might tend toward using a lithium-bromide absorption cycle with water vapor refrigerant that works with 70–95°C generator temperatures achievable using relatively low-cost flat-plate solar thermal collectors (Duffie and Beckman 1991).

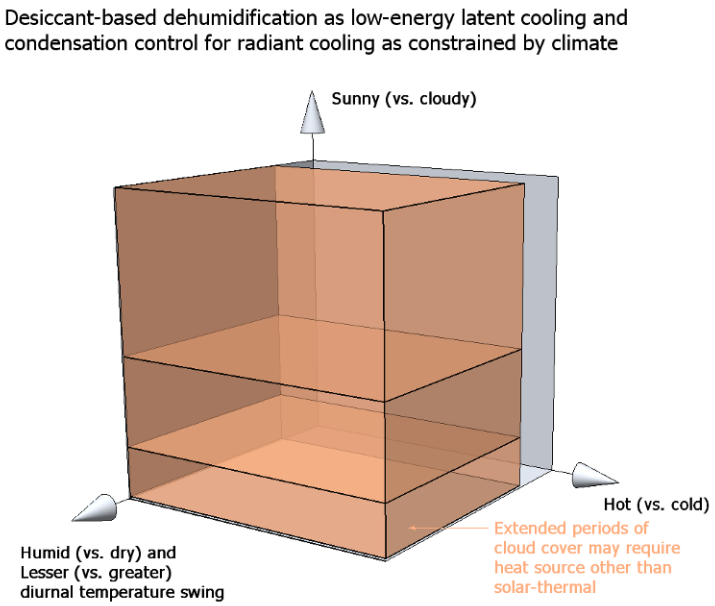

Figure A6: A range of desiccant-based technologies can provide dehumidification of ventilation air, and thus latent cooling condensation avoidance. Liquid desiccant systems using saltwater solutions, such as lithium chloride or calcium chloride, absorb moisture from intake air and can be regenerated at 60–70°C with heat from solar collectors (Henning et al 2004). Additionally, the concentration of salt in the regenerated solution is a relatively stable means of storing solar thermal energy over extended periods. However, commercially available systems are generally not appropriately design for solar regeneration.

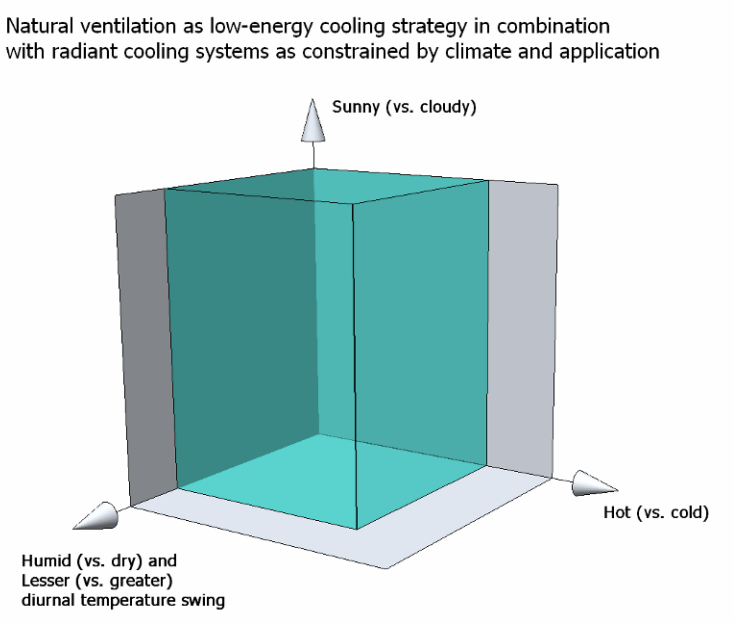

Figure A7: Natural ventilation appears to provide important opportunities for reduction of both fan energy and mechanical system first costs when used in combination with radiant cooling. However, it is of limited usefulness in notably hot climates and constrains radiant cooling capacity (as a function of supply water temperature and condensation avoidance) in humid climates.

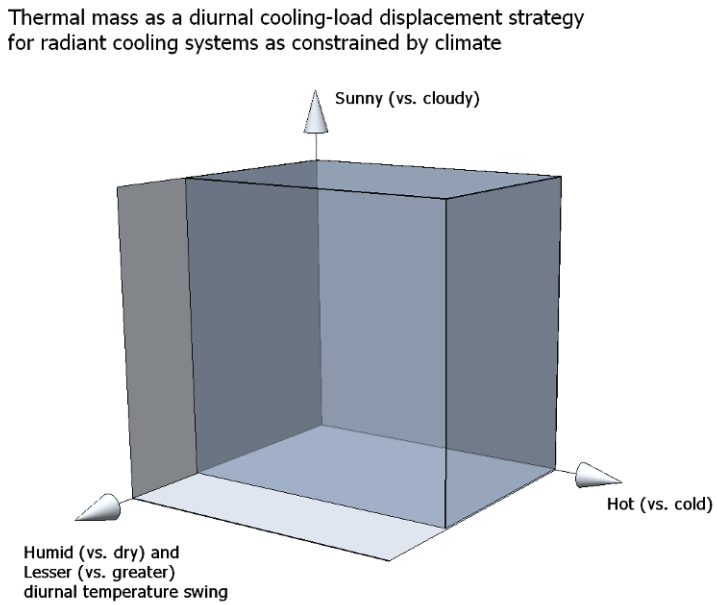

Figure A8: Thermal mass, while not a cooling source but a means of displacing cooling load over time, is most applicable in hot dry climates. However, this is mainly as a function of diurnal temperature swing, rather than humidity, per se. As described by Henning et al (2004), thermal storage can extend capacity for addressing diurnal swings and, to a lesser extent, capacity for multi-day cooling events—e.g., in the case of solar-thermal systems during a period of cloud cover or for evaporative systems during a period of elevated humidity.

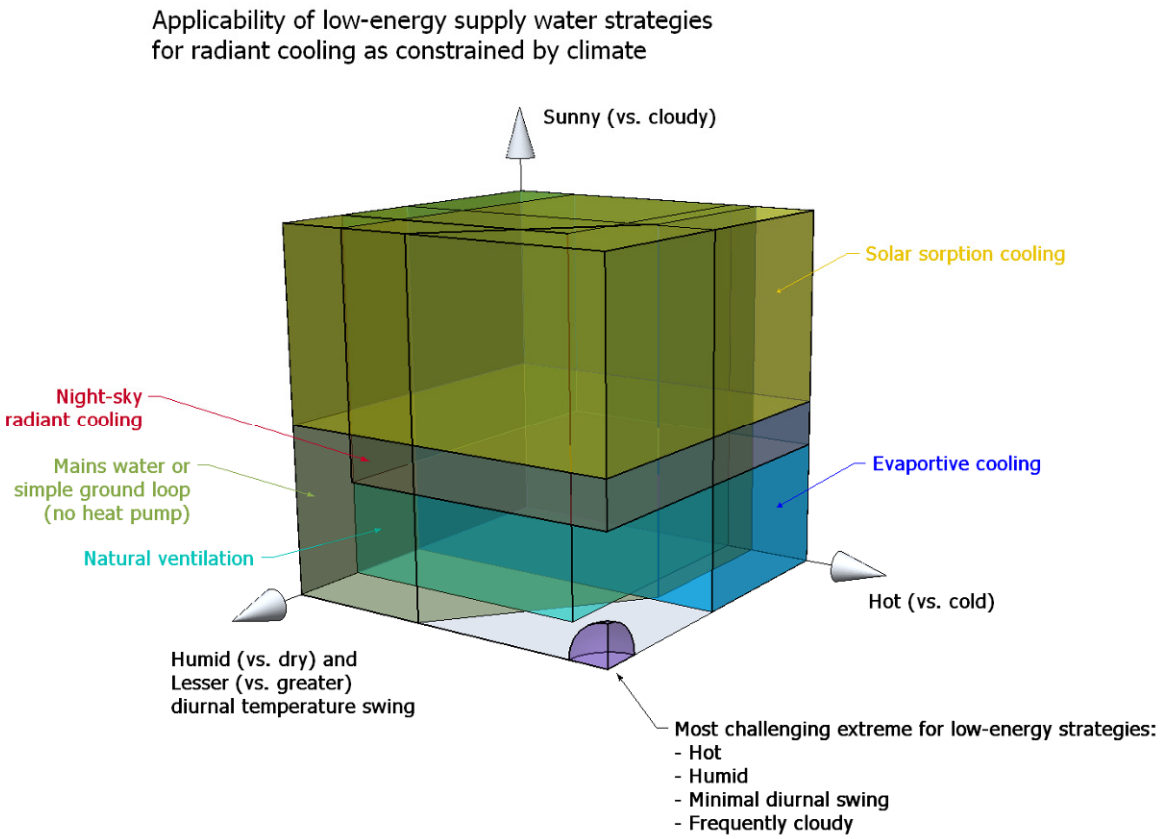

Figure A9: Even with their limitations, the low-energy cooling technologies and strategies discussed above collectively offer potential sources of cooling supply water and/or free cooling across most climates in the continental United States, albeit with limited capacity in some cases. The most challenging extreme climate includes is hot and humid with minimal diurnal swings and frequent cloud cover. This is typical of hot and/or rainy seasons in certain tropical and equatorial regions, but very uncommon within the continental United States. For these climates, some combination of desiccant-based dehumidification and air movement might be the most appropriate low-energy strategies to pair with radiant cooling.

REFERENCES

Alamdari Alamdari, F., and G.P. Hammond. 1983. “Improved data correlations for buoyancy-driven convection in rooms.” Building Services Engineering Research and Technology 4(3):106–12.

Awbi, H.B., and A. Hatton. 2000. “Mixed convection from heated room surfaces.” Energy and Buildings 32:153–66.

Baltimore Aircoil Company. 2000. “Closed Circuit Cooling Tower Selection Program” Release 6.2, www.BaltimoreAircoil.com

Bean, R., T. Doran, B. Olesen, and P. Simmonds. 2005. “Vertically Integrated Systems in Stand-Alone Multistory Buildings.” ASHRAE Journal, Vol. 47, No. 6, June 2005

Beausoleil-Morrison I. (1999), "Modeling Mixed Convection Heat Transfer at Internal Buildings Surfaces", Proc. Building Simulation '99, (1) 313-320, Int Building Performance Simulation Association, Kyoto Japan.

Carpenter, S R. Lay, 2003 “Radiant Cooling Systems – A Solution for LEED Buildings in Temperate Climates” Enermodal Engineering Ltd., Kitchener Ontario

Crawley, D. J. Hand, M. Kummert, and B. Grifith. 2005. “Contrasting the Capabilities of Building Energy Performance Simulation Programs.” U.S. Department of Energy; Univ. of Strathclyde, Glasgow, Scotland; Univ. of Wisconsin, Madison; and National Renewable Energy Laboratory.

Fanger, P.O., Ipsen, B.M., Langkilde, G., Olesen, B.W., Christensen, N.K. and Tanabe S. 1985, “Comfort Limits for Asymmetric Thermal Radiation”. Energy and Buildings, 8, 225–236.

Feustel, H. 1994. “Hydronic Radiant Cooling Systems.” Center for Building Science News (Fall issue), Lawrence Berkeley Laboratory

FT Energy EDR Design Brief. 2002. “Radiant Cooling Design Brief” prepared by Financial Times Energy, Boulder, CO for Energy Design Resources. www.energydesignresources.com

Gough, Martin 2007. “Water Side Economizer Design Spec (simulation).” An internal document of Integrated Environmental Solutions, Inc, 29 August 2007.

Gough, Martin 2007. Proprietary tool for calculating adjusted slab conductivity based upon Gough’s 1986 approximate solution to Laplace's equation.

Hauser, G., C. Kempkes, and B. W. Olesen. 2000. “Computer Simulation of Hydronic Heating/ Cooling System with Embedded Pipes” ASHRAE Transactions, Vol 106; part 1, pages 702-712

Hodder, S.G., Loveday, D.L., Parsons, K.C. and Taki, A.H. 1998, “Thermal Comfort in Chilled Ceiling and Displacement Ventilation Environments: Vertical Radiant Temperature Asymmetry Effects”. Energy and Buildings, 27: 167–173

Huizenga, C., D. K. Arasteh, E. Finlayson, R. Mitchell, B. Griffith, and D. Curcija. 1999. “Teaching Students About Two-Dimensional Heat Transfer Effects in Buildings, Building Components, Equipment, and Appliances Using THERM 2.0.” ASHRAE Transactions 1999, 105(2): 488-502

Kulpmann, R.W. 1993. Thermal comfort and air quality in rooms with cooled ceilings—Results of scientific investigations. ASHRAE Transactions 1993, 99(2): 488-502.

Laouadi, A. 2003. “Development of a radiant heating and cooling model for building energy simulation software.” Building and Environment 39 (2004) 421 – 431

Loveday, D.L., K.C. Parsons, A.H. Taki, and S.G. Hodder. 2002. “Displacement Ventilation Environments with Chilled Ceiling: Thermal Comfort Design within the Context of the BS EN ISO 7730 versus Adaptive Debate”. Energy and Buildings, 34: 573–579.

McCarry 2003. “Lower building energy usage with radiant heating and cooling.” Presentation at USGBC Greenbuild Conference, November, 2003.

McCarry, B. 2006. Personal communication. Stantec, Vancouver, BC, Canada

McNall Jr. P.E. and R.E. Biddison. 1970. "Thermal and Comfort Sensations of Sedentary Persons Exposed to Asymmetric Radiant Fields," ASHRAE Transactions 1970, 76 (1), 123–136.

Meierhans, R.A. 1996. "Room air conditioning by means of overnight cooling of the concrete ceiling." ASHRAE Transactions 1996, 102(2).

Mikler, V. 1999. In-house radiant cooling design guidelines. Cobalt Engineering, Vancouver, BC

Moore, T., F. Bauman, and C. Huizenga. 2006. "Radiant Cooling Research Scoping Study." Internal Report of the Center for the Built Environment, University of California, Berkeley

Moore, T. 2007. "Radiant Cooling Strategies and Applications: Initial Simulation Results" Internal Report of the Center for the Built Environment, University of California, Berkeley

Mumma, S.A. 2001. "Dedicated outdoor air in parallel with chilled ceiling systems." Engineered Systems 18(11):56–66.

Novoselac, A., B. Burley, and J. Srebric, 2006, "New Convection Correlations for Cooled Ceiling Panels in Room with Mixed and Stratified Airflow," HVAC&R Research, v12, no.2

Olesen, B.W. and R. Nielsen. 1981. "Radiant Spot Cooling of Hot Working Places". ASHRAE Transactions, 87 (1).

Olesen, B.W. 1987. "Possibilities and Limitations of Radiant Floor Cooling." ASHRAE Transactions 1987, 103(1).

Olesen, B.W. 2000. "Hydronic Radiant Heating and Cooling of Buildings Using Pipes Embedded in the Building Structure." 41 AICARR Conference.

Roth, K., D. Westphalen, J. Dieckmann, S. D. Hamilton, W. Goetzler. 2002. "Energy Consumption Characteristics of Commercial Building HVAC Systems Volume III: Energy Savings Potential" U.S. Dept. of Energy Building Technologies Program.

Seidl, R. 2005. "Indirect Evaporative Cooling Systems Using Cooling Towers," Presented as part of a workshop titled "Innovations in Evaporative Cooling and Water Treatment" December, 2005, Pacific Energy Center, San Francisco, CA

Simmonds, P., S. Holst, W. Gaw, and S. Reuss. 2000 "Using Radiant Cooled Floors to Condition Large Spaces and Maintain Comfort Conditions." ASHRAE Transactions 2000, 106(1)

Stetiu, C. 1999. "Energy and Peak Power Savings Potential of Radiant Cooling Systems in U.S. Commercial Buildings," Energy and Buildings, v.30, no.2

Zweifel, G. and M. Achermann. 2003. "RADTEST – The Extension of Program Validation Towards Radiant Heating and Cooling." Proc. Eighth International IBPSA Conference, Eindhoven, Netherlands, August 11-14, 2003

BIBLIOGRAPHY

Bauman, F. 2003. *Underfloor Air Distribution (UFAD) Design Guide*. Atlanta: ASHRAE, American Society of Heating, Refrigerating, and Air-Conditioning Engineers.

Bauman, F., H. Jin, and T. Webster. 2006. "Heat Transfer Pathways in Underfloor Air Distribution (UFAD) Systems." To be published in ASHRAE Transactions 2006, 112 (2).

Carpenter S. and J. Koklo, 1988. "Radiant Heating and Cooling, Displacement Ventilation with Heat Recovery and Storm Water Cooling: An Environmentally Responsible HVAC System," ASHRAE Transactions, v. 4, part.

Chantrasrisalai, C., V. Ghatti, D.E. Fisher, and D.G. Scheatzle. 2003. "Experimental Validation of the EnergyPlus Low-Temperature Radiant Simulation," ASHRAE Transactions, 109(2):614-623.

Conroy, C. and S.A. Mumma. 2001. "Ceiling radiant cooling panels as a viable distributed parallel sensible cooling technology integrated with dedicated outdoor-air systems." ASHRAE Transactions 2001, 107(1):571–579.

Jeong, J., S. A. Mumma and W. P. Bahnfleth. 2003. "Energy conservation benefits of a dedicated outdoor air system with parallel sensible cooling by ceiling radiant panels." ASHRAE Transactions 2003, 109(2).

Keller, B. "Low Temperature Heating and Cooling Systems for Low-Energy Buildings, Proved in Practice" Institute of Building Technology, ETH-Z (Swiss Federal Institute of Technology), Zurich, Switzerland

Mumma, S.A. 2002. "Chilled ceilings in parallel with dedicated outdoor air systems: Addressing the concerns of condensation, capacity, and cost." ASHRAE Transactions 2002, 108(2):220–231.

Lee 2004, "Sustainable Solution to a Building Mechanical System – Simulation of Thermo-Active Slab with Thermal Mass using TAS," Proc. eSim 2004, Vancouver, BC

Olesen, B W. 2002. Radiant Floor Heating in Theory and Practice. ASHRAE Journal, July 2002, pp. 19-26.

Rea, M., R. Zechin, B.Olesen, and M. De Carli, 2001. New Technologies in Radiant Heating and Cooling Università Degli Studi Di Padova, Dipartimento di Fisica Tecnica, Tesi di Dottorato in Energetica, XIV Ciclo

Shank, K. and S.A. Mumma. 2001. "Selecting the supply air conditions for a dedicated outdoor air system working in parallel with distributed sensible cooling terminal equipment." ASHRAE Transactions 2001, 107(1):562–570.

Simmonds, P. 1996. "Practical applications of radiant heating and cooling to maintain comfort conditions." ASHRAE Transactions 1996, 102(1): 659-666.

Strand, R.K. and K.T. Baumgartner. 2005. "Modeling radiant heating and cooling systems: integration with a whole-building simulation program." Energy and Buildings 37 (2005) 389–397

Strand, R.K., D.E. Fisher, R.J. Liesen, C.O. Pedersen. 2002 "Modular HVAC Simulation and the Future Integration of Alternative Cooling Systems in a New Building Energy Simulation Program."

Weber, T. and G. Johannesson. 2005. "An optimized RC-network for thermally activated building components." Building and Environment 40 (1): 1-14.

Zhen, T. and J. A. Love. 2006. "Radiant Slab Cooling: A Case Study of Building Energy Performance" Proc. SimBuild 2006, Cambridge, MA, August 2-4, 2006

Zmrhal, V., J. Hensen, and F. Drkal. 2003. Modeling and Simulation for a Room with Radiant Cooling Ceiling. Proc. Eighth International IBPSA Conference, Eindhoven, Netherlands, August 11-14, 2003.

LIST OF FIGURES AND TABLES